# Electrochemical characterization of nanostructured $SnO_2$ and $TiO_2$ for potential application as dielectric materials in sulfonated-polyaniline-based supercapacitors.

**LUNDI VINCENT NGQONGWA**

**A full thesis submitted in fulfillment of the requirements for the degree of**



**MAGISTER SCIENTIAE**

**In the Department of Chemistry, University of the Western Cape.**

**Cape Town, South Africa**

**Supervisor: Prof. Emmanuel I. Iwuoha**

**Co-supervisors: Dr. Tesfaye T. Waryo & Prof. Priscilla G.L. Baker**

**November 2010**

## DECLARATION

I declare that *Electrochemical characterization of nanostructured $SnO_2$ and $TiO_2$ for potential application as dielectric materials in sulfonated-polyaniline-based supercapacitors* is my own work, that it has not been submitted before for any degree or examination in any other university, and that all the sources I have used or quoted have been indicated and acknowledged by complete references.



**LUNDI VINCENT NGQONGWA**

**Signature: …….** **Date: …….**

## DEDICATION AND ACKNOWLEDGEMENT

I would like to take this opportunity to sincerely express my gratitude to the following bodies in absolutely no specific order for a tremendous contribution to my entire academic life. I doubt it would have been possible for me to get to this level without their support, whether financial or just social.

- The University of the Western Cape for granting me an opportunity to study in my all-time favourite institution.
- Rural Education Access Programme (REAP), without them, I would not have been able to pay for my registration at this University.
- A tremendous contribution to postgraduate studies have made possible by the formerly known as Department of Minerals and Energy of South Africa.
- South African National Energy Research Institute for making it possible to further my research in the energy field.
- Profs. E.I. Iwuoha and P.G. L. Baker, thank you very much for seeing my potential and guiding me all the way.
- To my postdoctoral fellow, Dr. Tesfaye T. Waryo, thank you very much for putting in time to this work. Your tremendous effort is gracefully appreciated.
- National Research Foundation is highly appreciated for the inspiration to aim for a PhD qualification.
- To Amagenge, (my friends) *Hola bafethu!* Thanks gents for the fun time together. I wish I could mention all of you by names, but you know time is our enemy here!
- To all SensorLab's research team, *you guyz rock!* Thank you very much for your selflessness.

- This is dedicated to me, my mother (Mavis Ngqongwa), my two sisters and brother, and to the entire Ngqongwa family. I would not have done it without their love and support.
- To my beloved and late granny and grandfather, from my mother's side, I still feel your presence, may the Holy Spirit be with you.
- I thank God Almighty for all the blessings and for keeping up with me through all the hard times.
- To Miss NL Hlasela, thank you very much my love for being there when I needed you most.

# TABLE OF CONTENT





## CHAPTER 1

## INTRODUCTION

**CHAPTER 2**

**LITERATURE REVIEW**

## CHAPTER 3

## RESEARCH DESIGN AND METHODOLOGY



## CHAPTER 4

## RESULTS PRESENTATION AND DISCUSSION

**CHAPTER 5**

**CONCLUSIONS AND RECOMMENDATIONS**

## LIST OF PUBLICATIONS

1. **Lundi V. Ngqongwa,** Tesfaye Waryo, Masiskini Milua, Priscilla Baker, Emmanuel Iwouha, *Metal oxide/polyaniline-composite supercapacitor materials studied at a carbon microelelectrode surface.* (**submitted manuscript**)

2. Masiskini Milua, Tesfaye Waryo, **Lundi V. Ngqongwa**, Priscilla Baker, Emmanuel Iwouha, *Hydroxy-Iron/β-Cyclodextrin-film Amperometric sensor for the Endocrine Disruptor substance Bisphenol A in an aqueous media with reduced fouling effects.* **(In press. Analytical Letters)**

## List of Schemes



## List of Tables

## List of figures

## LIST OF ABBREVIATIONS

| | |
|---|---|
| PANI | Polyaniline |
| ANi | Aniline |
| PSSA | Poly-(4-styrene) sulfonic acid |
| ECs | Electrochemical capacitors |
| EDLC | Electrochemical double layer capacitor |
| $C_{dl}$ | Double layer capacitance |
| $C_{pseudo}$ | Pseudocapacitance |
| SCs | Supercapacitors |
| KC*l* | Potassium chloride |
| HC*l* | Hydrochloric acid |
| M | Molarity |
| m | Mass |
| g | grams |
| F | Farads |
| $I_p$ | Peak current |
| $E_p$ | Peak potential |
| CA | Chrono Amperometry |
| CP | Crono-Potentiometry |
| CC | Chrono-Coulometry |
| Q | Charge |
| E | Energy |

| | |
|---|---|
| *n* | Number of electrons |
| $e^-$ | Electrons |
| *e*V | electron volts |
| Red | Reduction |
| Ox | Oxidation |
| ΔE | Change in potential |
| n | Nano |
| cm | centimetre |
| *l* | Litre |
| GCE | Glassy carbon electrode |
| Ag/AgCl | Silver/Silver chloride |
| TEM | Transmission Electron Microscopy |
| SEM | Scanning Electron Microscopy |
| CV | Cyclic Voltammetry |
| EIS | Electrochemical Impedance Spectroscopy |
| FTIR | Fourier Transform Infrared Spectroscopy |
| SC | Specific capacitance |
| C | capacitance |
| V | Volts |
| A | Amperes |
| Zi or Z'' | Imaginary impedance |
| Zr or Z' | Real impedance |
| Hz | Hertz |

| | |
|---|---|
| Rs | Solution Resistance |
| Rct | Charge transfer resistance |
| CPE | Constant Phase Element |
| W | Warburg element |
| ICPs | Intrinsic conducting polymers |
| CPs | Conducting polymers |
| HEV | Hybrid electric vehicles |

**SYMBOLS**



| | |
|---|---|
| μ | Micro |
| ν | Scan rate |
| Ω | Ohm |
| η | Coulombic efficiency |
| $\omega$ | Frequency |
| ∞ | Infinity |

# ABSTRACT

**Electrochemical characterization of nanostructured $SnO_2$ and $TiO_2$ for potential application as dielectric materials in sulfonated-polyaniline-based supercapacitors.**

L.V. Ngqongwa

*M. Sc full thesis, Department of Chemistry, University of the Western Cape, South Africa*

Electrochemical capacitors provide a mode of electrical charge and energy storage, complementary to that by batteries. Electrochemical capacitors are a special kind of capacitors based on charging and discharging the interfaces of high specific-area material such as porous carbon material or porous oxides of some metals. They can store electric charge and corresponding energy at high densities in a highly reversible way, as does a regular capacitor, and hence can be operated at specific power densities (watts/kg) substantially higher than can most batteries.

In this research project, nanostructured composites based on Tin dioxide ($SnO_2$) and Titanium dioxide ($TiO_2$) with poly-4-styrene sulfonic acid (PSSA) doped polyaniline (PANI) conducting polymer has been investigated based on their structural, electrical and electrochemical properties. The synthesis of conducting polymers and their metal oxide or composites have been carried out chemically or electrochemically according to methods modified from the literature. Layer-by-layer construction of nano-Metal Oxide/PSSA doped polyaniline composites were successfully constructed by electroanalytical methods on the surface of a glassy carbon working electrode (GCE).

The constructed nanocomposites were studied and characterized by cyclic voltammetry, chrono-potentiometry, chrono-amperometry, Fourier Transform Infra-red Spectroscopy (FTIR), High Resolution Transmission Electron Microscopy (HRTEM) and Electrochemical Impedance Spectroscopy (EIS). The constructed electrode material was in a minimal mass of $1.1893e^{-6}$ g and showing improved capacitance on a glassy carbon electrode with surface area of 0.07 $cm^2$. An increased specific capacitance values for the $SnO_2$ base composite from 0.01148 $F.g^{-1}$ of GCE//PANI-PSSA to 1.956 $F.g^{-1}$ of the GCE//PANI-PSSA/$SnO_2$ electrode and from 6.69121 $F.g^{-1}$ of the GCE//PANI-PSSA electrode to 9.4246 $F.g^{-1}$ when $TiO_2$ was deposited to form GCE//PANI-PSSA/$TiO_2$ electrode, and thus, showing potential application as electrode material for electrochemical supercapacitors. The $SnO_2$ based layer-by-layer composite, however, shows better specific capacitance than the $TiO_2$ based composite in most occasions.



**November 2010**

## KEYWORDS

Polyaniline

Poly-4-styrene sulfonic acid

Tin dioxide ($SnO_2$)

Titanium dioxide ($TiO_2$)

Supercapacitors

Electrochemical impedance

Cyclic voltammetry

Electropolymerization

Conducting polymers

Galvanostatic charge-discharge

Glassy carbon electrode

# CHAPTER 1

# INTRODUCTION

## 1.1 Introduction to capacitors and supercapacitors

All capacitors store energy as well as charge. The charges are generally stored on conductive plates, the positively charged plate called the anode and the negatively charged plate being the cathode. In order to keep the charges separate, the medium between the anode and cathode, called the *dielectric*, must be non-conductive – an electrical insulator. The two plates are configured so that very little movement occurs between them as they are charged and the force on the dielectric increases. As the stored charge increases, the electric field across the dielectric increases. This situation gives rise to a voltage which increases proportionally with the charge. The ratio of the charge magnitude on each plate to the electric potential between the plates is known as capacitance. The energy stored in a capacitor is the energy required to move the stored charge through the potential of the capacitor. The capacitance depends mostly on the plate geometry and the nature of the dielectric. It (the capacitance) is directly proportional to the "dielectric constant" and inversely proportional to the thickness of the dielectric



Simplest forms of capacitors store energy in a thin layer of dielectric material that is supported by metal plates that act as the terminals for the device. The capacitance of the dielectric capacitor depends on the dielectric constant *K*. and the thickness of the dielectric material and its geometric area *A*.

In a battery, energy is stored in chemical form as active material in its electrodes. Energy is released in electrical form by connecting a load across the terminals of the battery allowing the electrode materials to react electrochemically with the ions required in the reactions to be transferred through the electrolyte in which the electrodes are immersed. Energy is stored in the double-layer capacitor as charge separation in the double-layer formed at the interface between the solid electrode material surface and the liquid electrolyte in the micropores of the electrodes

As the charge and voltage on a given capacitor are increased, at some point the dielectric will be unable to separate the charges from each other. The dielectric then exhibits dielectric breakdown, or high conductivity in certain areas, which tends to lower the stored energy and charge, generating internal heat. This phenomenon, undesirable in most capacitor applications, occurs at the capacitor's breakdown voltage. Capacitor destruction can occur in such situations. Normally, breakdown ratings for dielectrics are expressed as a maximum field strength which is basically the ratio of the applied voltage to the dielectric thickness.



The mass energy density of a capacitor is the ratio of the amount of energy the capacitor can store at its working voltage to the capacitor mass, including package. The working voltage of a capacitor is defined as the maximum rated voltage for a given application. The working voltage is generally less than the breakdown voltage. An exception to this rule could occur if the transient peak voltage were able to exceed the steady-state breakdown voltage. The volumetric energy density of a capacitor is defined as the ratio of the energy stored to the capacitor volume, including package [1].

## 1.2 Introduction to working principle of a supercapacitor

A capacitor is a device used for storing electric charge [2-3]. A simple parallel plate capacitor (shown in Figure 1.1) consists of two parallel conductive plates separated by an insulating layer called a dielectric. The insulating layer prevents electric charges from flowing between the two plates.

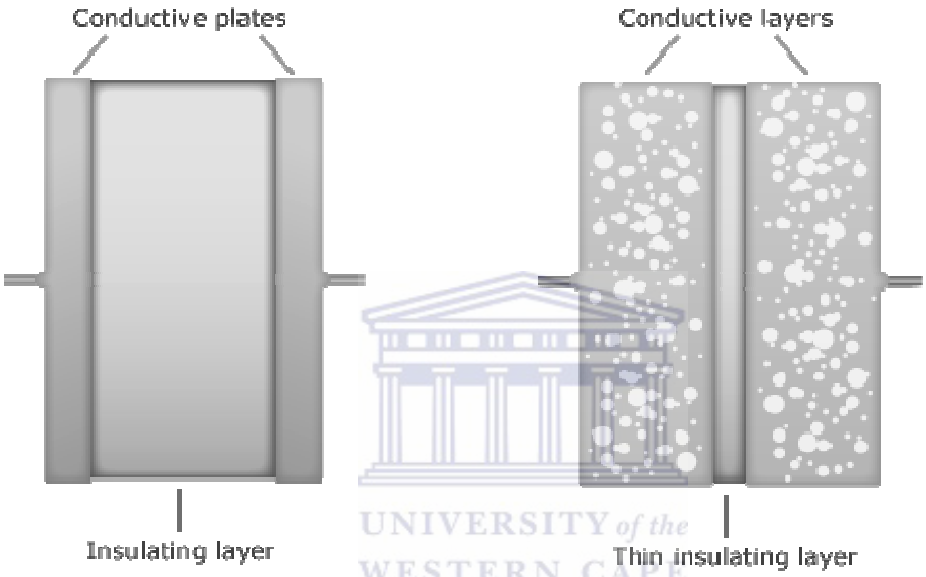



***Figure 1.1: Parallel plate capacitor and Supercapacitor.***

***images abducted from: http://www.bigshotcamera.org/sections/learn/power/cap.ht***

If the ends of a capacitor are connected to a power source, the voltage from that power source will drive the electrons from one of the capacitor's conductive plates to the other, *charging* the capacitor. Disconnecting the power source will trap (or *store*) the charges on the capacitor's plates. One plate will be negatively charged with electrons and the other be positively charged with an equal number of ions. The amount of charge that can be stored on these plates depends on a property of the capacitor known as capacitance.

A capacitance of a capacitor depends on the surface areas of its plates, the type of

insulating material between its plates, and the distance between its plates [4]. In general, the larger the capacitor, the more charge it can store. Once a capacitor is charged, it can be used as a power source.

Recent breakthroughs in materials science have given rise to a new type of capacitor called a supercapacitor. Rather than having two plates separated by a thick insulation layer, supercapacitors use two thick layers of conducting material separated by a very thin, often a few nanometers wide, insulating layer, as shown in Figure 1.1. The two conducting layers are made of a porous material to dramatically increase their surface area. Since the charges can be held inside the plates' pores in addition to outside on their surfaces, supercapacitors can store significantly greater amounts of charge than regular capacitors can.



**1.3 Characteristics of conventional capacitors**

Capacitors store energy in an electrostatic field rather than as a chemical state as in batteries.

- No chemical actions involved which means very long cycle life is possible.
- No limit on the cell voltage imposed by the so called cell chemistry as with galvanic cells.
- The terminal voltage is directly proportional to the state of charge which limits range of applicability.

***1.3.1 Low power capacitors***

Capacitors are probably the most common form of non-chemical energy storage and are widely used in low power applications. Supercapacitors, Ultracapacitors or EDLC

(Electric Double Layer Capacitors) as they are also called, look very much like batteries. They have double layer construction consisting of two carbon electrodes immersed in an organic electrolyte. See below

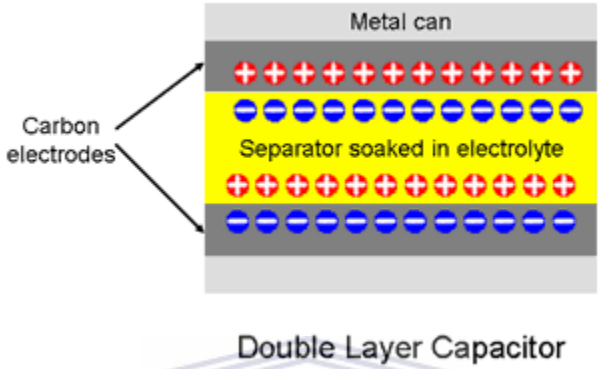


***Scheme 1.1: Schematic diagram of a double layer capacitor.***

***Image abducted from: http://www.4-lithium-batteries.com/tech-ultracapacitor.html***



During charging, electrically charged ions in the electrolyte migrate towards the electrodes of opposite polarity due to the electric field between the charged electrodes created by the applied voltage. Thus two separate charged layers are produced. Although similar to a battery, the double layer capacitor depends on electrostatic action. Since no chemical action is involved, the effect is easily reversible and the typical cycle life is hundreds of thousands.

Capacitors have a low energy density of less than 15 Wh/Kg but a very high power density of 4,000 W/Kg and capacitance values of thousands of Farads are possible. Although the power density is very high the cell voltage is limited to about 2.3 Volts to

avoid electrolysis of the electrolyte with the consequent emission of gas. Voltage equalization to spread the available charge evenly between the capacitors in a series chain may also be needed for many applications.

#### 1.3.1.1 Advantages

- Cell voltage determined by the circuit application, not limited by the cell chemistry.
- Very high cell voltages possible
- High power available.
- High power density.
- Simple charging methods.
- Very fast charge and discharge.
- Can not be overcharged.
- Long cycle life of more than 500,000 cycles.
- No chemical actions.
- 10 to12 year life
- Low impedance



#### 1.3.1.2 Shortcomings

- Linear discharge voltage characteristic prevents use of all the available energy in some applications.
- Power only available for a very short duration.
- Low capacity.
- Low energy density.
- Cell balancing required for series chains.
- High self discharge rate. Much higher than batteries.

### 1.3.2 Applications requiring a short duration power boost.

#### 1.3.2.1 Low power

- Capacitors are broadly used as power back-up for memory functions in a wide range of consumer products such as mobile phones, laptops and radio tuners.
- Used in pulsed applications to share the load and for providing peak power assistance to reduce the duty cycle on the battery to extend battery life in products or devices using mechanical actuators such as digital cameras. Also used for energy storage for solar panels, and motor starters.



#### 1.3.2.2 High power

- The shortcomings above render supercapacitors not suitable as primary power source for electric vehicles and hybrid electric vehicle applications, however their advantages make them ideal for temporary energy storage for capturing and storing energy from regenerative braking and for providing a booster charge in response to unexpected power demands.
- Since the capacitor is normally connected in parallel with the battery in these applications, it can only be charged up to the battery upper voltage level and it can only be discharged down to the battery lower discharge level, leaving considerable unusable charge in the capacitor, thus limiting its effective or useful energy storage capacity.

Using supercapacitors in EVs and HEVs to facilitate regenerative braking can add 15% to 25% to the power range of the vehicle.

At the same time, supercapacitors can provide an effective short duration peak power boost allowing the prime battery to be downsized. It should be noted however that while supercapacitors can be used to provide the increased range and short term power, it is at the cost of considerable added weight and bulk of the system, and this should be weighed against the advantages of using higher capacity batteries [5].

Supercapacitors are also used to provide rapid acting short term power back up for UPS applications. By combining a capacitor with a battery-based uninterruptible power supply system, the life of the batteries can be extended. Batteries provide power only during the longer interruptions, reducing the peak loads on the battery and permitting the use of smaller batteries [5].



**1.4 Carbon Nanotube Enhanced Supercapacitors**

Recent developments at MIT (metal-insulator-transition) have shown that the performance of supercapacitors can be significantly improved by using nanomaterials. The energy storage capability of a capacitor is directly proportional to its capacitance which in turn is proportional to the area of the plates or electrodes. Likewise the current carrying capability is directly proportional to the area of the electrodes. By using vertically aligned, single-wall carbon nanotubes which are only several atomic diameters in width instead of the porous, amorphous carbon normally employed, the effective area of the electrodes can be dramatically increased. While the achievable energy density of 60Wh/Kg still can not match the level obtainable in Lithium Ion batteries (120Wh/kg),

the power densities achieved of 100kW/kg are three orders of magnitude better than batteries [5].

### 1.5 Motivation of study

In the field of energy storage, two main parameters are fundamental for storage devices: the energy density and the power density. The first parameter defines the amount of energy that can be stored in a given volume or weight. The power density defines the way this energy can be stored into the device. The more this parameter is high, the more the time for loading and unloading the amount of needed energy is reduced. The ideal storage device should propose both a high energy density, together with a high power density.

This is unfortunately not the case, and compromises have to be done. Considering the battery technologies, the energy density is high, but with a poor power density. The opposite is the main characteristic of capacitors, a limited power density with a high power density. New components, such as the supercapacitors, offer today an alternative to this dilemma. They are compromise between batteries and conventional capacitors. Their main characteristic is to propose both a high energy density together with a high power density. This leads to new applications for energy storage, even if the energy density is still lower than that one of the batteries [6]. The major advantage of the two energy storage technologies is that none replaces each, they both work together and there is no fear of batteries being replaced by capacitors or vise versa.



### 1.6 Objectives of research project

- To develop alternative material for application in electrochemical capacitors

- To investigate the capacitance of selected metal oxide-based dielectric materials
- To develop new materials for better energy storage with improved charge and discharge properties.
- To develop and investigate novel nanocomposite of metal oxides and conducting polymers for application in electrochemical capacitors.
- To outline electrochemical, electrical and physical properties of the developed $SnO_2$-PANI/PSSA and/or $TiO_2$-PANI/PSSA nanocomposite.
- To characterize the synthesized nanocomposite of both metal oxides and polyaniline doped with polystyrene sulfonic acid (PSSA) using thermogravimetric analysis:
- X-ray diffraction (XRD) and energy dispursive X-ray spectroscopy (EDX) for detailed information about the chemical composition and crystallographic structure of natural and manufactured materials, Scanning Electron Microscopy (SEM) for information about the sample's surface topography, and Transmission Electron Microscopy (TEM) for information on size, shape and arrangement of the particles which make up the sample under investigation. Electrochemical characterization will be performed using chronopotentiometry, cyclic voltammetry and electric conductivity measurements will be done by electrochemical impedance spectrometry (EIS).



### 1.7 Problem statement

In recent years, due to environmental issues and depleting fossil fuels, interest in the development of alternative energy storage/conversion devices with high power and

energy densities catering the present day demands has increased to a greater extent. Supercapacitors (SCs) or electrochemical capacitors are energy storage devices that have gained importance in recent years owing to their technological significance ranging from satellites to consumer electronic devices [7]. Supercapacitors, also called electrochemical capacitors (ECs) or ultracapacitors, have attracted considerable attention over the past decades because of their higher power density and longer cycle life than secondary batteries and their higher energy density compared to conventional electrical double-layer capacitors. To develop an advanced supercapacitor device, an active electrode material with high capacity performance is indispensable. From the materials point of view, porous carbon materials, conducting polymers, and transition-metal oxides are fundamental candidates used as supercapacitor electrode materials [8].

The characteristics required for using one certain material as supercapacitor electrode are a capacitive behavior, a large surface area, a high conductivity, and electrochemical stability. The best example is the amorphous and hydrated ruthenium oxide ($RuO_2.xH_2O$), which yields remarkably high specific capacitance (720–780 F $g^{-1}$). However, the high cost of such metal oxides has stimulated researcher to identify other cheap materials that exhibit similar behavior [9].

Among all of these metal oxides, $RuO_2$ in its amorphous hydrous form ($RuO_2.xH_2O$) has been found to be the best material for supercapacitor applications due to its high specific capacitance, high specific energy density, high electrochemical reversibility, and long cycle-life. Nevertheless, an intrinsic problem with $RuO_2.xH_2O$ is that only a very thin layer takes part in the charge-storage mechanism while the underlying active material remains unreacted. Further, $RuO_2.xH_2O$ suffers from poor high-rate capability and is also

expensive [10]. Amorphous hydrated $RuO_2$ systems, with high specific capacitances (>700 F g−1) and cycling ability have been reported, but although $RuO_2$ gives high specific capacitance, it has disadvantages of high cost and toxic nature [11-13].

# CHAPTER 2

# LITERATURE REVIEW

## 2.1 Background literature

Electrochemical capacitors have drawn much attention as charge-storage devices for electrical energy owing to their ability to deliver high power and survive high number of cycle counts [14-16]. Due to the increasing demand for new improved charge-storage devices of high specific power and long durability, there has been growing interest in the development of novel electrode materials for the electrochemical capacitors, such capacitors can be utilized as supplementary high power charge storage devices for electrical vehicles, digital telecommunication systems, computers, memory backup systems solar cells and fuel cells. Electrochemical capacitors have also greater energy densities than common conventional dielectric capacitors [17].



Charge storage in electrochemical capacitors can originate from double layer capacitance arising from charge separation at the electrode-electrolyte interface and from the so called pseudocapacitance arising from fast reversible Faradaic (redox) reactions occurring at, or near, the electrode surface [18]. The combination of double layer capacitance with [19] pseudocapacitance should produce supercapacitors characterized by high energy densities and increased value of specific capacitance [3, 19]. Energy storage mechanism of electrochemical supercapacitors arises not only from charging of electrochemical double layer at the electrode-electrolyte interface, but also from pseudocapacitance involving reversible Faradaic charge transfer reactions (conducting polymers, noble metal oxides and high surface activated carbons) [20-21]. In electrochemical capacitors, carbon

powder, conducting polymers or conducting metal oxides are wildly used as active electrode materials. Conducting polymers and metal oxides store charges through the faradaic reactions called pseudocapacitance. Among these materials, conducting polymers and metal oxides with high surface areas are considered promising energy storage materials because the pseudocapacitors outshine the electrochemical double layer capacitance in terms of the interfacial area capacitance [19, 22].

Carbon nanotubes are attractive materials for supercapacitors because of their outstanding properties such as unique morphology, excellent electronic conductivity and useful mechanical performance. However, the relatively low capacitance and high cost of carbon nanotubes prohibit their application [19]. Among various transition metal oxide materials used in the pseudocapacitors, amorphous and hydrated ruthenium oxide has been reported to show a remarkably high specific capacitance ($720Fg^{-1}$) compared to other oxides [23-24].



Transition metal oxides such as hydrous ruthenium oxides, manganese oxides and nickel oxides have been demonstrated to be the electrode materials for electrochemical capacitors owing to their high specific capacitance. Among these oxides, a hydrous form of ruthenium oxide in aqueous $H_2SO_4$ possesses a high specific capacitance of $720Fg^{-1}$ at low scan rates of $2mVs^{-1}$ and excellent cycle-life stability. However, a disadvantage of ruthenium oxide is that it is very expensive for commercial use. Most of the researchers are, therefore, focused on alternative electrode materials that are inexpensive and exhibit capacitive behaviour comparable to that of ruthenium oxide [24].

Conducting polymers offer advantages of ease of synthesis and low cost [25] and can be chemically synthesized from a monomer, an oxidizing agent and a dopant [26].

Conventional aluminium electrolytic capacitors present many disadvantages such as high impedance and thermal instability, in addition to the problem of liquid electrolyte leakage, owing to the low-conductive ($10^{-2}$- $10^{-3}$ S/cm) and thermally unstable ionic liquid electrolyte. While tantalum electrolytic capacitors achieve improved thermal stability by employing pyrolytic manganese dioxide, the impedance frequency characteristics are not improved because of the low conductivity of manganese dioxide, in the range from ($10^{-2}$-$10^{-1}$) S/cm [26-27]. Tantalum oxide thin films are comprehensively studied in a wide range of industrial applications. Especially, tantalum oxide has received considerable attention for use as a capacitor material to replace thin $SiO_2$ layer in storage capacitor in scale down dynamic random access memories (DRAMs) because of their high dielectric constant values of about 20 and high chemical and thermal stabilities [28-29] compared with $SiO_2$ [28, 30-31]. DRAMs are a driving force for high-*k* dielectrics integration, and memories with high-*k* materials been fabricated. To date, $Ta_2O_5$ has merged as the strongest candidate as an active dielectric in dynamic memories [29]. Among the high-*k* materials like $ZrO_2$, $HfO_2$, $Ta_2O_5$, $Y_2O_3$, $TiO_2$ metal oxides, $Ta_2O_5$ is one of the most promising candidates to replace $SiO_2$ as a memory dielectric in storage capacitors, since it has excellent step coverage characteristics, high dielectric constant greater than 20, (depending on the conditions during growth), high breakdown field, relatively low leakage currents resulting in a high storage charge and chemically stable structure [32].

After discovering the new material class of intrinsic conducting polymers (ICP) approximately 25 years ago a lot of application possibilities have been developed. In the beginning, the properties of polyacetylene have been just an exotic feature of this

material. But after a while this behaviour (switching between metallic and insulating state to p/n doping, variable characteristics concerning conductivity, absorption and flexibility) has presented a vision for complex applications [33]. The possibility to adapt the usage of ICPs to production processes is an enormous advantage. Most known ICPs are represented by polypyrrole, polythiophene, polyaniline and their derivatives. ICPs belong to the substance class of combined electronic and ionic conductors with high redox-capacity consisting of soft material displaying according variable properties. It is mostly possible to obtain a copper-like conductivity by oxidizing ICPs [33]. Conducting polymers are frequently called "synthetic metals" because they present electric, electronic, magnetic and optical properties inherent to metals or semiconductors, while retaining mechanical properties of conventional polymers [34]. These properties are intrinsic to the doped material, being completely different from those originated from a mixture of a non-conductive polymer with a conducting material, such as metal or carbon powder. In intrinsic conducting polymers the conductivity is assigned to the delocalization of π-bonded electrons over the polymeric backbone, exhibiting unusual electronic properties, such as low energy optical transitions, low ionization potentials and high electron affinities. Delocalization of electron is a consequence of the presence of conjugated double bonds in the polymer backbone structure [34]. Conductive polymers such as polypyrroles, polyanilines, and polythiophenes have resistivities 10 to 100 times less than that of manganese dioxide. Since they are much less powerful oxidizing agents than manganese dioxide, the materials do not cause the capacitor to ignite upon failure [26].

## 2.2 Literature of the fourth generation capacitors: Supercapacitors

Batteries along with fuel cells rely on chemical reactions at the electrode to generate electrical energy. The behavior of certain electrode-electrolyte interfaces, however, resembles that of a conventional capacitor in that charge transfer across the interface over a limited voltage range is greatly impaired. Although potentials should be thermodynamically sufficient to drive one or more electron transfer processes, the rates at which such reactions proceed are negligibly small rendering the interface as effectively charged [35].

Theoretically, one plate of the capacitor is the electrode and the other is a collection of ions present in the electrolyte, forming a diffuse double layer of only a few nanometers thick. An appreciation of the advantage such an electrochemical capacitor, often referred to as supercapacitor or ultracapacitor, offers compared to batteries can be gleaned from the Ragone plot (figure 2.1), as shown in the figure, electrochemical capacitors have excellent specific power densities compared to batteries, but very modest when it comes to specific energy densities [35-36].

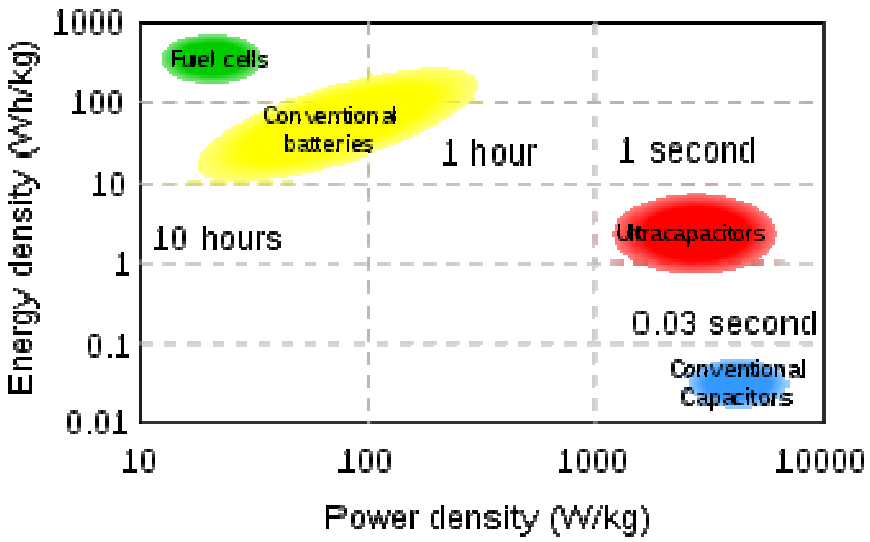


***Figure 2.1: Ragone plot differences of energy and power densities of Fuel cells, batteries and capacitors. Image abducted from*** *(www.englishgratis.com)*

Electrochemical capacitor also named as supercapacitor is a novel type of energy storage device whose capacitance is 20-200 times higher than that of electrolytic capacitors [37]. These electrochemical capacitors (ECs) are simply defined as charge storage devices which have higher energy densities than conventional dielectric capacitors and have higher power density than batteries [36, 38-39]. In hybrid electric vehicles [25], electrochemical capacitors are used in combination with batteries as they have higher power density than batteries for load leveling [38, 40]. The combination has excellent cold weather SLI (starting, lighting and ignition) [41] and increased battery life [38].

Supercapacitors are charge storage devices which possess high power density, excellent reversibility, and have longer cycle-life as compared to batteries. Supercapacitors derive their power from the charge storage at the electrode-electrolyte interface and can be classified as:

- redox supercapacitor, which utilize the pseudocapacitance arising from reversible faradaic reactions occurring at the electrode surface and
- Electrical double-layer capacitance, which utilize the capacitance arising from charge separation at the electrode-electrolyte interface. The key to the high specific power of a supercapacitor lies in the nature as well as well as the surface area of its electrode material. The ability of a supercapacitor to supply high power lies in the charge-storage occurring in the nanosize thick region at the interface of the electrode and the electrolyte. The nanomaterials with high surface area and high porosity are considered as the best performance electrode materials for supercapacitors [42].



### 2.2.1 Classification of electro-chemical capacitors

The capacitors can be generally classified as follows:

- Electrostatic capacitors.
- Electrolytic capacitors.
- Electro-chemical capacitors.

Electrostatic capacitors are typically made of two metal electrodes (parallel plates) separated by a dielectric. The dielectric is nothing, but is a non conducting material that is inserted between the parallel plates of the metal electrode material. The operating voltage of the capacitor depends upon the strength of the dielectric material that is measured in volts per meter. An electrolytic capacitor is similar in construction to an electrostatic capacitor but has a conductive electrolyte salt in direct contact with the metal electrodes. Aluminum electrolytic capacitors, for example, are made up of two aluminum conducting

foils (coated with an insulating oxide layer) and a paper spacer soaked in electrolyte. The oxide layer serves as the dielectric and is very thin, which results in higher capacitance per unit volume than electrostatic capacitors. ECs also use electrolyte solutions but have even greater capacitance per unit volume due to their porous electrode structure compared to electrostatic and electrolytic capacitors [43].

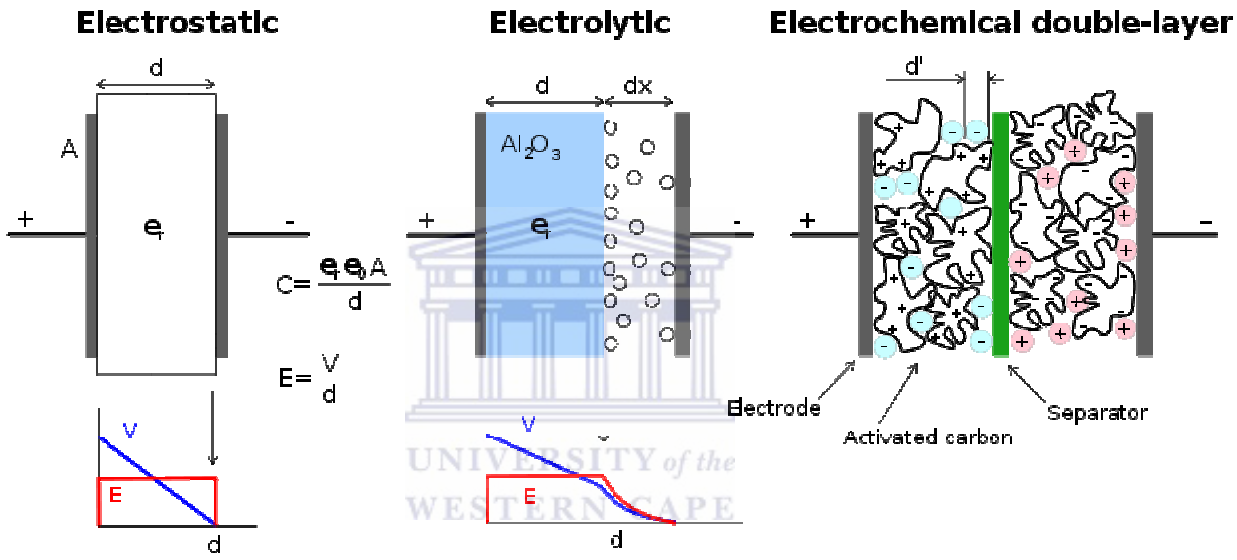


***Figure 2.2. Schematic presentation of electrostatic capacitor, electrolytic capacitor and electrical double layer capacitor.***

***Images abducted from*** *(www.printedelectronicsworld.com)*

### 2.2.1.1 Electrostatic capacitors

***Table 2.1. Comparison of the properties of battery, electrostatic capacitor and electrochemical capacitors.***

| | ***Battery*** | ***Electrostatic capacitor*** | ***Electrochemical Capacitor*** |
|---|---|---|---|
| Discharge time | 0.3 - 3 h | $10^{-3}$ to $10^{-6}$ s | 0.3 – 30 s |
| Charge time | 1 - 5 h | $10^{-3}$ to $10^{-6}$ s | 0.3 – 30 s |
| Energy density | 10 – 100 | <0.1 | 1 - 10 |

| | | | |
|---|---|---|---|
| (Wh/Kg | | | |
| Specific power (W/Kg) | 50 – 200 | > 10 000 | ~1000 |
| Charge-discharge efficiency | 0.7 - 0.85 | ~1 | 0.85 – 0.98 |
| Cycle life | 500-2000 | >500 000 | >100 000 |

Table 2.1 summarizes the differences expected between batteries and ECs. Due to such differences, the corresponding electrochemical behavior is also different. It can be seen from the table that the energy density of EC is 10 times higher than electrostatic capacitor; in addition, the EC has the advantages of high power density, short charge-discharge time, high charge–discharge efficiency and long cycle life compared with battery. Therefore, the EC has filled the gaps between the electrostatic capacitor and battery [44].

Capacitors are made from two metallic electrodes, mainly Si, placed in mutual opposition with an insulating material called the dielectric between the electrodes for accumulating an electrical charge. The charge accumulating principle can be described as follows: when a battery is connected to the capacitor, flow of current induces the flow of electrons so that electrons are attracted to the positive terminal of the battery and so they flow towards the power source. As a result, an electron deficiency develops at the positive side, which becomes positively charged and an electron surplus develops at the negative side, which becomes negatively charged. This electron flow continues until the potential difference between the two electrodes becomes equal to the battery voltage. Thus the capacitor gets charged. Once the battery is removed, the electrons flow from the negative side to the side with an electron deficiency; this process leads to discharging [44-45].

### 2.2.1.2 Electrolytic capacitors

*Table 2.2: History of electrolytic capacitors*

| *Generation* | *Type* | *Electrolyte* | *Developed* |
|---|---|---|---|
| 1st | Al electrolytic capacitors | Liquid electrolyte | 1908 |
| 2nd | Ta solid capacitors | $MnO_2$ | 1953 |
| 3rd | Al solid capacitors | TCNQ complex salt | 1982 |
| 4th | Conductive polymer capacitor | Polypyrrole | 1988 |

7,7,8,8-tetracyanoquinodimethane (TCNQ)

Electrolytic capacitors are similar to batteries in cell construction but the anode and the cathode materials remain the same. They are mainly tantalum and aluminum and ceramic capacitors where solid/liquid electrolytes are used with a separator between two symmetrical electrodes. A typical aluminum electrolytic capacitor includes an anode foil and a cathode foil processed by surface enlargement and/or formation treatment. The dielectric film is usually fabricated by anodizing high purity aluminum foil for high voltage application in boric acidic solutions. The thickness of the dielectric is related to the working voltage of the capacitor. Electrolytic aluminum capacitors are mainly used as power supplies for automobiles, space vehicles, computer, etc [45].



#### *2.2.1.2.1 Qualities of a semiconductor used in electrolytic capacitors*

A semiconductor or solid electrolyte needs to have the following qualities to be adopted in a solid electrolytic capacitor:

- high conductivity;
- processability to impregnate elements of capacitors;
- solid adhesion to dielectric films;

- heat-resistance and a long life;
- causing no reaction from metals used as dielectric films,
- or not causing deterioration of the voltage-proof;
- ability to restore dielectric films, and highly voltage-proof, and
- stable temperature characteristics.

The development of a semiconductor that satisfies all these conditions is very difficult and only three semiconductors listed in Table 2.2 have been obtained [46].

#### 2.2.1.3 Electrical double layer capacitors

Energy is stored in the double-layer capacitor as charge separation in the double-layer formed at the interface between the solid electrode material surface and the liquid electrolyte in the micropores of the electrodes [47].



The capacitor is charged and the electrical energy stored in the capacitor is discharged at loads. EDLCs based on carbon electrodes has been used for memory back-up device since 1978 for many electrical appliances like VCRs, camera etc. In 1980s, the EDLCs were used for the energy source to drive wrist watches with solar cells. In 1990s, they were used as actuator back-up sources for toys, electric appliances, home equipment etc. Recently, EDLCs with higher capacitances are under development for higher electric power sources in electric vehicle systems and electric power storage systems. Typical potentiodynamic electrochemical response of carbon nanotube in aqueous electrolyte shows a symmetrical and rectangular cyclic voltammetric curve as a trademark for double layer capacitance [48]. Theoretically, specific capacitance of an activated carbon is directly proportional to the specific surface area. However, in reality it does not happen.

It was reported that the some activated carbons with smaller surface area give a larger specific capacitance than those with a larger surface area; for instance, M-30 with a BET surface area of 2571 $m^2/g$ gave the specific capacity of 62.9 $Fg^{-1}$ while M-30 with a BET surface area of 2130 $m^2/g$ gave a specific capacity of 100 $Fg^{-1}$ [49]. The relation between the surface area of the activated carbons and their electrochemical performance has been discussed by Shi et al [49-50].

### 2.3 Impedance of Supercapacitors

It has been noted that different types of electrochemical supercapacitors exhibit specific capacities many orders of magnitude higher than the film and electrolytic capacitors known before. It must be added at once, however, that the behavior of supercapacitors differs appreciably from that of ideal film (parallel plates separated by thin layer of air) capacitors. In contrast to film capacitors, supercapacitors have a noticeable and sometimes rather high internal resistance (impedance). This resistance is caused by many factors. With the aim of having a maximum specific surface area and thus maximum specific capacity, highly disperse materials are used in the electrodes of all types of supercapacitors. The pores of these materials are filled with electrolyte through which current flows when the capacitor is operated. The resistance of the electrolyte in the branched system of fine and ultra-fine pores is high, causing considerable ohmic losses. In highly disperse systems, ohmic voltage losses also develop between the individual grains of electrode material. Another factor is hindered diffusion and migration of ions in the system of fine pores, but these processes are necessary for the formation and decay of

the counterion layers in the solution next to the electrode when there is a change in the amount of charge in the electrode.

The influence of all these factors increases with the current density in the capacitors. During charging with very low currents, their influence is insignificant, so that the capacitors readily and without losses are charged to almost their full capacity. However, the main purpose of these capacitors is high-current discharge, which is attended by appreciable voltage losses and, as a result, a drastically lower value of the capacity that can be realized in practice when discharge is terminated at a given final voltage [51].

**2.4 Preparation of conducting polymers.**

Conducting polymers are suitable systems for supercapacitors on account of their ease of processability and excellent reversibility behavior. These polymers utilize their conjugated backbones to transfer electrical charge from the current collector to the electrolyte. Conducting polymers are referred to as either n-doped (reduced state) or p-doped (oxidized state) relative to their neutral state. The mechanism of charge storage is three-dimensional, since the amount stored is proportional to the extent of electroactive species absorbed on the electrode [52].

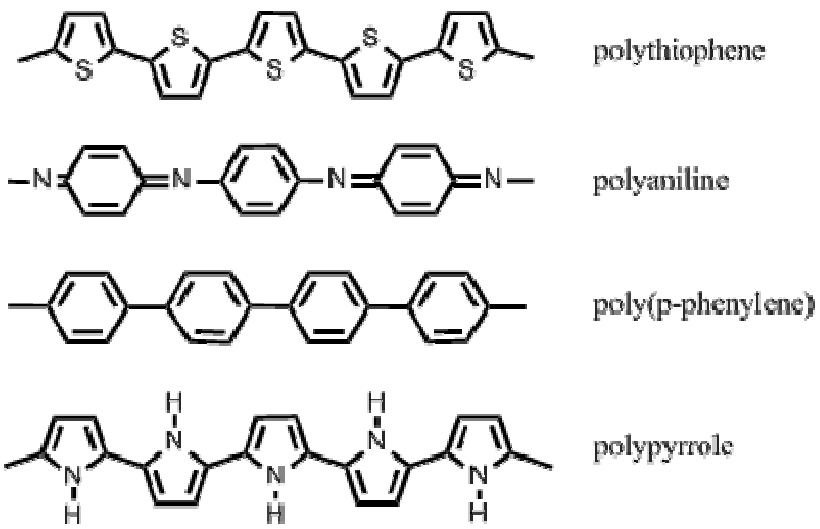


***Figure 2.3 Structures of conducting polymers, polythiophene, polyaniline, poly(p-phenylene) and polypyrrole.***



Of the intrinsically conducting polymers, polyaniline, polypyrrole and polythiophene have been greatly exploited for practical applications in many areas of human needs. The structural feature common to conducting polymers is their alternating single and double bond lattice structure which allows for the transfer of charge carriers upon excitation by the use of appropriate dopant. *Figure 2.3* shows the conjugated systems of polythiophene, polyaniline, poly(para-phenylene) and polypyrrole. Other electronic polymers are poly-acetylene, poly-(phenylenevinyl-ene), polyfuran, polyindole, polycarbazole and other poly-(heteroaromatic vinylenes). Doping materials can include iodine, bromine, lithium, sodium, mineral acids and surfactants[53-54].

The preparation techniques aim at getting a product with excellent conductivity and good environmental stability. The limitations posed by the processibility of these polymers limits their relative applications. Thus researchers aim at fashioning out preparation

procedures for synthesis of conjugated polymers that are soluble in either or both aqueous and organic solvents for a target use. The conducting polymer may be made by a variety of techniques including cationic, anionic, radical chain growth, co-ordination step growth polymerization or electrochemical polymerization. The electrochemical polymerization of conducting polymers is generally achieved by galvanostatic, potentiostatic or potential scanning voltammetry [53-56].

The conductivity and yield of the polymeric product are enhanced by doping, use of oxidizing or reducing agent or protonic acid to give a highly delocalized polycation or polyanion. New technologies such as *intrinsic* i.e. doped conducting polymer or *extrinsic* i.e. composite conducting polymer are now used to describe different conducting polymers. Literally, the intrinsically conducting polymers, ICPs, are essentially conjugated organic polymers which are either electrical insulators or semiconductors that the conductivity has been boosted by several orders of magnitude through doping to make the electronic polymers. The extrinsic conducting polymers are polymer composites made up of a non-conducting polymer that its matrix have been sintered or sputtered with particles of a metal or carbon black to make it conductive [53].



**2.5 Polyaniline as conducting polymer.**

Organic conducting polymers have attracted interest in recent years because they exhibit a wide range of novel electrochemical properties. Among the most studied is polyaniline (PANI), which has been studied extensively as an important conducting material that possesses interesting electrical, electrochemical and optical properties [55]. Some conducting polymers that have been investigated for chemical sensors are polypyrrole,

polyacetylene, polyaniline (PANI), polythiophene, etc. Among these conducting polymers, polypyrrole and polyaniline are widely investigated. Polypyrrole films are not easily processible whereas polyaniline is soluble in common organic solvents from which free standing films can be cast. PANI is also considered to be one of the most technologically promising conducting polymers because of its easy preparation, low cost, and relatively stable electrical conductivity in air [57]. The continuous growing interest in the study of PANI is caused by these diverse, unique properties, and its promising potential in commercial application. Polymer films can be deposited on electrode surfaces very readily. Polymerization of the monomer aniline can be achieved either chemically or electrochemically. Electrochemically, the polymer can be grown on the electrode surface pulse, galvanostatic, potentiostatic or potentiodynamic technique [55-56]. The latter being proffered because of the homogenous film produced and a strong adherence to the electrode surface [55], and achieved by scanning the electrode potential in the oxidative linear sweep mode or the cyclic voltammetric mode in a solution containing aniline [56].



The conductivity of PANI, which is of a metallic character, depends on the preparation procedure. The structure of PANI is also affected by conditions employed during film preparation, such as electrode potential, concentration of monomer, the pH of the electrolyte, and additives such as surfactants. The conductivity of PANI depends also on the degree of protonation of the different polymeric species that constitute the polymer [56-57]. PANI films produced in non-acidic media are usually non-conducting [56]. PANI can be converted rapidly between base and salt forms by treatment with acid or base. The reversible redox forms, pH-switching property, and the electrical conductivity

of PANI have been appreciated for developing a suitable electrochemical sensor. PANI loses electrochemical activity and electronic conductivity because of the deprotonation of the nitrogen sites of the oxidized form [58]. *Figure 2.4* presents the accessible oxidation states of PANI.

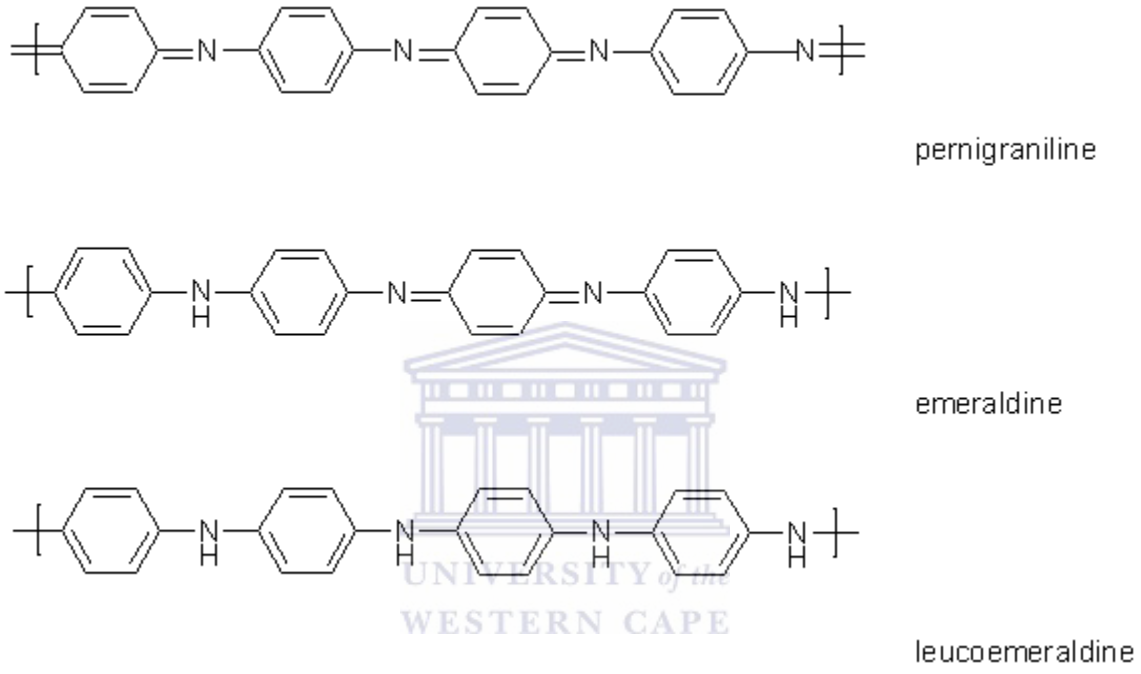




***Figure 2.4 Accessible oxidation stated of polyaninline***

Polymerized from the aniline monomer, polyaniline can be found in one of three idealized oxidation states [59]

- **leucoemeraldine** - white/clear
- **emeraldine** - green or blue
- **pernigraniline** - blue/violet

Polyaniline (PANI) is one of the most extensively studied conductive polymers and has attracted considerable attention over recent years due to its environmental compatibility

as well as its electrical properties for many technological applications [60]. Amongst the available intrinsically conducting polymers (ICPs), polyaniline (PANI) is found to be the most promising because of its ease of synthesis, low cost monomer, tenable properties, and better stability compared to other ICPs. ICPs are inherently conducting in nature due to the presence of a conjugated π electron system in their chemical structure. ICPs have a low energy optical transition, low ionization potential and a high electron affinity [61]. A high level of conductivity (near metallic) can be achieved in ICPs through oxidation-reduction as well as doping with a suitable dopant [62].

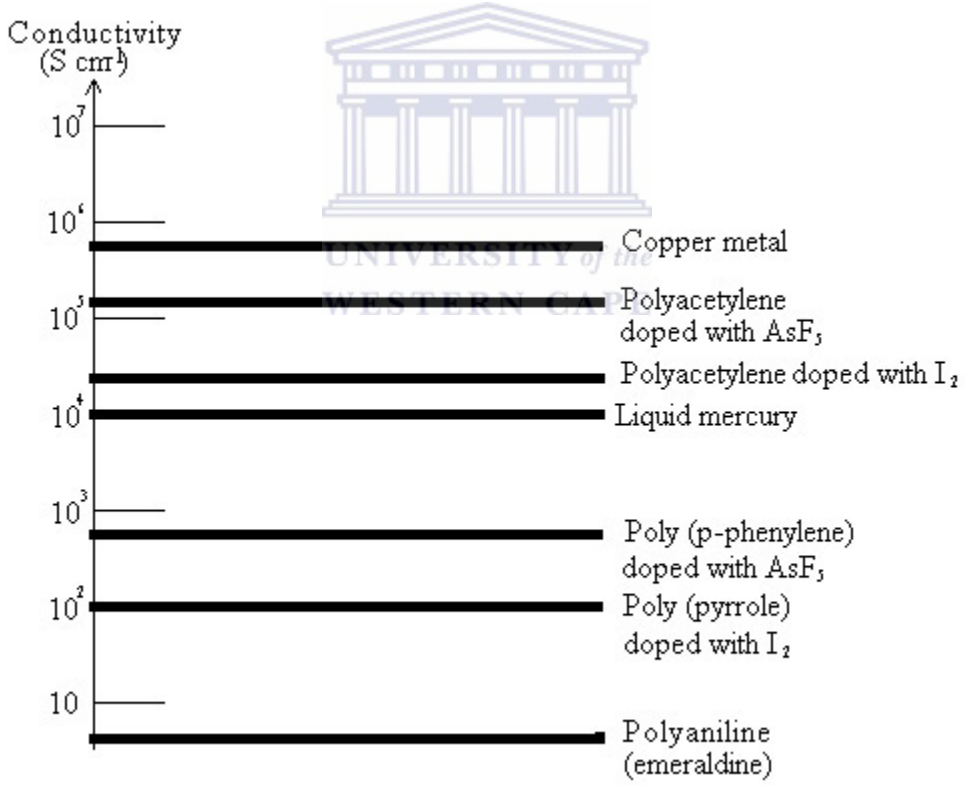

Logarithmic conductivity ladder locating some metals and conducting polymers

***Chart abducted from:* (*www.homepage.ntlworld.com/colin.pratt/applcp.htm*)**

## 2.6 The use of Carbon electrode

Pure carbon exists in two basic crystalline forms, the hard, rigid cubic structure of diamond and the softer anisotropic layered structure of graphite. Graphitic carbon has a wide range of applications and is arguably as important as diamond. There is also a large family of carbon materials derived from pitches and polymeric precursors or produced by various deposition techniques. These materials are often referred to as amorphous or glassy carbon. Glassy carbon is a hard material which typically fails suddenly when loaded in tension or compression [63]. Several forms of carbon have been used as cathodes with the most common of them being glassy carbon, glassy cloth, and graphite. Carbon electrodes are very convenient when large surface is essential. Graphite electrodes are very useful as anodes, electrodes of natural graphite, however, are not as resistant towards corrosion as platinum electrodes and thus have a limited lifetime. Graphite is available in many forms, one resembling cloth and another being glassy carbon. Glassy carbon (vitreous carbon) can be used in many cases when platinum was previously used [64].



## 2.7 Transition metal oxides

Metal oxides present an attractive alternative as electrode material because of high specific capacitance at low resistance making it easier to construct high energy, high power supercapacitors. Though, however, the most beneficial metal oxide known for providing high capacitance is $RuO_2$. Extensive research into ruthenium oxide has been conducted for military application as it is presumably that cost is less of an issue than it is for commercial ventures. However, academic institutions have focused on searching for

cheaper materials other than $RuO_2$ and the rarity of this particular metal oxide is also a factor which diverted researchers towards other metal oxides [44-45, 47]. Some of the metal oxides that have been studied for SC electrode materials are NiO, $Ni(OH)_2$, $MnO_2$, $Co_2O_3$, $IrO_2$, FeO, $TiO_2$, $SnO_2$, $V_2O_5$ and MoO but yet none of these oxides are used in commercial production of EDLCs as they are still in lab-scale research [45].

### 2.7.1 Titanium (IV) Oxide ($TiO_2$)

Among transition metal oxides, $TiO_2$ is non-toxic, inexpensive and available in abundance. It being an n-type semiconductor, the charges on the surface are more than the other regions due to the attractive contribution of the positively charged depletion region [45]. Titanium dioxide exists in three modifications with different crystal lattice structures and therefore alternating physical properties. These are rutile, anatase and brookite. Rutile is thermodynamically the most stabile form.



Titanium dioxide is a naturally occurring oxide of the element titanium. Also referred to as titanium (IV) oxide or titania, this substance also occurs naturally as three mineral compounds known as anatase, brookite, and rutile. However, it is most commonly extracted from titanium tetrachloride by carbon reduction and re-oxidization. Alternatively, it may be processed from another oxide called ilmenite, which is subjected to reduction with sulfuric acid to achieve pure titanium dioxide. There are a number of industrial applications for this mineral. For one thing, it has very high refraction properties. In fact, titanium dioxide is one of the whitest materials known to exist on Earth, which has earned it the nickname "titanium white." For this reason, it is often included in many cosmetic preparations to reflect light away from the skin. It is also a

major component of sun block to deter the absorption of ultraviolet (UV) rays from the sun, the concentration of which determines the product's Sun Protection Factor (SPF) [65-66].

Titanium itself is a relatively unnoble metal which, similar to aluminium, is only stable in the atmosphere because of an oxide passivation layer. It has a pronounced tendency to form oxides which are very stable. The far most preferred oxidation state is that of $Ti^{+4}$. Expectedly, titanium dioxide is chemically hardly reactive. Titanium dioxide is insoluble in water. Calcinated titania, especially in the rutile modification, is insoluble or only moderately soluble even in hot, concentrated acid. Small amounts of oxygen are easily withdrawn from titanium dioxide. In that case $Ti^{+3}$ is generated, that leads to a grayish color of titania due to the fact that $Ti^{+3}$ within the $TiO_2$ lattice is dark blue, almost black. This reduction on the surface is, however, reversible. Even the oxygen in the air suffices to recover $Ti^{+4}$, which is not colored [66]. Titanium oxide possesses specific dielectric constant in the range of 16-100 compared to common typical dielectric materials [67].



### 2.7.2 Tin (IV) Oxide ($SnO_2$)

Tin is a fairly corrosion-resistant metal, widely used in many applications in industry. Investigations of its electrochemical behavior (passivation, corrosion) are therefore of considerable interest, since the corrosion resistance of tin in humid atmospheres and in aqueous solutions is attributed to the presence of a passive oxide/ hydroxide film on the metal surface. Since electrochemical processes at metallic electrodes are often affected by the presence of a surface oxide film, knowledge of the semiconducting properties of such films is necessary in order to understand their influence in film growth, charge transfer,

*etc*. These films are most frequently non-stoichiometric oxides and of amorphous or polycrystalline structure. The principles of the band theory of solids have been quite successfully extended to this type of materials and it is known that the presence of a semiconducting oxide film determines the charge distribution and the potential drop at the metal-metal oxide-electrolyte interface, *i.e.*, the character of the double layer. since $SnO_2$ is one of the most studied metal oxides due to its wide applications ranging from electrochemistry to optics, solar cells or gas sensor. There are several contributions concerning the study of tin in different electrolytic media. In alkaline solutions, the anodic passivation of tin is a complex, multi step process that is due to the presence of an oxide layer on the metal surface. Both the composition and the thickness of the passive film change continuously with potential and pH [68].

$SnO_2$ displays n-type semiconducting properties, and the presence of oxidizing and reducing agents is known to have dramatic effects on the electronic properties of the material surface [69]. As has been commented above, Tin oxide is an n-type semiconductor due to the existence of the native donor levels. These levels have energies of 0.03-0.034 eV and 0.14- 0.15 eV below the conduction band edge, and are generally attributed to single and double ionization of oxygen vacancies, as unrelaxed vacancies are above, i.e., within the conduction band. The position of the Fermi level is fixed and would be between the conduction band edge and the intrinsic Fermi level position (that is very close to the mid of the band gap), because $SnO_2$ presents a negligible concentration of electronic band-gap states at their geometrically ideal surfaces [70].

## 2.8 Use of Nanotechnology and significance to the Environment and Energy aspects

Nanotechnology is the popular term for the construction and utilization of functional structures with at least one characteristic dimension measured in nanometers. Such materials and systems can be rationally designed to exhibit novel and significantly improved physical, chemical, electrical and biological properties, phenomena, and processes because of their size. When characteristic structural features are intermediate in extent between isolated atoms and bulk materials, in the range of about (1 to 100 nm), the objects often display physical attributes substantially different from those displayed by either atoms or bulk materials. Properties of matter at the nanoscale are not necessarily predictable from those observed at larger scales. Important changes in behavior are caused not only by continuous modification of characteristics with diminishing size, but also by the emergence of totally new phenomena such as quantum size confinement, wave-like transport, and predominance of interfacial phenomena. Once it is possible to control feature size and shape, it is also possible to enhance material properties and device functions beyond what are already established.



Nanotechnology has the potential to significantly impact energy efficiency, storage, and production. It can be used to monitor and remediate environmental problems; curb emissions from a wide range of sources; and develop new, “green” processing technologies that minimize the generation of undesirable by-product effluents. The impact on industrial control, manufacturing, and processing will be impressive and result in energy savings. Several technologies that utilize the power of nanostructuring, but that were developed without benefit of the new nanoscale analytical capabilities, illustrate this

potential [71]:

## 2.9 Electrode processes

The term electrode processes includes all phenomena which, as a result of applying a voltage to an electrode, lead to a current flow through that electrode. The course of an electrode process is greatly influenced by the nature of the phase boundary of the working electrode and its associated electrical double layer. The importance of this region cannot be over-emphasized since the potential applied to the cell exists only across the double layers of the working and reference electrodes when there is no current flow through the cell; there being no potential drop across the cell solution under zero current conditions. In cells with supporting electrolytes the double layers are only a few nanometers thick yet all the electrochemical reactions occur there. Most voltammetric and polarographic analysis utilize electrode processes in which electrons or ions are exchanged between the two phases. As a result of this analyte will be either oxidized or reduced depending on the potential of the working electrode. Such an electrode process is referred to as a charge transfer reaction and produces a flow of charge, which is a current, through the electrode. This is summarized in equation 2.1:



$$Ox + ne^- \leftrightarrow Red \qquad \textit{(eqn. 2.1)}$$

Where *Ox* and *Red* represent the analyte in its oxidized and reduced forms respectively, and *n* is the number of electrons, $e^-$, which reacted with each molecule unit of the analyte.

A current flow that results from the oxidation or reduction of a substance is known as a Faradaic current, $i_F$, and its magnitude depends on the concentration profile of that

substance in the region of the electrode surface. This profile depends on the concentration of the substance in the cell solution and on the kinetics of all steps in the associated electrode process. If the profile is controlled by the diffusion of the analyte to the electrode, the faradaic current is known as a diffusion current, if controlled by the kinetics of a step in the electrode process, as a kinetic current, and if controlled by a catalytic process, as a catalytic current.

As a result of the electrode process, the concentration of an analyte at the electrode surface drops until it reaches an equilibrium value determined by the potential of the working electrode and the *standard electrode potential,* $E^{o}_{ox/red}$, of the charge transfer reaction (equation 2.1). Once equilibrium is reached it might be expected that the current would fall to zero. But this is not observed. It is found that the charge transfer reaction can be maintained even in a stationary solution. Hence the decrease in concentration of the analyte at the electrode surface due to the electrode reaction must be countered by supplementation of the analyte from the bulk solution in the cell. In addition, any soluble electrode reaction products must be moving out into the bulk solution. This movement of material to and from the electrode surface may be achieved by a number of mechanisms.

The analyte in the test (cell) solution may be transported to the electrode surface by *convection*. This is facilitated by movement of the solution relative to the electrode, for example by stirring or by the action of the mercury dropping from the capillary of the dropping mercury electrode (DME).

The most important process for transporting molecules through the thin layer of solution (10-100μm) immediately in contact with the electrode surface is *diffusion*. This is the case for both the transport of analyte to the electrode surface and the transport of the

electrode reaction products away from the electrode surface into the bulk solution. Nernst called this important region adjacent to the electrode surface the *diffusion layer* [72].

Another mechanism by which ionic analytes may be transported in a cell arises when there is a current flow through the cell. The positive ions move towards the working electrode when it is negatively charged and the negative ions move in the opposite direction. This process is known as *migration* and leads to the *migration current,* $i_m$. All ions present in the cell solution contribute to the migration current in proportion to their charge, concentration and mobility. Because the concentration of the supporting electrolyte is usually more than one thousand times that of the analyte, the contribution of the analyte itself to the migration current can be neglected. In effect, in addition to the reducing the cell resistance, the supporting electrolyte caries the current through the cell solution although it is not involved in the current-determining electrode process at the working electrode.



**2.10 Capacitive currents**

The very simple representation of the electrode-electrolyte solution interface presented in Figure 2.5 omitted any detail of the electrode double layer as this was not essential for an understanding of the diffusion process.

When a potential is applied to an electrode from an external source, the charge that flows to the electrode resides on its surface. Because of electrostatic attraction, ions of opposite charge in the electrolyte solution will be attracted to the immediate vicinity of the electrode to form the electrochemical double layer.

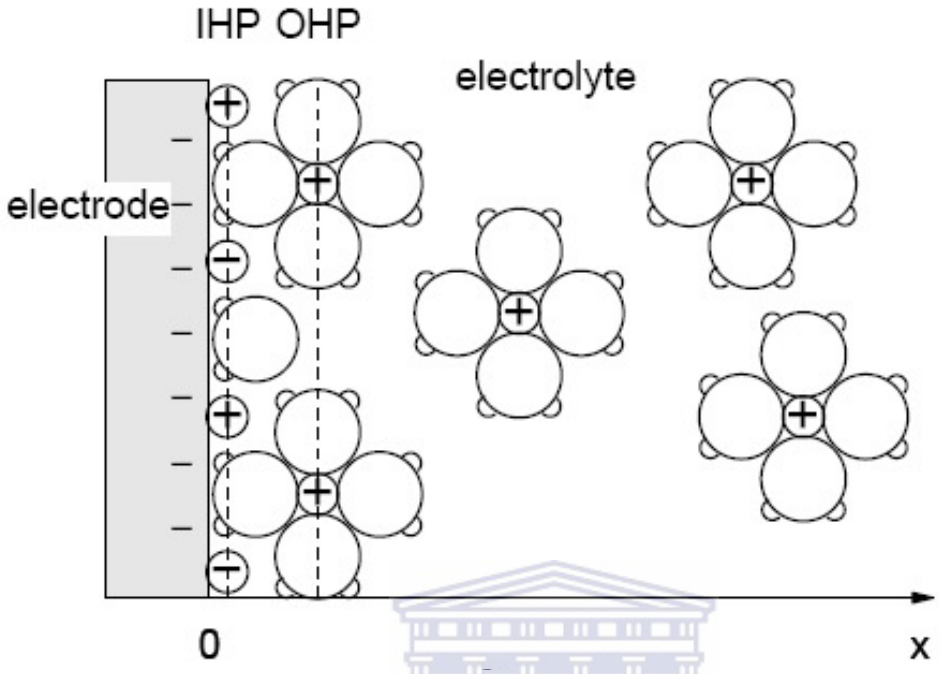


***Figure 2.5: Schematic diagram of electrode-electrolyte interface***



According to figure 2.5, there is a layer of solvent molecules in contact with the electrode surface and these molecules have their dipoles orientated by the electric field. The plane in which the centres of these adsorbed solvent molecules lie is referred to as the *Inner Helmholtz Plane,* IHP. There is then a layer of solvated ions of opposite charge to that of the electrode (metal). These ions lie in a plane referred to as the *Outer Helmholtz Plane,* OHP, and the region between this plane and the electrode surface is referred to as the *compact layer.*

The potential difference between the electrode and the solution occurs across the very narrow diffusion layer region near the interface. This charged interfacial region is equivalent to a parallel plate capacitor, one plate being the electrode surface and the other being the charge in the compact and diffuse region of the double layer. Like a capacitor,

the double layer at the interface has the ability to store charge and is characterized by a capacitance, *the double layer capacitance,* $C_{dl}$.

The capacitance of a parallel plate capacitor is proportional to the area of the plates and the dielectric constant of the material between them and inversely proportional to the distance between the plates but is dependent of the voltage. The structure of the double layer is not constant but varies with the nature and concentration of the electrolyte solution and with the potential of the electrodes.

The value of the double layer capacitance of an electrode is normally expressed as the double layer capacitance, $C_{dl}$, per unit area. It is related to the electrode potential and the charge on the electrode by the general formula for capacitor, namely:

$$C_{dl} = C_{dl}^{*} / A \quad = Q / (\Delta E A) \qquad \textit{(eqn. 2.2a)}$$

This, because Cdl varies with voltage is usually expressed in the differential form:

$$C_{dl} = \{dQ / d(\Delta E)\}/A \qquad \textit{(eqn. 2.2b)}$$



Where, $C_{dl}$ is the double layer capacitance per unit area in F $m^{-2}$, Q is the charge on the electrode in coulombs, $\Delta E$ is the potential applied to the cell in volts, relative to $E_m$, the potential of the electrocapillary maximum at which the charge on the electrode is zero, and A is the area of the electrode in $m^{-2}$ [72].

## 2.11 Characterization Techniques

### 2.11.1 Cyclic Voltammetry

Cyclic voltammetry is the most widely used technique for acquiring qualitative information about electrochemical reactions. The power of cyclic voltammetry results from its ability to rapidly provide considerable information on the thermodynamics of

redox processes and the kinetics of heterogeneous electron transfer reactions and on coupled chemical reactions or adsorption processes. Cyclic voltammetry is often the first experiment performed in an electroanalytic study. In particular, it offers a rapid location of redox potentials of the electroactive species, and convenient evaluation of the effect of media on the redox process.

Cyclic voltammetry consists of scanning linearly the potential of a stationary working electrode (in an unstirred solution), using a triangular potential waveform (figure 2.6). Depending on the information sought, single or multiple cycles can be used. During the potential sweep, the potentiostat measures the current resulting from the applied potential. The resulting current-potential plot is termed a *cyclic voltammogram.* The cyclic voltammogram is a complicated, time-dependent function of a large number of physical and chemical parameters.

Figure 2.7, illustrates the expected response of a reversible redox couple during a single potential cycle. It is assumed that only the oxidized form O is present initially. Thus, a negative-going potential scan is chosen for the first half-cycle, starting from a value where no reduction occurs.

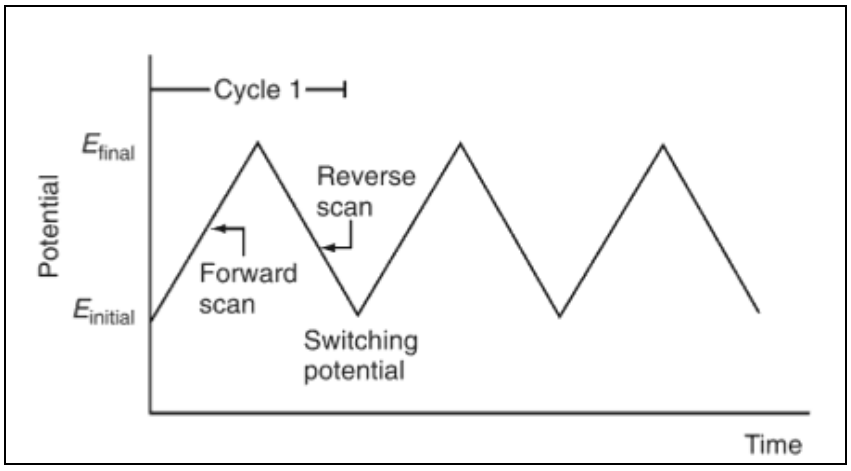


***Figure 2.6: A Potential against Time type of voltammetry***

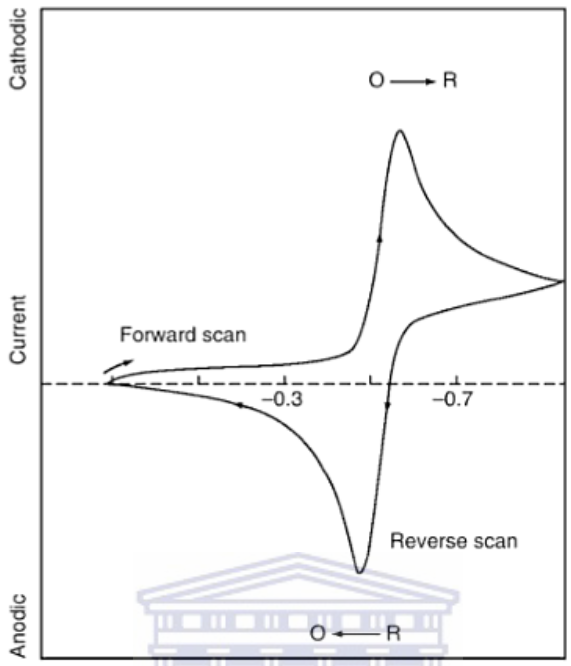


***Figure 2.7: Typical cyclic voltammogram for a reversible O + ne⁻ ↔ R redox process.***



As the applied potential approaches the characteristic $E^o$ for the redox process, a cathodic current begins to increase, until a peak is reached. After traversing the potential region in which the reduction process takes place, the direction of the potential sweep is reversed. During the reverse scan, R molecules (generated in the forward half-cycle, and accumulated near the surface) are reoxidized back to O, resulting in an anodic peak. The characteristic peaks in the cycle voltammogram are caused by the formation of the diffusion layer near the electrode surface. These can be best understood by carefully examining the concentration-distance profiles during the potential sweep [73].

### 2.11.1.2 Data interpretation

The cyclic voltammogram is characterized by several important parameters. Four of these observables, the two peak currents and two peak potentials, provide the basis for the diagnostics developed by Nicholson and Shain for analyzing the cyclic voltammetric response [73-74].

#### *2.11.1.2.1 Reversible systems*

The peak current for a reversible couple (at 25°C) is given the Randles-Sevcik equation:

$$i_p = (2.69 \times 10^5) n^{3/2} A C D^{1/2} v^{1/2} \qquad \textit{(eqn. 2.3)}$$

Where $n$ is the number of electrons, $A$ the electrode area (in $cm^2$), $C$ the concentration (in $mol/cm^3$). $D$ is the diffusion coefficient (in $cm^2/s$), and $v$ the potential scan rate (in V/s). Accordingly, the current is directly proportional to concentration and increases with the square root of the scan rate. Such dependence on the scan rate is indicative of electrode reaction controlled by mass transport. The reverse-to-forward peak current ratio, $i_{p,r}/i_{p,f}$, is unity for a simple reversible couple. This peak ratio can be strongly affected by chemical reactions coupled to the redox process. The current peaks are commonly measured by extrapolating the preceding baseline current.



The position of the peaks on the potential axis ($E_p$) is related to the formal potential of the redox process. The formal potential for a reversible couple is centred between $E_{pa}$ and $E_{pc}$.

$$E^o = (E_{pa} + E_{pc})/2 \qquad \textit{(eqn. 2.4)}$$

The separation between the peaks potentials (for a reversible couple) is given by

$$\Delta E_p = E_{pa} - E_{pc} = 0.059V/n \qquad \textit{(eqn. 2.5)}$$

Thus, the peak separation can be used to determine the number of electrons transferred, and as a criterion for a Nernstian behaviour. Accordingly, a fast one-electron process exhibits a $\Delta E_p$ of about 59 mV [73].

**2.11.1.3 The effects of absorption, capacitance and the electrode double layer.**

Solvent splitting and electrolytic side reactions are an extremely common contribution to non faradaic current ($I_{non\text{-}faradaic}$). In solution, all electrodes are surrounded by a layer of water molecules, ions, and other atomic or molecular species [75]. The two Helmholtz layers are often said to comprise the electrode double-layer or electric double-layer. The extent to which ions, etc. adsorb an electrostatic attraction with the surface of an electrode is determined by the material from which the electrode is made (the substrate). At equilibrium, the rate of adsorption is the same as the rate of desorption, thus ensuring that the fraction of the electrode surface covered with adsorbed material is constant. The double-layer is important because faradaic charge, the useful component of the overall charge, represent the passage of electrons through the double-layer to effect redox changes to the material in solution [75-76].



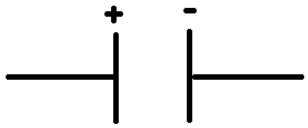


***Scheme 2.1: A representation of a typical capacitor in a circuit diagram***

Scheme 2.1 above represents a typical representation of a typical capacitor. In elementary physics, a capacitor is usually depicted as comprising two layers which are separated by a distance and bear different amounts of charge as seen in practice by the formation of a

difference in potential between the two plates. The electric double-layer around the electrode will similarly behave as a capacitor since the inner layer is different from the outer layer in terms of number of ions adsorbed, and hence the total number of charge it comprises [75].

#### 2.11.1.4 Linear-Sweep and Cyclic Voltammetry

The principal difference polarography and voltammetry is the nature of the working electrode (WE). In polarography, a dropping-mercury electrode (DME) is used as the working electrode, while the working electrode employed during voltammetry is usually solid.

Like polarography, voltammetry is a microanalysis technique, so only a small proportion of the solution is ever modified by the processes occurring at the electrode. The potential of the working electrode is ramped at a scan rate of $v$. The resultant trace of current against potential is termed a voltammogram. In linear-sweep voltammetry (LSV), the potential of the working electrode is ramped from an initial potential $E_i$ to a final potential $E_f$. Figure 2.8 below shows a linear-sweep voltammogram for the reduction of a solution-phase analyte, depicted as a function of scan rate.

During cyclic voltammetry, the potential is similarly ramped from an initial potential $E_i$ but, at the end of the linear sweep, the direction of the potential scan is reversed, usually stopping at the initial potential or it may commence an additional cycle. The potential at which the reverse occurs is known as the switch potential ($E_\lambda$). Almost universally, the scan rate between $E_i$ and $E_\lambda$ is the same as that between $E_\lambda$ and $E_i$. Values of the scan rate $v_{forward}$ and $v_{backward}$ are always written as positive numbers.

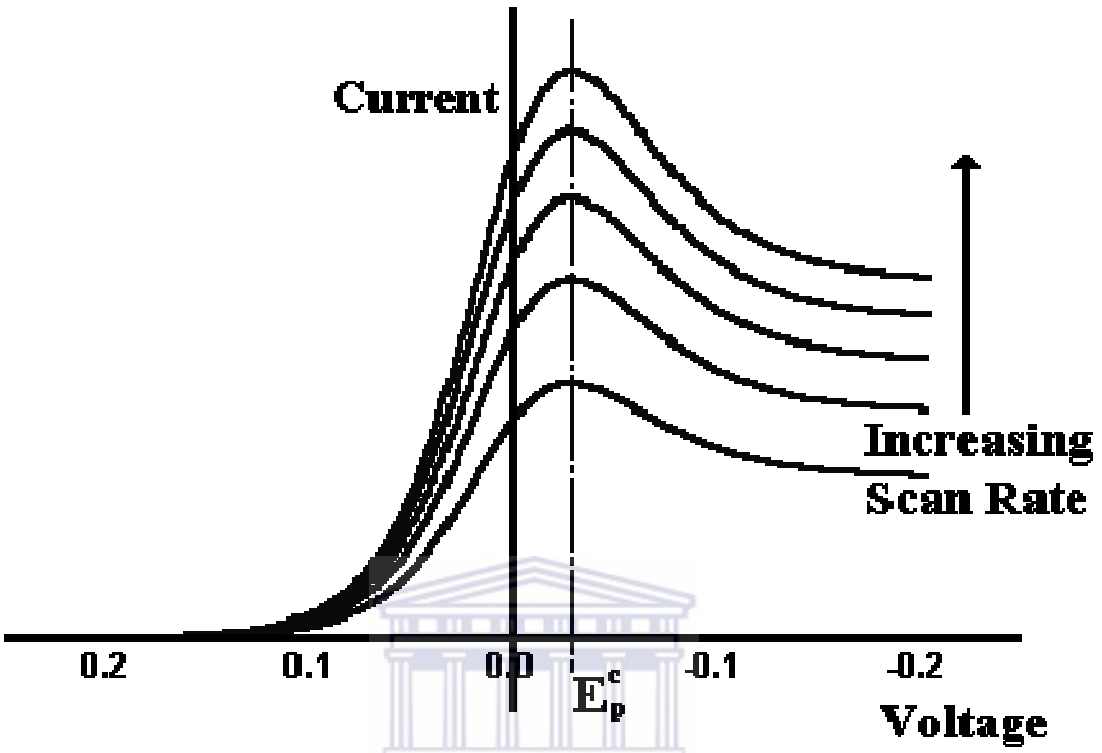


***Figure 2.8: linear-Sweep voltammogram***



***Abducted from:*** *http://www.cartage.org.lb/en/themes/sciences/Chemistry*

Figure 2.9 below, shows a voltammogram for a simple solution-phase couple, such a plot is known as a Cyclic Voltammogram (CV).the adjective *cyclic* arises from the closed loop drawn within the plot. The shape of the CV shown in figure 2.9 is typical for a couple that is wholly reversible in thermodynamic sense, other simple diagnostic tests for electro-reversibility are listed in Table 2.3.

***Table 2.3: Diagnostic tests for the electrochemical reversibility of redox couple carried out by using cyclic voltammetry.***

| | |
|---|---|
| 1 | $I_{pc} = I_{pa}$ |
| 2 | $E_{pc}$ and $E_{pa}$ are independent of the scan rate |
| 3 | $E^{o'}$ is positioned midway between $E_{pc}$ and $E_{pa}$, so that $E^{o'} = (E_{pa} + E_{pc})/2$ |
| 4 | $I_p$ is proportional to $v^{1/2}$ |
| 5 | The separation between $E_{pc}$ and $E_{pa}$ is 59 mV/$n$ for an $n$-electrode couple |

There is seen to be a peak formed in both the forward and reverse sides of the CV. These peaks are of similar shape and, if fully reversible, their magnitudes will be identical. Oxidation has occurred during the forward part of the CV, with reduction taking place during the reverse part. If the scan was going negative from $E_i$, then reduction would occur during the forward part of the scan, and oxidation during the reverse.

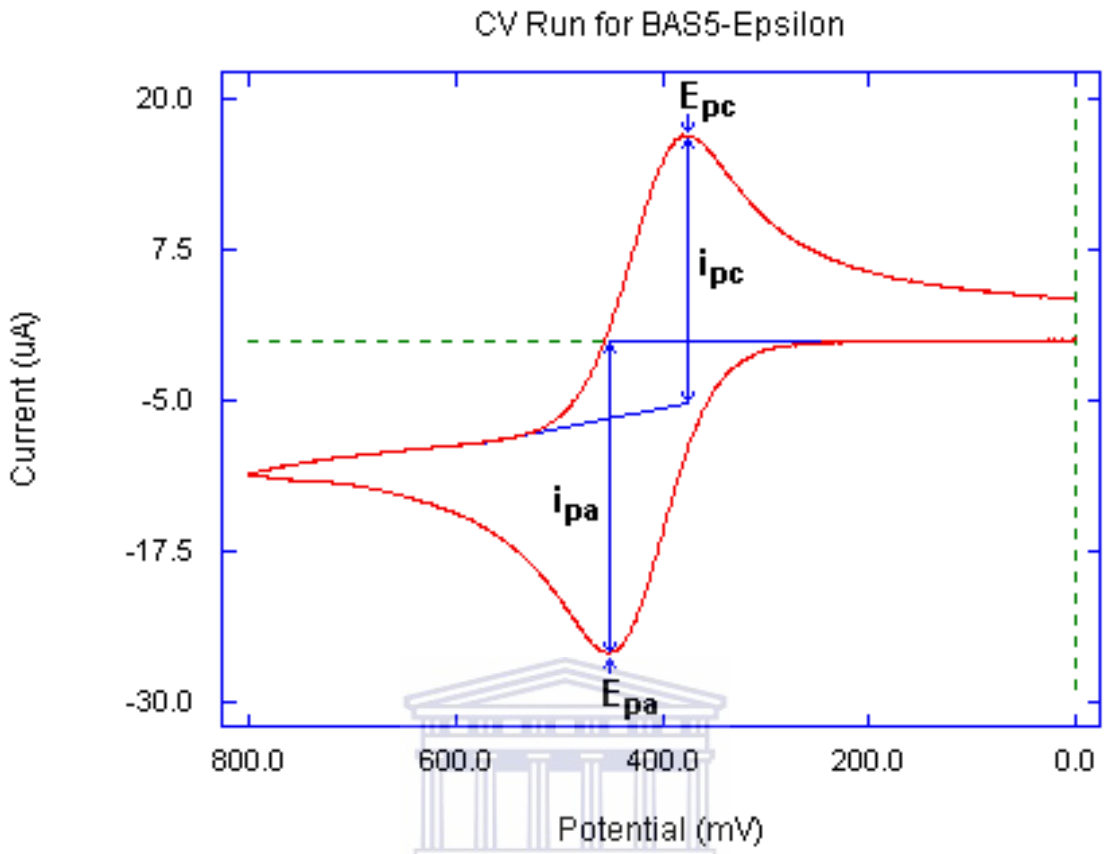




***Figure 2.9: A typical cyclic voltammogram***

***Abducted from:*** *http://www.basinc.com/mans/EC_epsilon/Techniques/CycVolt/cv.html*

As with other forms of voltammetry, the magnitude of the current is proportional to the concentration, so the equality between the $I_{p(forward)}$ and $I_{p(backward)}$ implies a qualitative retrieval of electromodified material. At the completion of the CV, when the potential has returned to $E_i$, there is still a slight current, indicating that a small amount of material has still not been reduced. This slight residual current would dissipate to zero if we were to force the potential of the electrode to more negative potentials beyond $E_i$.

### 2.11.1.5 Double-Layer Capacitance

When the potential applied to an electrode immersed in an electrolyte solution is decreased from zero, the surface charge becomes negative and the net space charge of the double-layer must increase to maintain overall electrical neutrality. Similarly, an increase in electrode potential must induce a net negative space charge. From the point of view of the external electric circuit, the double layer thus behaves as a capacitor, serving to store electric charge. Capacitance is defined as the ratio of charge stored to voltage applied [76].

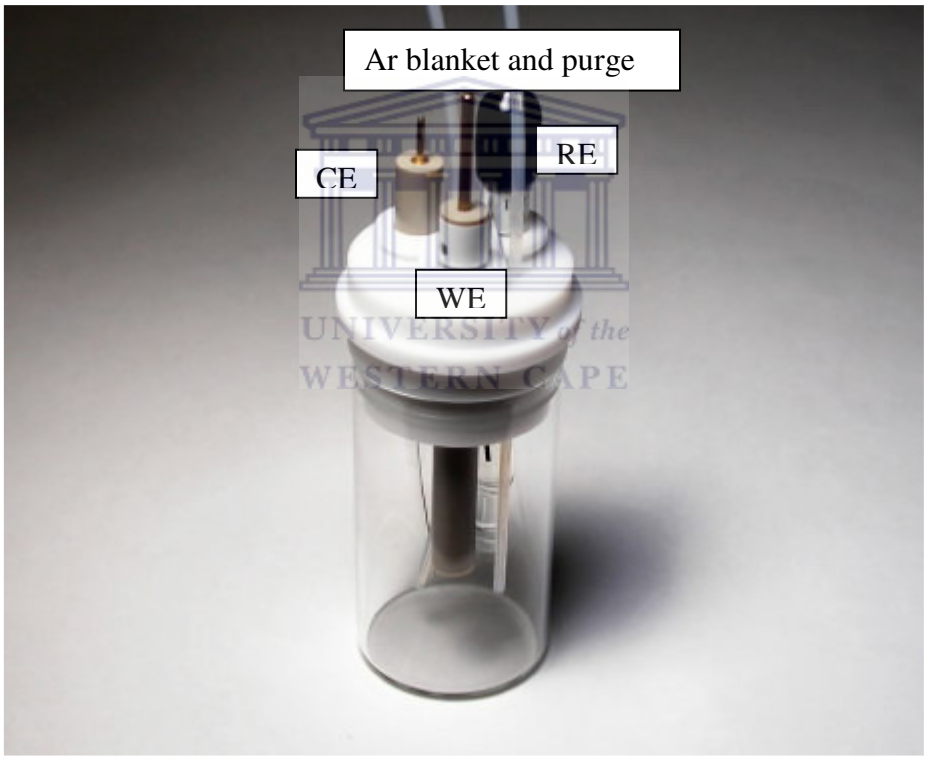


***Figure 2.10: Three electrode cell***

***Image abducted from: http://www.bio-logic.info/potentiostat/glassware_cells.html***

#### 2.11.1.6 Cell Electrodes

An electrochemical cell or device must consist of at least two electrodes and one electrolyte. In a less formal sense, we use electrode to indicate the electronic conductor and electrolyte to indicate the ionic conductor in an electrochemical cell. The first electrode of the three electrode compartment cell shown in figure 2.10 as WE is the working electrode also known as the test electrode. This is the electrode at which the electrochemical phenomena being investigated are taking place. Its function is to serve as a location for electrochemical measurements. It may or may not be constructed of inert material [77].

The second functional electrode is the reference electrode (RE), which is also known as the unpolarized electrode or unpolarizable electrode. This is the electrode whose potential is constant enough that it can be taken as the reference standard against which the potential of the other electrodes in the cell can be measured. It should not be, and normally is not, constructed of inert material [77].



The third functional electrode is the counter electrode, which is also known as the auxiliary electrode. This is the electrode that serves as a source or a sink for electrons so that current can be passed through the cell. In general, neither its current nor potential is measured or known. It is usually constructed of inert material [77].

### 2.11.2 Electrochemical impedance spectroscopy

#### 2.11.2.1 Introduction

The basic experiment of electrochemical impedance spectroscopy (EIS) consists in applying a small, sinusoidal voltage or current signal to an electrochemical cell,

measuring the system's response (current or voltage, respectively) with respect to amplitude and phase (or, equivalently, real and imaginary part), determining the impedance of the system by complex division of ac voltage by ac current, and repeating this for a certain range of different frequencies. This frequency-domain analysis requires that the system under investigation [78]:

- is linear or at least can be linearized with respect to signal amplitudes in its working point and
- is stationary or at least quasistationary for the time of measurement. Interpretation of the results and proper modelling requires
- that the experimental setup allows some idealization like separating between working electrode and reference electrode or maintaining the concentrations of reactants essentially constant at the interface.



The trend away from corrosive aqueous solutions and towards solid state technology was inevitable in electrochemical energy engineering, if only for convenience and safety in bulk handling. As a consequence, the characterization of systems with solid-solid or solid-liquid interfaces, often involving solid ionic conductors and frequently operating well above room temperature, has become a major concern of electrochemists and material scientists.

At an interface, physical properties-crystallographic, mechanical, compositional, and particularly, electrical-change precipitously and heterogeneous charge distributions (polarizations) reduce the overall electrical conductivity of a system. Each interface will polarize in its unique way when the system is subject to an applied potential difference.

The rate at which a polarized region will change when the applied voltage is reversed is characteristic of the type of interface, slow for chemical reactions at the triple phase contacts between atmosphere, electrode and electrolyte, appreciably faster across grain boundaries in the polycrystalline electrolyte. The electrical response of a heterogeneous cell can vary substantially depending on the species of charge present. Electrochemical impedance (EI) is a powerful method of characterizing many of the electrical properties of materials and their interfaces with electronically conducting electrodes. It may be used to investigate the dynamics of bound or mobile charge in the bulk or interfacial regions of any kind of solid or liquid material, ionic, semi-conducting, mixed electronic-ionic, and even insulators (dielectrics) [79].



Electrochemical methods based on alternating currents can be used to obtain insights into corrosion mechanisms and to establish the effectiveness of corrosion control methods, such as inhibition and coatings. In an alternating-current circuit, impedance determines the amplitude of current for a given voltage. Impedance is the proportionality factor of between voltage and current. In electrochemical impedance spectroscopy (EIS), the response of an electrode to alternating potential signal of varying frequency is interpreted on the basis of circuit models of the electrode/electrolyte interface. Figure 2.11 shows two circuit models that can be used for analyzing EIS spectra.

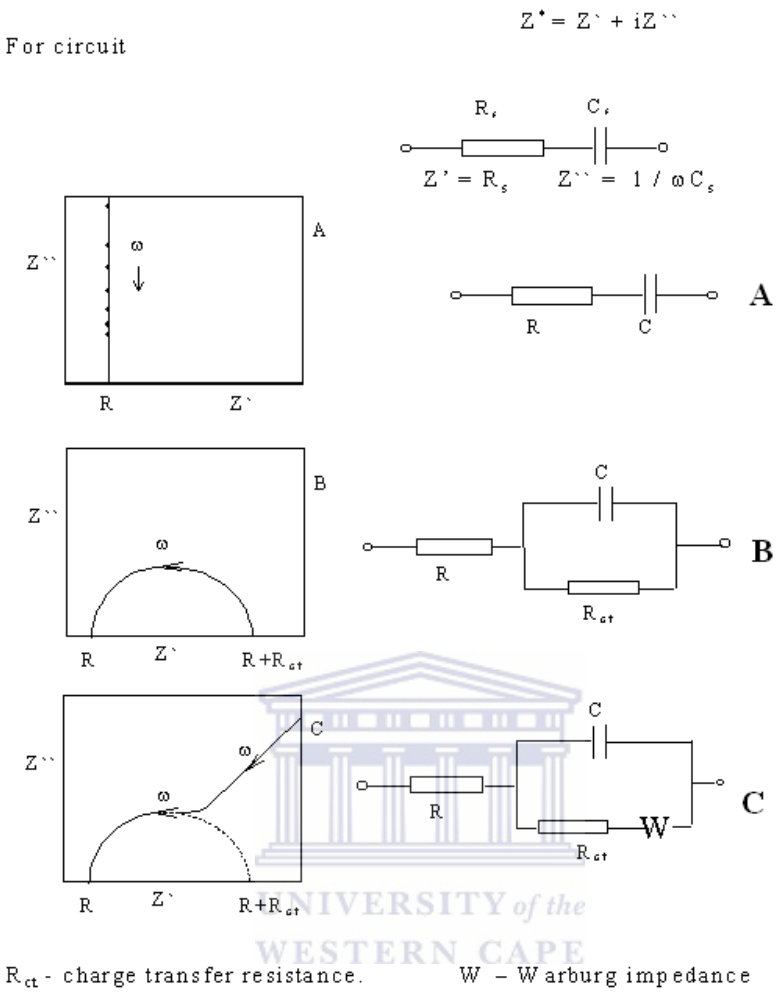


***Figure 2.11: Electrical equivalent circuit model used to represent an electrochemical interface undergoing corrosion in the absence of diffusion control and Electrical equivalence circuit model when diffusion control applies; W is the Warburg impedance.***

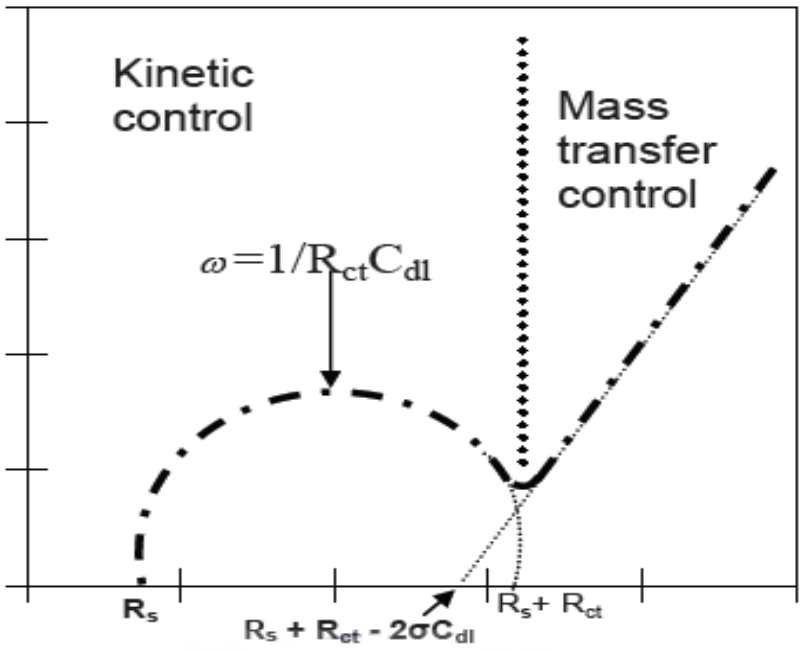


***Figure 2.12: A Nyquist plot showing kinetic and mass transfer control regions depicted when an analyte is analyzed***.



The simplest model for characterizing the metal-solution interface, Figure 2.11(B), includes the three essential parameters, $R_s$ (the solution resistance), $C_{dl}$ (the double layer capacitance), and $R_{ct}$ (the charge transfer resistance). When direct-current measurements are carried out (i.e., frequency is zero), the impedance of the capacitor approaches infinity. In parallel electrical circuits, the circuit with the smallest impedance dominates, with the result that, under these conditions, the sum of $R_s$ and $R_{ct}$ is measured. If $R_s$ is significant, the corrosion rate is underestimated [80-81].

When diffusion control is important, another element, $Z_D$ or W, sometimes called the Warburg impedance, is added in series with $R_{ct}$, as shown in Figure 2.11(C). Figure 2.12 however, displays a Nyquist plot (also referred to as Cole-Cole plot) showing the regions of kinetics and diffusion (or mass transfer control) when a Warburg element is involved.

In electrochemical impedance spectroscopy, the impedance of the corroding metal is analyzed as a function of frequency. A sinusoidal potential change is applied to the corroding electrode at a number of frequencies, ω. At each frequency, the resulting sinusoidal current waveform is out of phase with the applied potential signal by an amount, the phase angle, θ, that depends on the circuit parameters. The current amplitude is inversely proportional to the impedance of the interface. The electrochemical impedance, Z(ω), is the frequency-dependent proportionality factor in the relationship between the voltage signal and the current response,

$$Z(\omega) = \frac{E(\omega)}{i(\omega)}\sqrt{-1} \qquad (2.6)$$

Where E is the voltage signal, $E = E_0 \sin(\omega t)$; $i$ is the current density, $i = i_o \sin(\omega t + \theta)$; Z is the impedance (ohms-$cm^2$); and $t$ is the time in seconds [79, 82].

Impedance is a complex number that is described by the frequency-dependant modulus, |Z|, and the phase angle, θ, or alternatively, by the real component, Z', and the imaginary component, Z''. The mathematical convention for separating the real and imaginary components is to multiply the magnitude of the imaginary component by $j$ [$=\sqrt{-1}$] and report the real and imaginary values as a complex number [82].



**2.11.2.2 Equivalent Circuits and Representation of Electrochemical capacitance Behavior.**

***Table 2.4: Demonstration of electrochemical Impedance plots with corresponding equivalent circuits.***

| Equivalent circuit | Corresponding Nyquist plot |
|---|---|
| 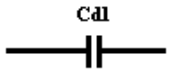 Ideally polarizable interfacial capacitance | 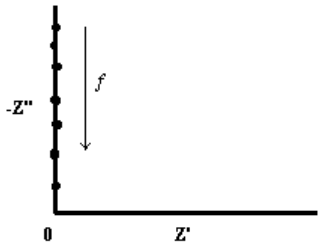 |
| 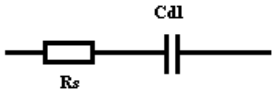 Interfacial capacitance with ohmic series resistance, Rs, e.g solution or circuit resistance. | 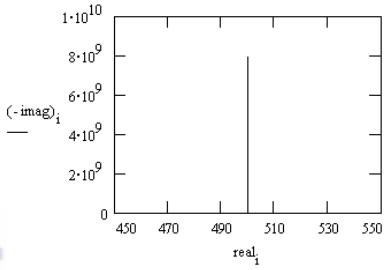 |
| 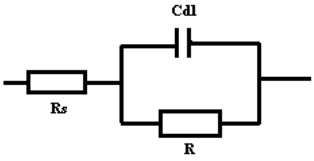 Interfacial capacitance with Rs and parallel ohmic leakage resistance R. | 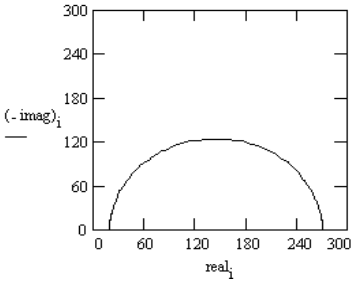 |
| 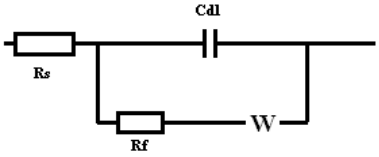 Interfacial capacitance with Rs, and parallel Faradaic leakage resistance, Rf, with coupled diffusional impedance, W, (Randles circuit). | 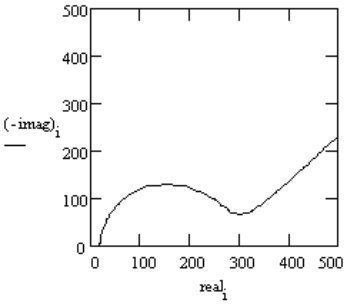 |

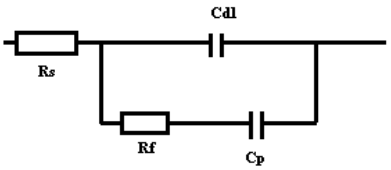


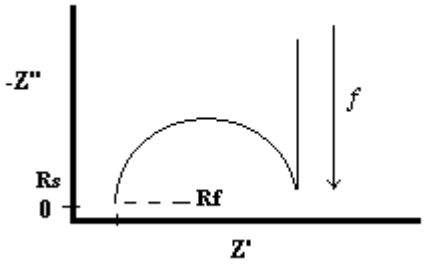


Interfacial capacitance with Rs and Faradaic pseudocapacitance, Cp, charge via faradaic resistance, $R_F$.

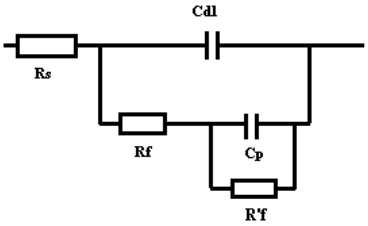


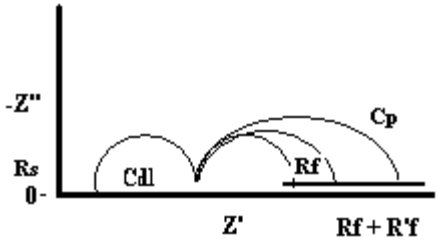


Interfacial capacitance with Rs and Faradaic pseudocapacitance Cp charged via a faradaic resistance, Rf, with Cp leaked by a desorption faradaic resistance, $R'_F$.



The representation of impedance spectra of electrochemical systems in terms of the ac response behavior of equivalent circuits has become a common practice in the field. A physically reasonable circuit is chosen and values of its *C*, *R* and *L* components are selected to give the best fit to the observed frequency spectral response over a wide range of frequencies. It should be noted, however, that a particular, selected circuit model may not uniquely represent the impedance behavior of the system; nevertheless, the circuit modeling approach is widely used, aided by special computer programs.

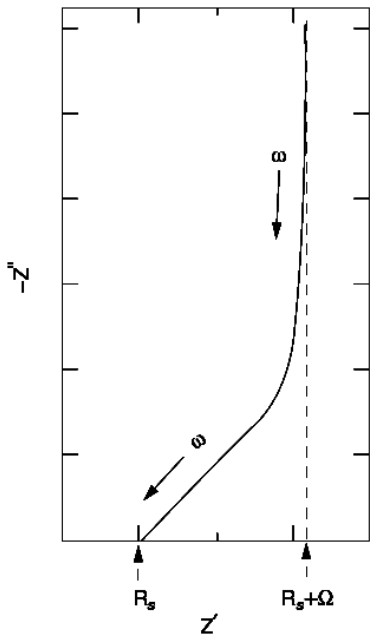


***Figure 2.13: Characteristic form of a complex-plane impedance plot for a porous capacitor electrode with series resistance Rs (intercept at $\omega \rightarrow \infty$ ) and cumulative distribution resistance, $\Omega$.***



The impedance spectra of porous carbon supercapacitor electrodes have a characteristic inflected form as shown typically in Figure 2.13. Three regions can be distinguished in this type of complex-plane plot. At relatively high frequencies, a linear relation between $-Z''$ and $Z'$, initially arises having a near 45° slope (for $-Z''$ plotted with the same scale sensitivity as that of $Z'$) which is characteristic (at such frequencies) of transmission-line behavior, in contrast to a Warburg 45° phase-angle plot which arises only at low frequencies when a diffusion-controlled process is determining the impedance spectrum. Note that the high-frequency 45° line extrapolates (first region) with respect to $-Z'' \rightarrow 0$, to an intercept on the $Z'$ axis that gives the resistance, *Rs* (ESR) in series with the

capacitor device. In well-conducting solutions, ESR values for double-layer supercapacitor electrodes can be as low as fractions of milliohms in well-designed devices. Progressing to lower frequencies (second region) in Figure 2.13, a knee or smooth inflection arises, going into an (ideal) vertical, third region of the complex plane plot in which almost pure capacitive behavior is manifested ($-Z''$ simply increasing according to $1/jwC$). Extrapolating the vertical section of the plot in Figure 2.13 to zero – $Z''$ gives another intercept on the $Z'$ axis equal to $Rs + \Omega$, where $\Omega$ represents an effective internal resistance of the distributed $RC$ network of the porous electrode. $\Omega$ is often appreciably larger than the ESR, $Rs$, and determines, with $Rs$, the time response and power-spectrum of the distributed $RC$ network and thus practical aspects of device performance. $\Omega$ can have values up to tens of m$\Omega$ depending on the type of porous electrode material and the electrolyte used in the device [83].



### 2.11.3 Electron Microscopes

#### 2.11.3.1 Introduction

Just as "light microscope" is a generic term covering a range of instruments for producing magnified images using glass lenses and visible or ultra violet light, so the name 'electron microscope' does not refer to a specific design of instrument but to a family of instruments which produce magnified images by the use of electrostatic or electromagnetic lenses with fast-moving electrons as illumination. They all share the ability to give images of high or very high resolution over a very useful depth of field. Within the electron microscope family there are two well-defined ranges of microscope, corresponding to transmission and reflection (metallurgical) light microscopes, which

look directly at the internal structure of translucent specimens and the outside features of bulk material, respectively.

The transmission electron microscope (TEM) is a direct derivative of the compound light microscope, making use of the shorter wavelength electron illumination. In its simplest form, its magnification is achieved by exactly the same lens arrangement as in its light counterpart. It has also been developed further to make the fuller use of the special properties of electron illumination; principally the higher resolution, but also the ability to carry out various forms of elemental and crystallographic microanalysis.

The electronic equivalent of the metallurgical or reflected light microscope, used to study the outside of specimens rather than their internal arrangement, is the Scanning Electron Microscope (SEM). This finds applications throughout the magnification range between a hand lens and the TEM. This instrument differs from traditional microscopes in forming its image sequentially. Its most advanced forms owe much to developments in electron sources and short-focus electron lenses. Whereas the TEM has developed by going up in voltage, the SEM has done the reverse in order to approach true surface imaging [84].

### 2.11.3.1.1 Transmission Electron Microscope

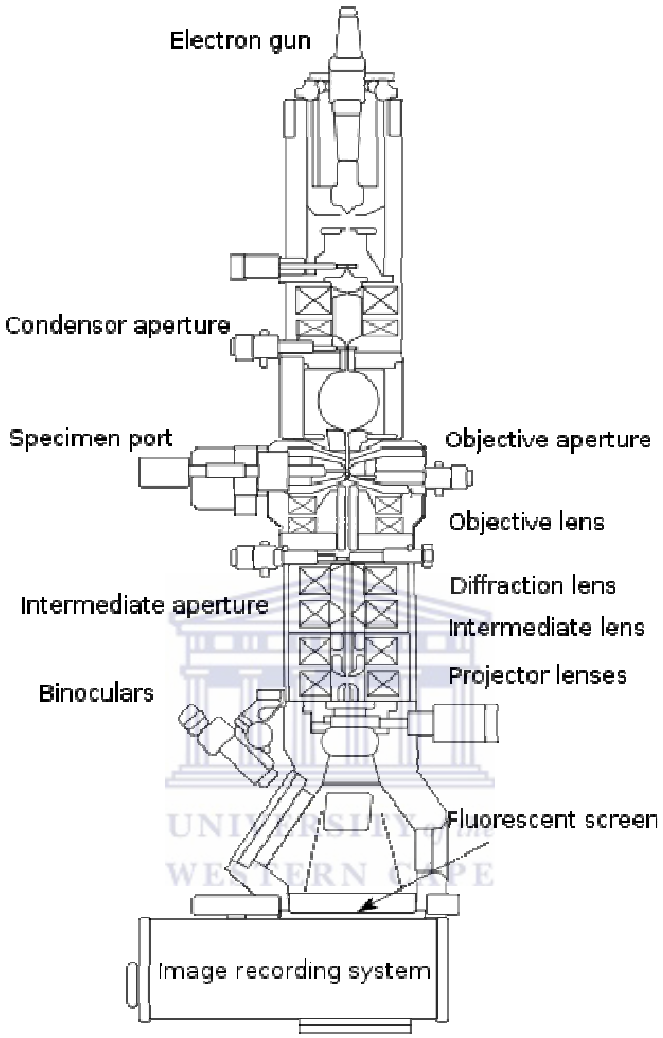


***Scheme 2.2: Schematic diagram of Transmission Electron microscope (TEM). Image a**bducted from:* *http://en.wikipedia.org/wiki/Transmission_electron_microscopy*

The transmission electron microscope (TEM) operates on the same basic principles as the light microscope but uses electrons instead of light. What you can see with a light microscope is limited by the wavelength of light. TEMs use electrons as “light source” and their much lower wavelength make it possible to get a resolution a thousand times better than with a light microscope.

Materials scientists have traditionally examined metals, alloys, ceramics, glasses, polymers, semiconductors and composite mixtures of these materials with sporadic adventures into wood, textiles and concrete. In addition to thinning them from the bulk state, particles and fibers of some of these materials are also commonly studied and, in such shapes, they are sometimes thin enough for direct TEM examination. Nanotechnology is defined as the ability to understand and control matter at dimensions of roughly 1 to 100 nanometers, where unique phenomena enable novel applications. Encompassing nanoscale science, engineering and technology, nanotechnology involves imaging, measuring, modeling and manipulating matter at this fore mentioned length scale.

When nanoscale materials are created, they come with specific dimensional limits in 1D, 2D or 3D and the TEM is well suited to observing them precisely because of these limits. Nanotubes, nanowires, quantum dots, nanoparticles, and most catalysts particles can be viewed as 1D structures and they can be put into a TEM without further modification, since 1D is always thin enough for direct observation [85].



#### 2.11.3.1.2 Working principle of TEM

In a conventional transmission electron microscope (CTEM or TEM for short), a thin specimen is irradiated with electron beam of uniform current density; the electron energy is in the range of 60-150 keV (usually 100 keV) or 200 keV-3 MeV in the case of the high-voltage electron microscope (HVEM). Electrons are emitted in the electron gun by thermionic emission from tungsten hairpin cathodes or $LaB_6$ rods or field emission from pointed tungsten filaments. The latter are used when high gun brightness is needed. A

two-stage condenser-lens system permits variation of the illumination aperture and the area of the specimen illuminated. The electron intensity distribution behind the specimen is imaged with a three or four-stage lens system, onto a fluorescent screen. The image can be recorded by direct exposure of a photographic emulsion inside the vacuum. The lens aberrations of the objective lens are so great that it is necessary to work with very small objective apertures, of the order of 10-25 mrad, to achieve resolution of the order of 0.2-0.5 nm. Bright-field contrast is produced either by absorption of the electrons scattered through angles larger than the objective aperture (scattering contrast) or by interference between the scattered wave and the incident wave at the image point (phase contrast). The phase of the electron waves behind the specimen is modified by the wave aberration of the objective lens. This aberration and the energy spread of the electron gun, which is of the order of 1-2 eV, limits the contrast transfer of high spatial frequencies.

Electrons interact strongly with the atoms by elastic and inelastic scattering. The specimen must therefore be very thin, typically of the order of 5 nm-0.5 μm for 100 keV electrons, depending on the density and elemental composition of the object and the resolution desire. Thicker specimens can be investigated in a high-voltage electron microscopy. TEM can provide high resolution because elastic scattering is an interaction process that is highly localized to the region occupied by the screened Coulomb potential of an atomic nucleus, whereas inelastic scattering is more diffuse, spreads out over about a nanometer. TEMs are used not only in the high-resolution mode, in which the contrast is caused by elastic and inelastic scattering, but also in microanalysis modes, which information is collected from the emitted x-rays and the energy losses of inelastically scattered electrons from cathodoluminescence and electron-beam-induced currents. For

every application, knowledge of the dependence of the electron-specimen interactions on specimen and imaging parameters is essential. The most efficient modes of operation of the instrument can then be selected and the letter can be tuned to give the best possible performance [86].

### 2.11.4 Chrono-potentiometry

In this technique a constant current is passed between the working and auxiliary/counter electrodes in a suitable cell containing a still solution of a base electrolyte and the electroactive species, the potential of the working electrode versus a reference electrode is recorded as a function of time [87].

Instruments containing both a potentiostat and a galvanostat, and hence can perform both controlled potential (potentiostatic) and controlled current (galvanostatic) experiments. Although potentiostatic experiments are much more common, there are some applications for which a galvanostat is advantageous.



The galvanostat uses a three electrode configuration, in which a current is applied between the auxiliary and working electrodes, and the potential of the working electrode (measured with respect to the reference electrode) is monitored. The basis of controlled current experiments is that a redox (electron transfer) reaction must occur at the surface of the working electrode in order to support the applied current. For example, if ferricyanide is present in the solution, then a reducing current will lead to the reduction of ferricyanide to ferrocyanide at the working electrode. Common applications of the galvanostat include constant current stripping potentiometry and constant current electrolysis, including applications where a constant rate of electrolysis in important,

such as electrodeposition and battery studies. One advantage of all constant current techniques is that the ohmic drop due to solution resistance is also constant, as it is equal to the product of the current and the solution resistance. The ohmic distortion can therefore be simply corrected by a constant potential offset. In contrast, in potentiostatic experiments (e.g., cyclic voltammetry), the current, and hence the ohmic drop, varies with potential, and correction is more complicated [88].

### 2.11.5 Chrono-amperometry/Chrono-coulometry

Chronoamperometry (**CA**) and chronocoulometry (**CC**) have the same potential wave form - the potential step - which is one of the simplest potential wave forms. In **CA**, the current is monitored as a function of time, whereas in **CC**, the charge is monitored as a function of time. It is important to note that the basic potential step experiment on an instrument is **CA**; that is, *during* the experiment, the *current* is recorded as a function of time. However, *after* the experiment, the data can also be displayed as *charge* as a function of time (the charge is calculated by integrating the current). Hence, chronocoulometry data can be obtained [88].



### 2.11.6 Fourier Transform Infrared (FTIR) Spectroscopy

Fourier Transform Infrared (FTIR) Spectroscopy bases its functionality on the principle that almost all molecules absorb infrared light. Only the monatomic (He, Ne, Ar, etc) and homopolar diatomic ($H_2$, $N_2$, $O_2$, etc) molecules do not absorb infrared light. Molecules only absorb infrared light at those frequencies where the infrared light affects the dipolar moment of the molecule. In a molecule, the differences of charges in the electronic fields

of its atoms produce the dipolar moment of the molecule. Molecules with a dipolar moment allow infrared photons to interact with the molecule causing excitation to higher vibrational states. The homopolar diatomic molecules do not have a dipolar moment since the electronic fields of its atoms are equal. Monatomic molecules do not have a dipolar moment since they only have one atom. Therefore, only homopolar diatomic molecules and monatomic do not absorb infrared light [89].

FTIR analysis is technique that provides information about the chemical bonding or molecular structure of materials, whether organic or inorganic. It is used in analysis to identify unknown materials present in a chemical sample. The technique works on the fact that bonds and groups of bonds vibrate at characteristic frequencies. A molecule that is exposed to infrared rays absorbs infrared energy at frequencies which are characteristic to that molecule. During FTIR analysis, a spot on the specimen is subjected to a modulated infrared (IR) beam. The specimen's transmittance and reflectance of the infrared rays at different frequencies is translated into an IR absorption plot consisting of reverse peaks. The resulting FTIR spectral pattern is then analyzed and matched with known signatures of identified materials in the FTIR spectrum. Unlike SEM inspection or Energy Dispersive X-ray (EDX) analysis, FTIR spectroscopy does not require a vacuum, since neither oxygen nor nitrogen absorbs infrared rays. FTIR analysis can be applied to minute quantities of materials, whether solid, liquid , or gaseous [90].



### 2.12 Distinction of Pseudocapacitance and double layer capacitance

Many charge-storage mechanisms have been proposed for electrochemical capacitors; most notably double-layer capacitance and charge-transfer-reaction pseudocapacitance.

The large specific capacitance of supercapacitors is the results of one or a combination of above charge-storage mechanisms [91-92]. Double-layer capacitance arises from the separation of charge at the interface between a solid electrode and an electrolyte [93-94] whereas pseudocapacitance arises from fast, reversible faradaic reactions occurring at or near a solid electrode surface over an appropriate range of potential [95]. Utilization of the capacitance of the double-layer at electrode interfaces for electrical energy storage is the basis of so-called 'double-layer capacitors' or supercapacitors developed first, in principle, by *H.E. Backer (General Electric), US Patent No. 2 800 616 (1957)* and later by *J.C. Currie (Sohio), US Patent No. 4 730 239 (1988)* using high-area carbon powder materials and tetraalkylammonium salt electrolytes. Charge storage in double-layer capacitance is largely electrostatic in nature (separation of ion and electron charges) and, for this reason, charging/discharging is highly reversible and hundreds of thousands of cycles are typically attainable with a given element of charge being able to be admitted or withdrawn at virtually the same potential [96].



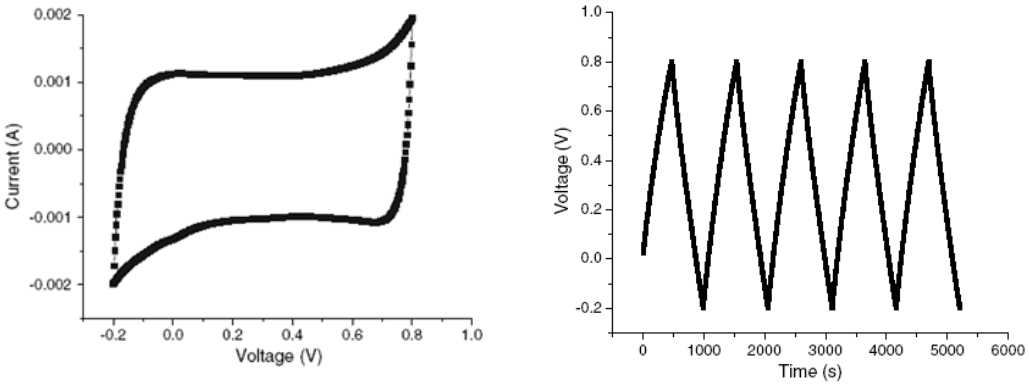


***Figure 2.14: Typical "rectangular shape" cyclic voltammogram along side with "ΛΛΛ" shaped galvanostatic charge-discharge curve of a double layer capacitance.***

Figure 2.14 above shows typical cyclic voltammogram of a double layer capacitor with a distinctive rectangular shaped CV. The rectangular cyclic voltammogram is usually due to the electrode-electrolyte interface at the electrode surface where there is no faradaic electron transfer reaction taking place [97-99]. The double layer is purely electrostatic in nature. This particular type of voltammogram is usually accompanied by a galvanostatic charge-discharge curve of straight or linear charge and discharge counterparts as evidence of no redox reaction taking place at the electrode surface [98]. However, figure 2.15 below shows a typical CV of an electrochemical capacitor with distinctive redox peaks as there are faradaic electron transfer reactions taking place at the electrode surface. This is noted by having a peak or a series of redox peaks at certain potentials which become more pronounced as the scanning rate is increased.

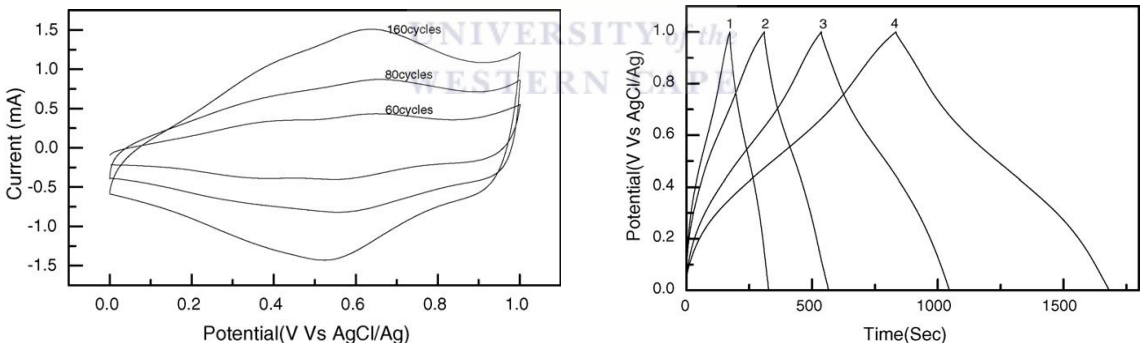


***Figure 2.15: Typical redox/electroactive cyclic voltammogram of electrode materials with non-linear galvanostatic charge-discharge curve exhibiting pseudo-capacitance.***

This cyclic voltammogram is also corresponding to its typical galvanostatic charge-discharge curve. The charging and discharging counterparts however, are neither

symmetrical nor linear. This is evidence of electron transfer redox reactions taking place at electrode surface.

# CHAPTER 3

# RESEARCH DESIGN AND METHODOLOGY

## 3.1 Experimental

### 3.1.1 The experimental design

The flow chart shown below is a sequential design of the experimental procedure performed during this study. For standardization of the glassy carbon electrode after each experiment, electrochemical measurements were taken in order to ascertain the cleanliness of the electrode and also to model its behavior in the presence of the control electrolyte. Electropolymerization process was conducted in acidic media (1M HCl) with a ratio of 2:1 mols of Aniline and poly-4-styrene sulfonic acid respectively.



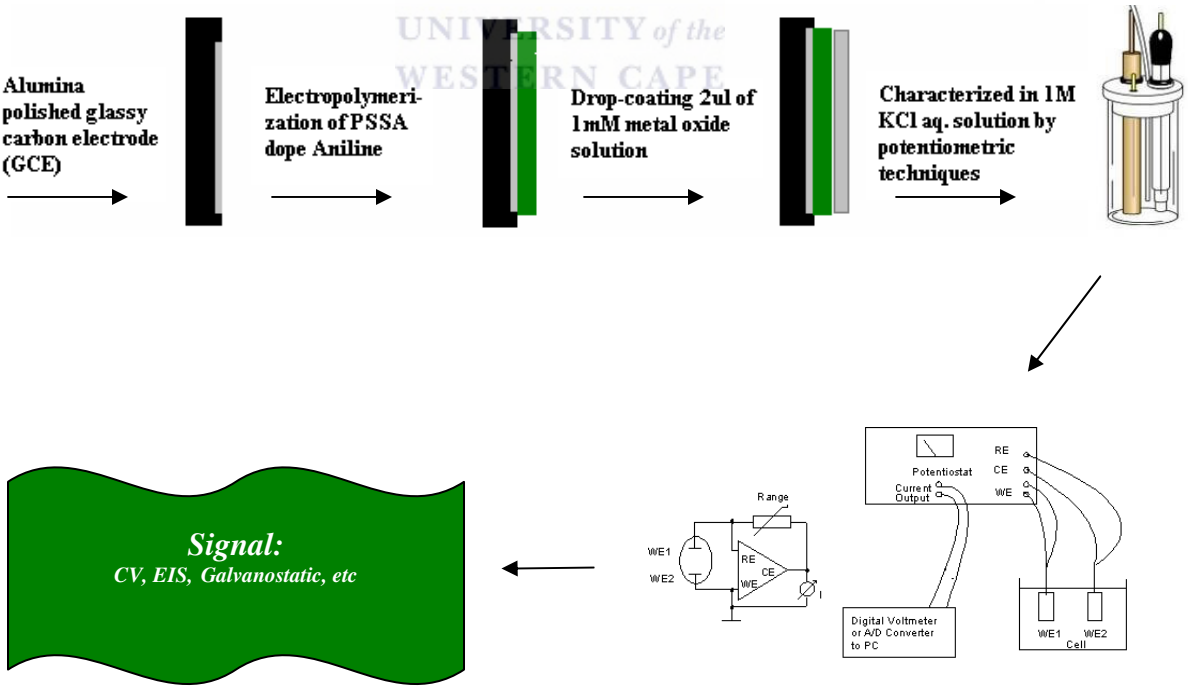


*Scheme 3.1: Flow chart of experimental design*

### 3.2. Chemicals

All inorganic materials were commercial materials of analytical grade and purity and were used without further purification. Aniline was doubly distilled before use and all materials were purchased from Sigma Aldrich (South Africa). Poly-4-styrene sulfonic acid and nanopowders of $SnO_2$ and $TiO_2$ were also used as received (Sigma Aldrich). Water used was purified with a reverse osmosis – ion exchange purification system (Millipore, Billerica, USA). Ultra high purity Argon gas was supplied by Afrox, South Africa.

### 3.3 Preparation of Solutions

Solutions were prepared using general analytical procedures and formula such as equations 3.1, 3.2 and 3.3 for preparation and dilution of solutions.



$$mass = \frac{Molar\,mass \times Molarity \times Volume}{1000} \qquad (eqn.\ 3.1)$$

$$Molarity = \frac{Density \times \%Purity \times 1000}{MW} \qquad (eqn.\ 3.2)$$

$$C_1V_1 = C_2V_2 \qquad (eqn.3.3)$$

Details of other calculations necessary will be found in the experimental and result sections.

### 3.4. Apparatus

All electrochemical experiments were carried out using a three-electrode electrochemical cell connected to the BAS100W (Bioanalytical Systems, Lafayette, USA) or the VoltaLab PGZ402 (Radiometer Analytical SAS, Lyon, France) electrochemical workstations. A glassy carbon working electrode (GCE) (3 mm diameter, BASi), a platinum wire counter electrode (99.9%, Sigma-Aldrich), and a Ag/AgCl (3 M NaCl) reference electrode (BASi) were employed. Cyclic voltammogram (CV), electrochemical impedance spectroscopy (EIS), chrono-amperometry and chrono-potentiometry were recorded with computers interfaced with these machines. TEM images were obtained with Technai $G^2$ F20X-TWIN MAT 200 kV Field emission high resolution transmission electron microscope. Attenuated Total Reflectance Fourier Transform Infrared (ATR-FTIR) spectra were recorded in the range of 4000-300 $cm^{-1}$ using a PerkinElmer Model spectrum 100 series.



### 3.5. Distillation of aniline

Distillation is a widely used method for separating mixtures based on differences in the conditions required to change the phase of components of the mixture. To separate a mixture of liquids, the liquid can be heated to force components, which have different boiling points, into the gas phase. The gas is then condensed back into liquid form and collected. Repeating the process on the collected liquid to improve the purity of the product is called double distillation. Although the term is most commonly applied to liquids, the reverse process can be used to separate gases by liquefying components using changes in temperature and/or pressure.

Distillation is used to purify a compound by separating it from a non-volatile or less-volatile material. When different compounds in a mixture have different boiling points, they separate into individual components when the mixture is carefully distilled. Aniline must be distilled on the day of use, the first and last 10% being discarded. Aniline is a highly toxic material, particularly when its vapor is inhaled, and the apparatus described in this report was devised to ensure minimum danger as well as maximum convenience in distilling this reagent [100]. The collection of the distilled product (aniline) was collected in an air-tight contained immersed in an ice bath and stored in a freezer.

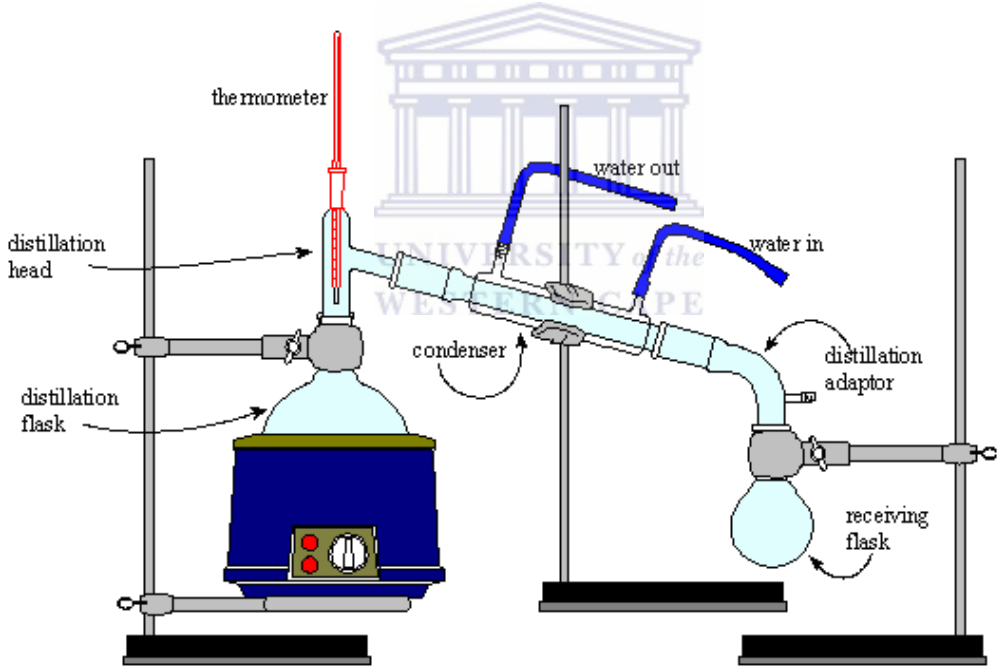


***Figure 3.1: Distillation apparatus for distillation of aniline.***

***Image abducted from*** *http://www.pharmainfo.net/reviews/fractional-distillation-binary-solvent-mixture*

The apparatus illustrated is used as a complete assembly and is taken apart only for periodic cleanings. The above Figure 3.1 shows the assembly of a distillation apparatus. The resultant product, which in this case was distilled aniline, was purged with argon gas and stored below freezing point in an eppendorf tube.

## 3.6. Casting of PANI/metal oxide composite films for characterization as super-capacitor materials

Before each experiment, the glassy carbon electrode (GCE) was thoroughly polished with 1.0, 0.3, and 0.05 μm slurries of alumina successively, and it was rinsed with de-ionized water after each polishing step. This was followed by a final cleaning in water in an ultrasonic bath for 5 to 10 minutes [101]. Modification of the GCE surface with films of PANI, $SnO_2$ and composite of both is described below. Electrochemical characterization experiments on the results films were carried out in aqueous KCl solution (1 M).



Respective electrolyte solutions (10 mL) were first degassed by bubbling Argon gas for 5 minutes and then a constant argon blanket was kept over the cell during all the electrochemical measurements and preparations.

### *3.6.1 Electropolymerization of aniline in the presence of PSSA*

PSSA-doped Polyaniline (PSSA-PANI) was deposited according to literature [102] by potentiodynamic electropolymerization at the surface of a bare glassy carbon electrode from a solution of aniline (50 mM) and PSSA (25 mM) in 1 M HCl while the potential was cycled from 0.2 V to 1.1 V[102] at 50 mV $s^{-1}$ for 5 cycles.

### *3.6.2 Electrode modification with $SnO_2$ and $SnO_2$/PANI-PSSA composite*

An aqueous dispersion of the metal oxide was prepared in glass vials with water (18.4 MΩ) and their concentrations were 10 mM with respect to the respective metal ion. $SnO_2$ films were cast by drop-coating the above aqueous dispersion of the oxide on the bare GCE or over the PANI/PSSA-modified GCE. $SnO_2$, PANI/PSSA, and $SnO_2$/PANI/PSSA films were let to dry in open air and first rinsed with water in order to remove loosely adsorbed particles before electrochemical measurements were carried out on them. The $SnO_2$ dispersion was always drop-coated layer-by-layer in droplets of 2 µL, letting a layer to dry before the drop-coating for the next layer was applied.

### *3.6.3 Electrode modification with $TiO_2$ and $TiO_2$/PANI-PSSA composite*



An aqueous dispersion of the Titanium dioxide was prepared in glass vials with water (18.4 MΩcm) and their concentrations were 1 mM with respect to the respective metal ion. $TiO_2$ films were cast by drop-coating the 1mM aqueous dispersion of the oxide on the bare GCE or over the PANI/PSSA-modified GCE. $TiO_2$, PANI/PSSA, and $TiO_2$/PANI/PSSA films were let to dry in open air and first rinsed with water in order to remove loosely adsorbed particles before electrochemical measurements were carried out. The $TiO_2$ dispersion was always drop-coated layer-by-layer in droplets of 2 µL. The samples were prepared by dispersing the nanopowders of $TiO_2$ and $SnO_2$ in acetone and placed drop-wise on cupper grid for TEM microscopic analysis.

# CHAPTER 4

# RESULTS PRESENTATION AND DISCUSSION

## 4.1 Transmission electron microscopic studies of the metal oxides

An electron microscope visualizes the structural information carried by scattered electrons. In a fixed-beam transmission electron microscope, scattered electrons emerging from the irradiated sample are collected over a narrow solid angle and focused by the objective lens onto the image plane [103]. Figure 4.1 shows transmission electron microscope (TEM) images of nano-$TiO_2$ transition metal oxide with the later image being a magnification of a less agglomerated part of the former image for a distinctive viewing of the particle size. The wideness of the $TiO_2$ metal oxide particle is estimated at ~10 nm. The shapes of the particles however, are flake-shaped and highly agglomerated. The TEM images were brought about to confirm the nano-structure of the metal oxide studied [104].

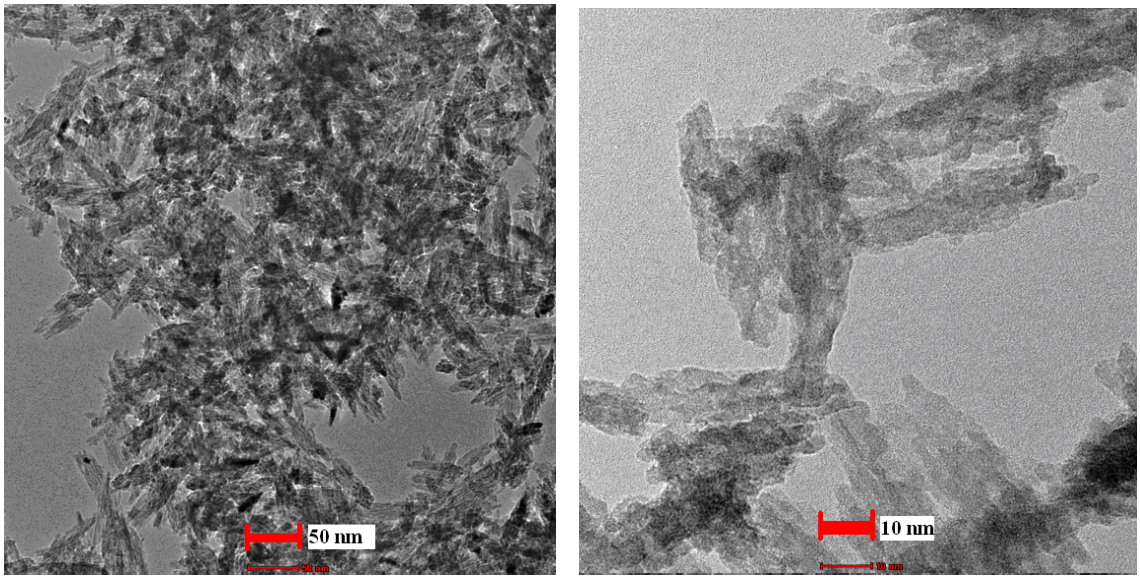


***Figure 4.1: Transmission electron microscope (TEM) images of nano-$TiO_2$ transition metal oxide***

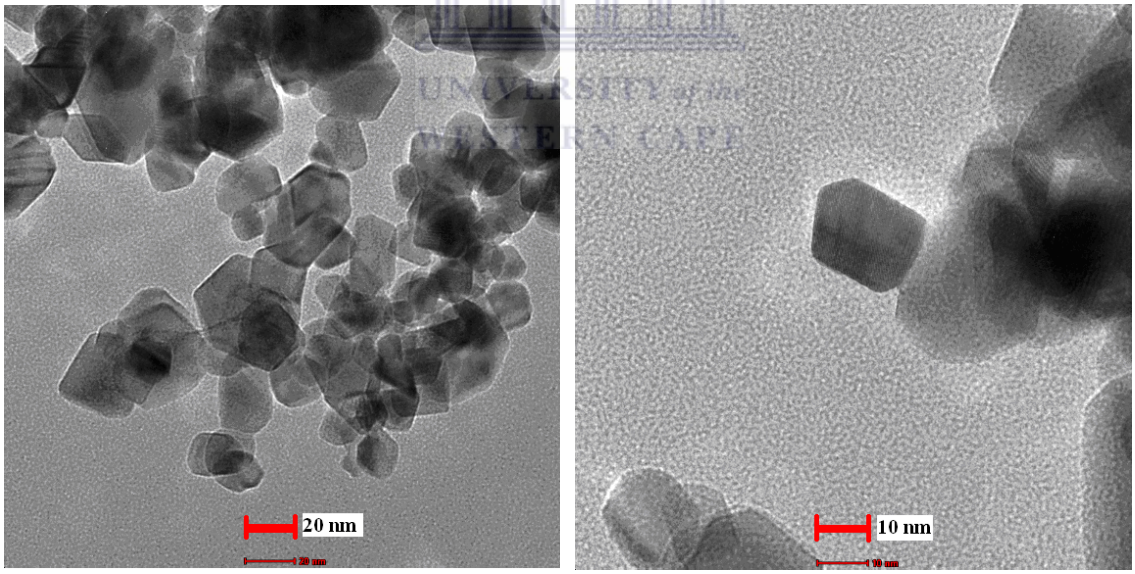


***Figure 4.2: TEM images of $SnO_2$ nanoparticles.***

Figure 4.2 shows images of Transmission electron microscopy (TEM) of the nanoparticles of $SnO_2$. The TEM images distinctly prove that the particles of Tin Dioxide

are indeed in nano-scale and that the particles are of irregular spherical shapes. The average particle size is believed to be approximately 10 nm in diameter. Both the metal oxides used have close to similar nanoparticles size of about 10 nm as also confirmed by Skandan *et. al* [104] and Liu *et. al* [105].

### 4.2. Potentiometric analysis: Cyclic voltammetry

#### 4.2.1 Analysis for the nano-$SnO_2$ metal oxide modified electrodes.

Figure 4.3(a) is the voltammogram of the potentiodynamic electrodeposition of polyaniline at the glassy carbon electrode in the presence of poly-4-styrene sulfonic acid in aqueous. HCl (1 M) characterized in 1M KCl aqueous electrolyte solution at scan rate of 50 $mVs^{-1}$. Because of the final cathodic scan with a stopping potential of -0.2 V, during the electropolymerization of aniline in acid media, the deposited film must be dominantly in its emeraldine form. Its mass was estimated as 946.7 ng from the following formula:



$$\text{Mass of deposited PANI} = \frac{Q \times MW}{F \times n} \qquad \textit{(eqn. 4.1)}$$

Where $Q$ is net charge of polymerization, $MW$ is the molecular weight of aniline, $F$ is Faraday's constant and $n$ is the average number of electrons involved per monomer unit.

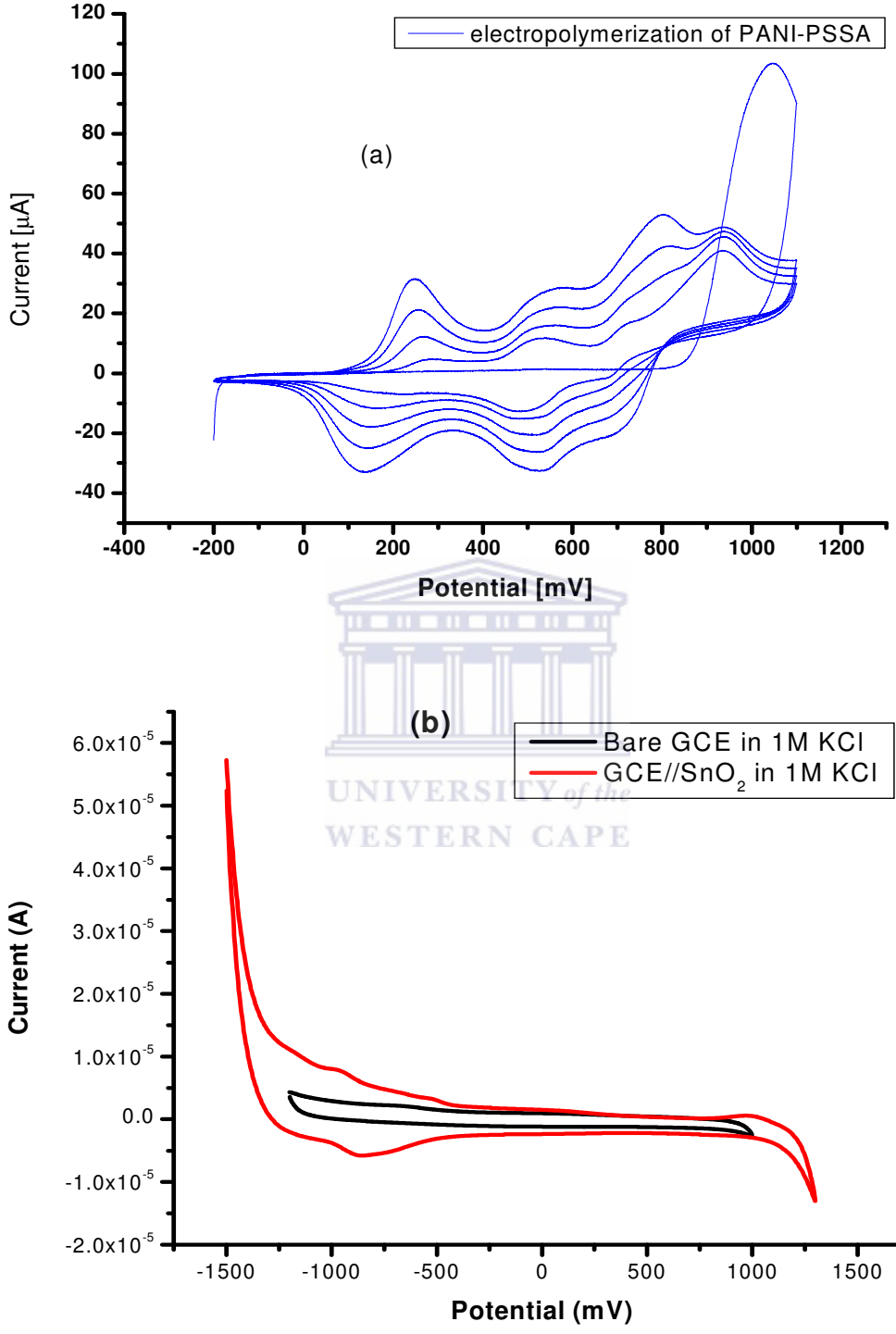

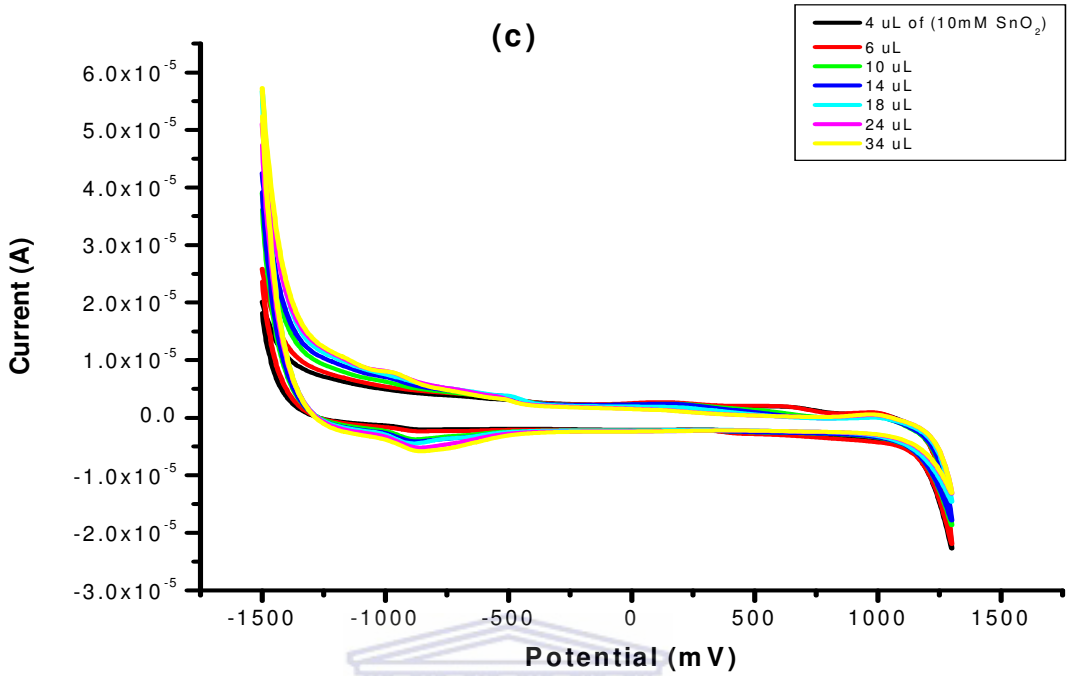


***Figure 4.3: (a) Electropolymerization of PSSA doped Aniline in 1M HCl electrolyte solution at a scan rate of 50 mV/s. (b) Drop-coating of 10 mM solution of $SnO_2$ onto a bare glassy carbon electrode (GCE). (c) The effect of coating with increase in volume and concentration of the 10 mM $SnO_2$ solution on the GCE.***



Figure 4.3 exhibited the two characteristic reversible peak pairs of polyaniline at formal potential of about 0.2 V ($\Delta Ep$ = 0.1 V) and 0.75 V ($\Delta Ep$ = 0.1 V).

The cyclic voltammograms in Figure 4.3(b) contrast the electrochemical behavior of the bare GCE and the $SnO_2$-film-modified GCE. One can see a significant increase in current density after the immobilization of $SnO_2$ film, especially in cathodic half-portion of the voltammogram. In Figure 4.3(c) shown are the cyclic voltammograms recorded with increasing amount of drop-coated $SnO_2$ film. One can also see that, as the amount, hence

as the thickness of the $SnO_2$ film was increased with successive drop-coating and drying, the current density increased in the same cathodic section of the voltammogram (i.e., from -0.5 V towards 1.5 V). Two cathodic processes, the formation of Tin (II) oxide (on-set potential ~ -0.4 V) and then the formation of Tin (0) (on-set potential ~ -1.3 V) might be occurring together with their respective reverse process. However, it appears that due to the third electrode reaction (perhaps the catalytic reduction of water) related with the formation of Tin(0) might have caused a high current hindering the complete reduction of the oxide. As a result of this, we could only see the occurrence of a single reversible redox peak pair with a formal potential of 0.913 V ($\Delta Ep$ = 0.115 V). This may be assigned to the Tin(IV)/Tin(II) inter-transformation. The mass of the metal oxide ($SnO_2$) film formed over the electrode's surface was estimated as 301.4 ng per 2 µL of its aqueous dispersion. The mass of the $SnO_2$ particles was calculated from a known molar mass and number of moles of the 2 µL aliquot of a 10 mM $SnO_2$ aqueous solution.



Figure 4.4 shows the cyclic voltammograms of the polyaniline/poly-4-styrene sulfonic acid (GCE//PANI-PSSA) modified electrode and that of the layer-by-layer modified GCE//PANi-PSSA/$SnO_2$ electrode with 2 uL of 1M $SnO_2$ aqueous solution. The mass of the metal oxide ($SnO_2$) was calculated to be $3.014 \times 10^{-7}$ g. In this Figure, it is clearly seen that the characteristic peaks of polyaniline [106] are still witnessed during cyclic voltammetric characterization of the PANI-PSSA modified electrode in 1M KCl aqueous electrolyte solution. The GCE//PANI-PSSA/$SnO_2$ modified electrode shows an increase in current density ($uA/cm.^2$) and a slight shift of the polyaniline peak potentials both cathodic and anodic.

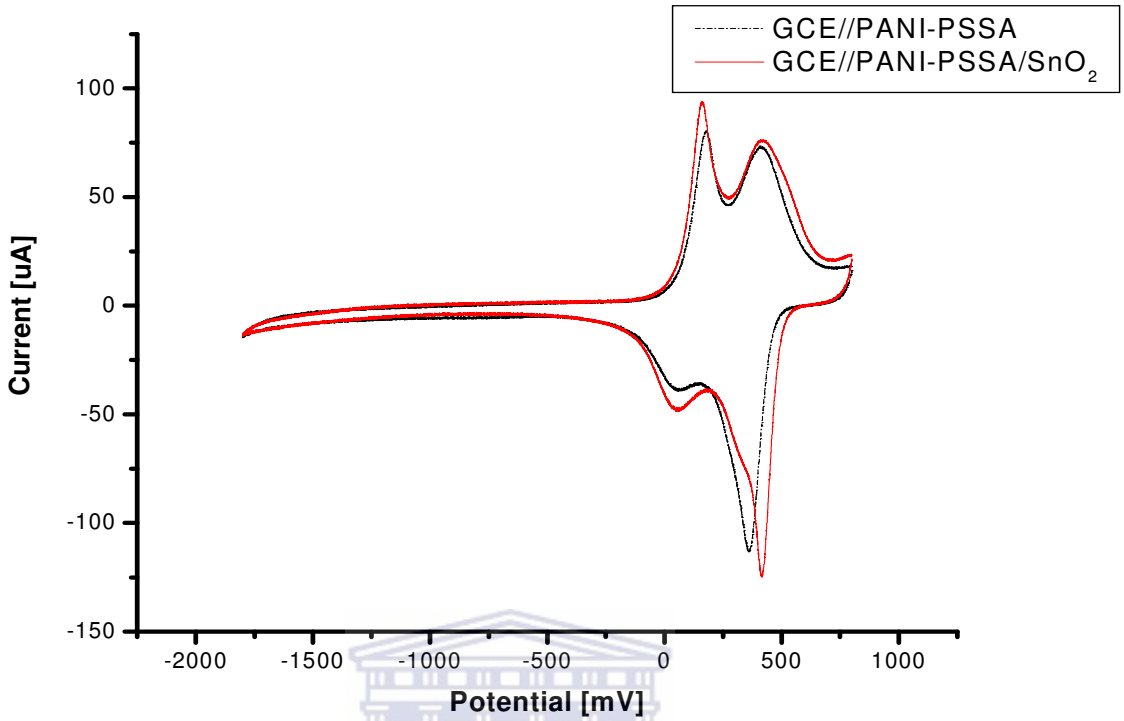




***Figure 4.4: Cyclic voltammogram of PANI-PSSA modified glassy carbon electrode and the PANI-PSSA/$SnO_2$ modified glassy carbon electrode at a scan rate of 50 mV/s in 1M KCl electrolyte solution.***

Specific capacitance of the electrode is calculated using equation 4.2, based on cyclic voltammograms, calculated from equation (eqn. 4.2) and gave capacitance of 1.976 $F.g^{-1}$ for the nano-$SnO_2$ modified (gce//PANI-PSSA/$SnO_2$ electrode and 1.0611 $F.g^{-1}$ for the GCE//PANI-PSSA. These values of capacitance of both the GCE//PANI-PSSA and gce//PANI-PSSA/$SnO_2$ electrodes display an improved capacitance when the metal oxide is incorporated onto the GCE//PANI-PSSA modified electrode forming the layer-by-layer nanocomposite.

$$\text{Specific capacitance } C = \frac{Q}{\Delta E \times m} \qquad \textit{(eqn. 4.2)}$$

Where, $C$ is specific capacitance, $Q$ is the deposition charge, $\Delta E$ is the change in potential and $m$ being the mass of the electrode material.

Figure 4.5 displays the effect of scan rate on the GCE//PANI-PSSA/$SnO_2$ modified electrode. The current density increases with an increase in sweep rate from 40-400 $mVs^{-1}$ and there is a constant shift in peak potential (Ep) for peaks *(a), (b)* and *(b')* of the characteristic peaks of the doped Polyaniline except for peak *(a')* as demonstrated by the linear fittings in Figures 4.8 and 4.9. The potential peak difference (ΔE) of the anodic and cathodic peaks decreases with increase in scan rate, the significance of this becomes more visible as the scan rate is excessively increased.

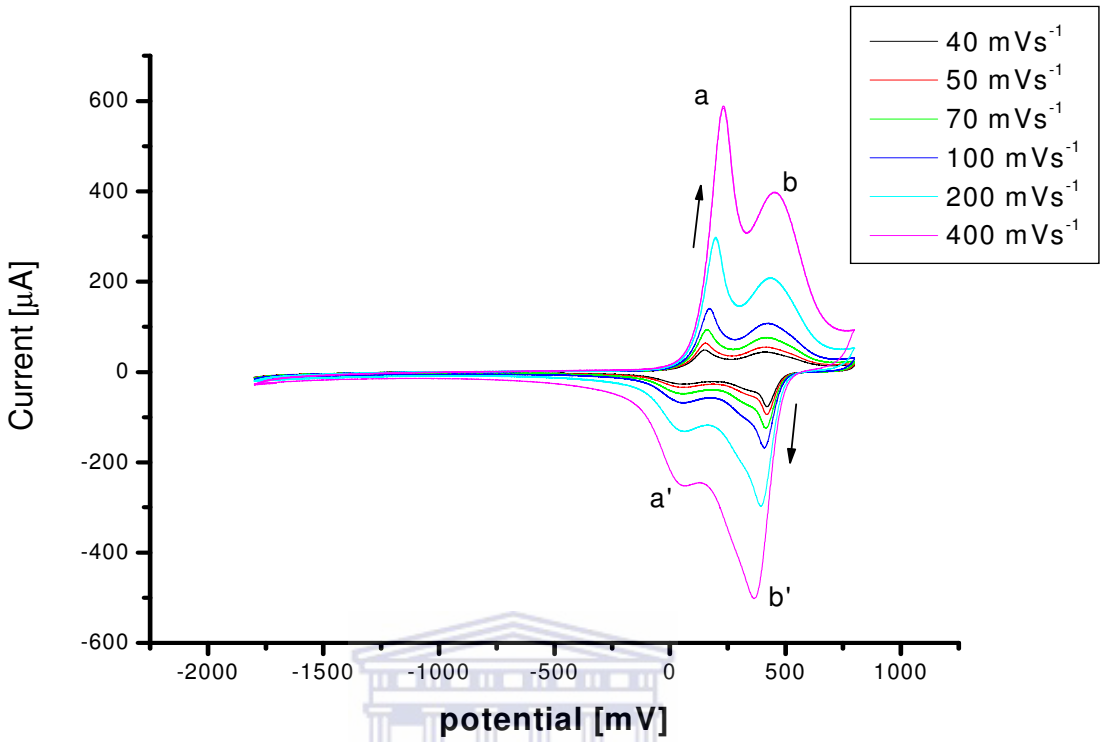


***Figure 4.5: Effect of scan rate on the PANI-PSSA/$SnO_2$ modified glassy carbon electrode.***



Figures 4.6 and 4.7 display the calibration plots of anodic and cathodic current peaks (Ipa and Ipc), against scan rate, respectively. A linear fit was obtained as characteristic of the constant increase in current density with increase in scan rate. A negative slope was obtained for the calibration curve of the cathodic current peaks (Ipc) due to the negative current values of peaks (*a'*) and (*b'*).

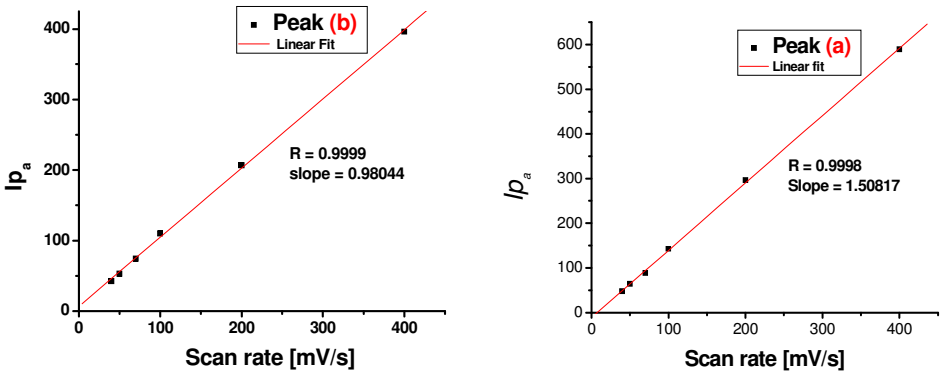


***Figure 4.6: Shows the calibration plots of the oxidation current peaks (Ipa) for the two anodic peaks: a and b of the GCE//PANI-PSSA/$SnO_2$ modified electrode.***

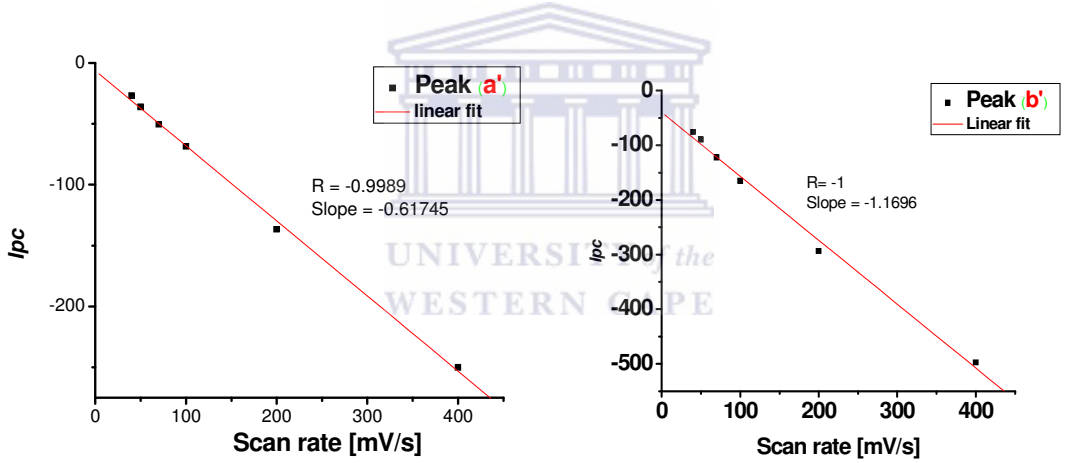


***Figure 4.7: Shows the calibration plots of the reduction current peaks (Ipc) for the two cathodic peaks: a' and b' of the GCE//PANI-PSSA/$SnO_2$ modified electrode.***

Figures 4.8 and 4.9 show calibration plots of oxidation and reduction potential peaks (Epa and Epc) against scan rate, respectively. A linear fit was obtained as characteristic of the constant shift in potential with increase in scan rate. A negative slope was obtained for the calibration curve of the reduction potential peaks (Epc) due to the potential (E)

values shift of peak (*b'*) towards the negative potentials. No slope observed for peak (*a'*) as due to the fact that there was no shift in potential (Epc) peak height observed at mostly all the scan rate used.

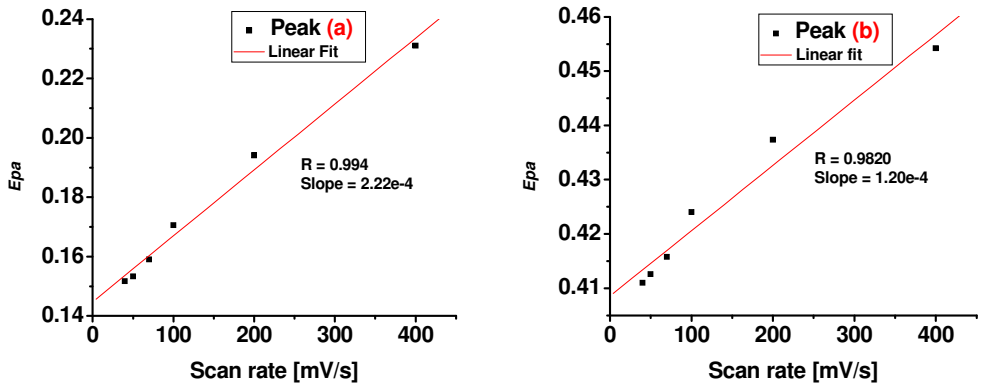


***Figure 4.8: Shows the calibration plots of the oxidation potential peaks (Epa) for the two anodic peaks: (a) and (b) of the GCE//PANI-PSSA/$SnO_2$ modified electrode.***



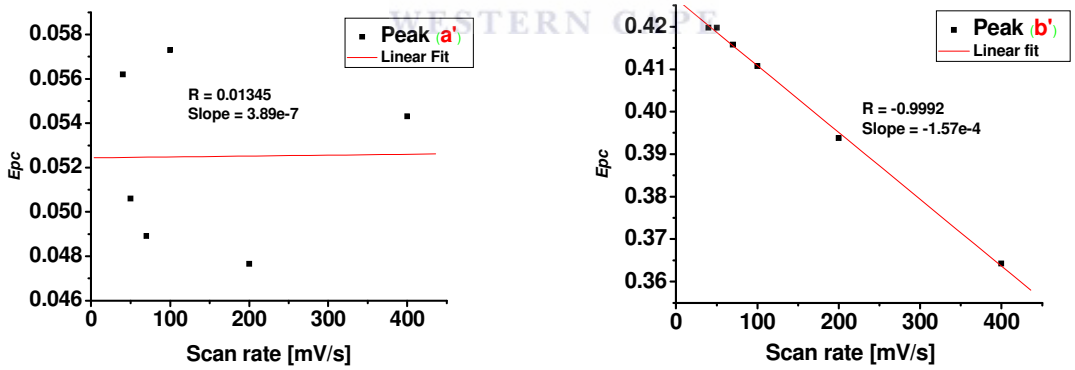


***Figure 4.9: Shows the calibration plots of the reduction potential peaks (Epc) for the two cathodic peaks: a' and b' of the GCE//PANI-PSSA/$SnO_2$ modified electrode.***

### 4.2.2 Analysis for the nano-$TiO_2$ metal oxide modified electrodes.

Electroanalysis of the constructed nanocomposite was done by electrochemical methods e.g. cyclic voltammetry. Figure 4.10 shows cyclic voltammograms of a bare glassy carbon (GCE) electrode along side with nano-$TiO_2$ modified glassy carbon electrode scanned at a rate of 50 mV/s between potentials of 1.3V and -1.9V. It is clearly observable that the current density of the $TiO_2$ modified electrode is higher than that of the bare electrode, moreover in the negative potentials region. The increase in current demonstrates that the deposited metal oxide shows good reversible electroactivity [107].

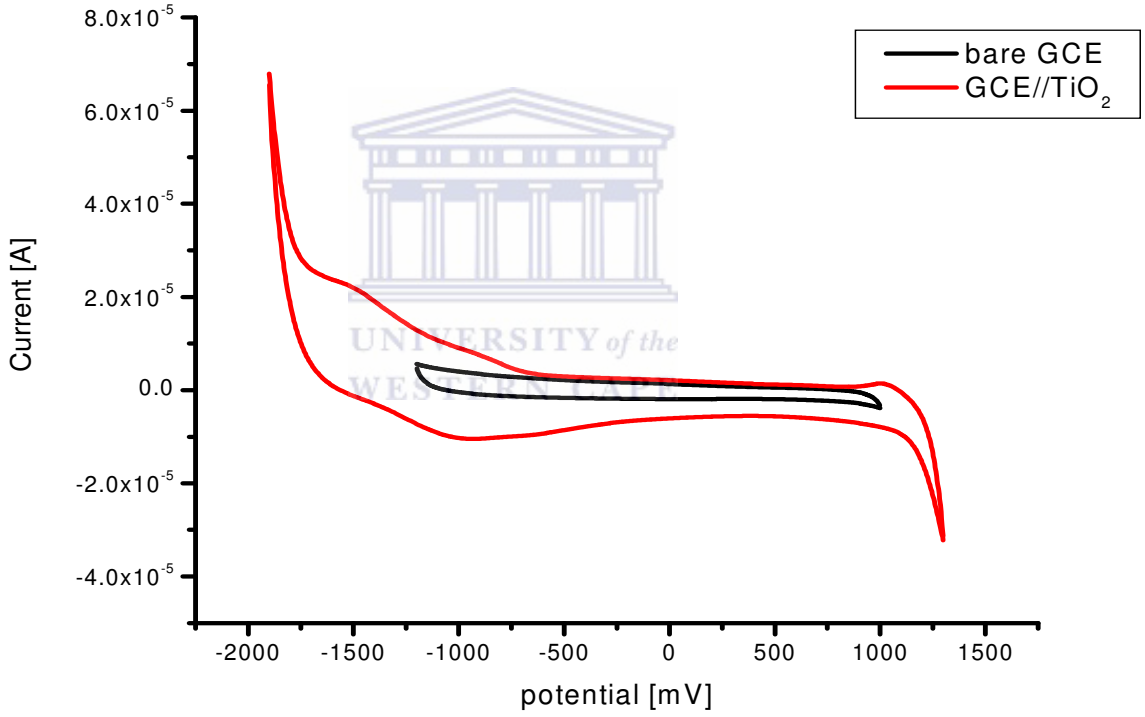


***Figure 4.10: Cyclic voltammetric comparison of the bare glassy carbon electrode (bare GCE) and $TiO_2$ modified electrode (gce///$TiO_2$) at scan rate of 50 $mVs^{-1}$ against Ag/AgCl reference electrode.***

The effect of concentration/quantity of the deposited $TiO_2$ on to the electrode is shown in figure 4.11. There is an increase in current density as more of the transition metal oxide is added on the electrode surface. Therefore, the current is directly proportional to the amount of nano-$TiO_2$ deposited on the electrode surface. The increase is only distinctly effective in the negative potential region of the cyclic voltammogram shown in Figure 3.

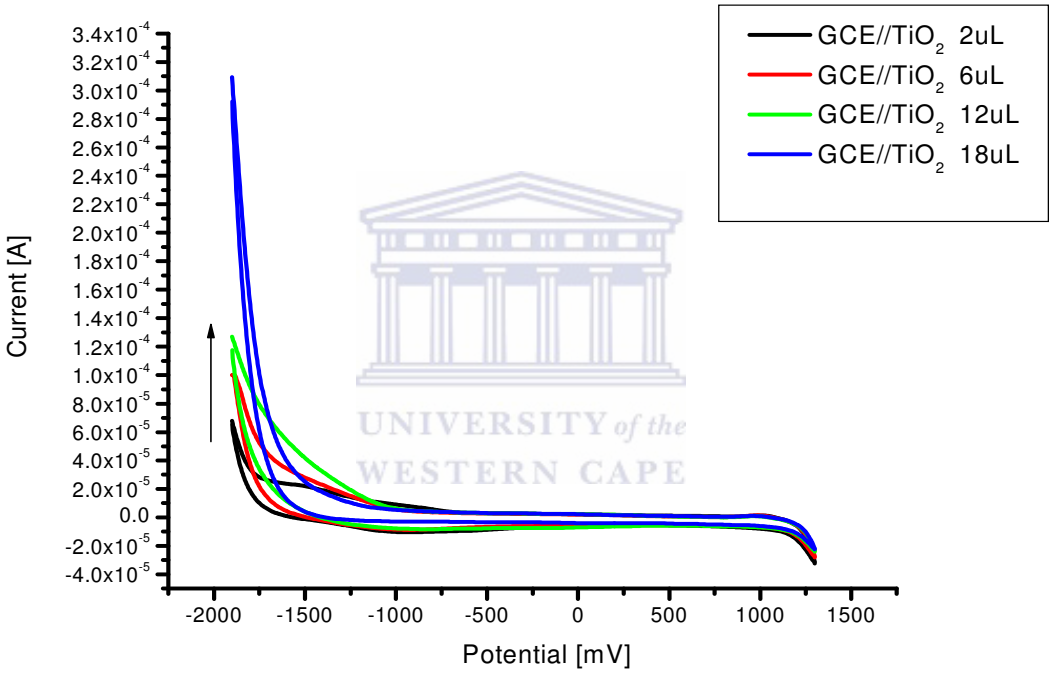


***Figure 4.11: Cyclic voltammograms of the effect of the quantity of the nano-$TiO_2$ metal oxide on a bare GCE at scan rate of 50 $mVs^{-1}$ against Ag/AgCl.***

Electropolymerization of polystyrene sulfonic acid doped aniline was conducted in acid medium by sweeping the potential from -0.2V to +1.1V at a sweep rate of 50 mV/s for a number of 5 cycles. Figure 4.12 shows a typical cyclic voltammogram of the polymerization of aniline in 1M HCl electrolyte solution. The PANI-PSSA layer was

seen to be redox active in the studied potential region exhibiting three set of peak both anodic and cathodic scans. Oxidation of Polyaniline, initially occurred at potential of about 0.9V resulting in the nucleation of polyaniline [55]. An increase in the amplitude of the redox peaks observed after repeated voltammetric scans is the indication of polymer deposition on the electrode surface and confirms its conductivity. The generally accepted structure of PANI is described as figure 2.3 (Chapter 2). The three separate oxidation states of PANI are: fully reduced form which is designated as leucoemeraldine base (LB); half-oxidized form which is designated as emeraldine base (EB); and fully oxidized form designated as pernigraniline base (PNB). All the three base forms LB, EB, and PNB can be protonated to corresponding salt forms designated as leucoemeraldine salt (LS), emeraldine salt (ES) and pernigraniline salt (PNS), respectively [108]. Figure 4.12 shows two main redox processes (I/I′ and III/III′) corresponding to transition from leucoemeraldine to emeraldine and emeraldine to pernigraniline states. Another redox process corresponding to incorporation of oligomers into the polymer matrix or degradation products of the polymer was noticed (II/II′) [109].

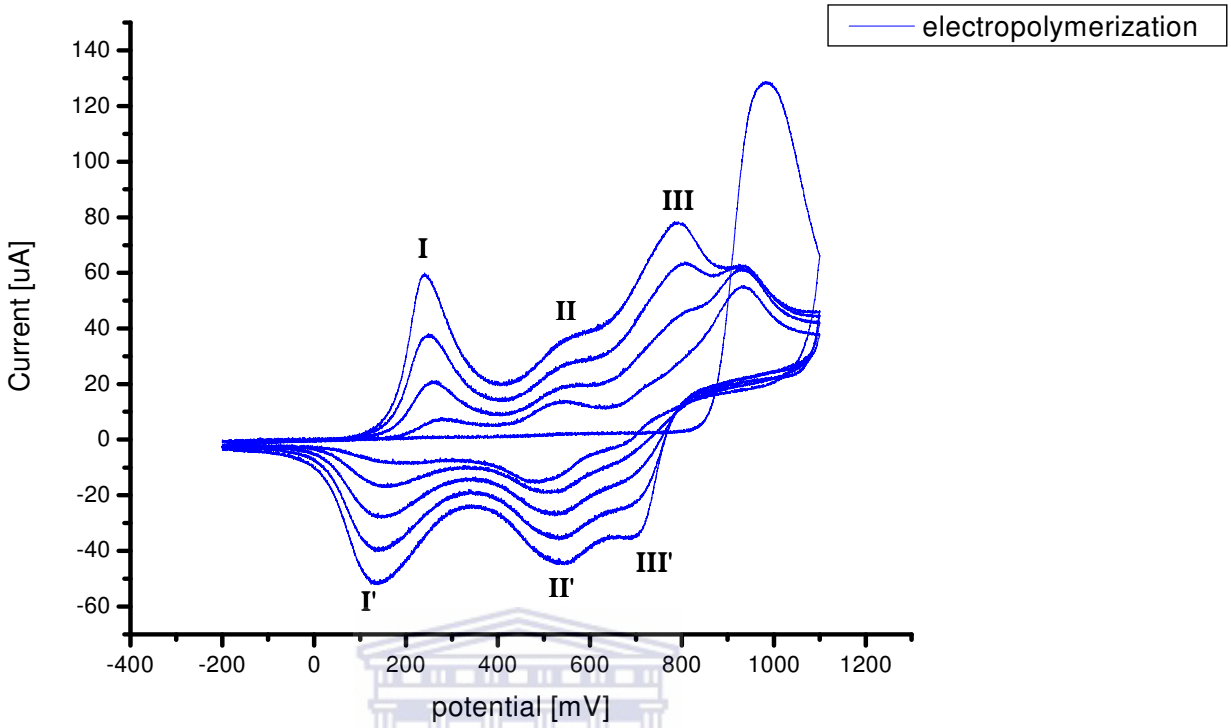


***Figure 4.12: Electropolymerization of 0.05M aniline and 0.025 M poly-4-styrene sulfonic acid in 1M HCl electrolyte solution at scan rate of 50 mV/s for 5 cycles against Ag/AgCl reference electrode.***



The mass of the polyaniline deposited on the surface of the glassy carbon electrode has been calculated using the following equation (eqn.4.3). An amount of $1.1887e^{-3}$ mg of polyaniline was obtained on a 0.0707 $cm^{-2}$ electrode surface area.

$$\text{Mass of deposited PANI} = \frac{Q \times MW}{F \times n} \qquad \textit{(eqn. 4.3)}$$

Where, $Q$ is the deposition charge, $MW$ is the molecular weight of aniline, $F$ is Faraday's constant and $n$ being the number of electrons involved in the polymerization process.

Specific capacitance of the electrode is calculated using equation 4.4, based on cyclic voltammograms, polyaniline modified GC (GCE//PANI-PSSA) electrode gives capacitance of 0.00532 $F.g^{-1}$ calculated from equation (eqn. 4.4) and a capacitance of 0.01303 $F.g^{-1}$ for the nano-$TiO_2$ modified (gce//PANI-PSSA/$TiO_2$ electrode.

$$\text{Specific capacitance } C = \frac{Q}{\Delta E \times m} \qquad \textit{(eqn. 4.4)}$$

Where, $C$ is specific capacitance, $Q$ is the deposition charge, $\Delta E$ is the change in potential and $m$ being the mass of the electrode material.



Figure 4.13 illustrates voltammetric type responses recorded for differently modified electrodes. PANI-PSSA modified electrode was characterized in 1M KCl electrolyte solution, still showing PANI-PSSA characteristic redox peaks. The figure also shows that the gce//PANi-PSSA/$TiO_2$ cyclic voltammogram is different from that of GCE//PANI-PSSA in the sense that an increase in peak current and a shift in peak potential for redox peak (*b)* and (*b')* are observed. As illustrated in figure 4.11 that current increases with increase in amount of $TiO_2$ deposited on the electrode surface, it is also evident in this figure (figure 4.13). The increase in current and the shift in potentials prove that the nano-$TiO_2$ material is actually deposited on the surface of the electrode. The two main redox peak couples in the gce//PANI-PSSA/$TiO_2$ electrode, (*a*) and (*b'*), become more intense as more nano-$TiO_2$ is deposited. The first peak (*a*) in the cyclic voltammetry of gce//PANI-PSSA/$TiO_2$ composite is due to the surface electron transfer at 0.15 V which has similar characteristics as that of PANI-PSSA. However, it is more intense than that of

GCE//PANI-PSSA. The behaviour of the similarities suggest that the incorporation of the nano-$TiO_2$ metal oxide on the doped polyaniline does not retard the properties of polyaniline itself in the sense of its conductivity and stability, therefore indicating a formation of a conductive composite of PANI-PSSA/nano-$TiO_2$. Peak (*b*) at potential of 0.48V, however, is due to quinoid structure in polyaniline [110] and the protonation peak from polymerization of polyaniline has fallen away when KCl was used as an electrolyte solution.

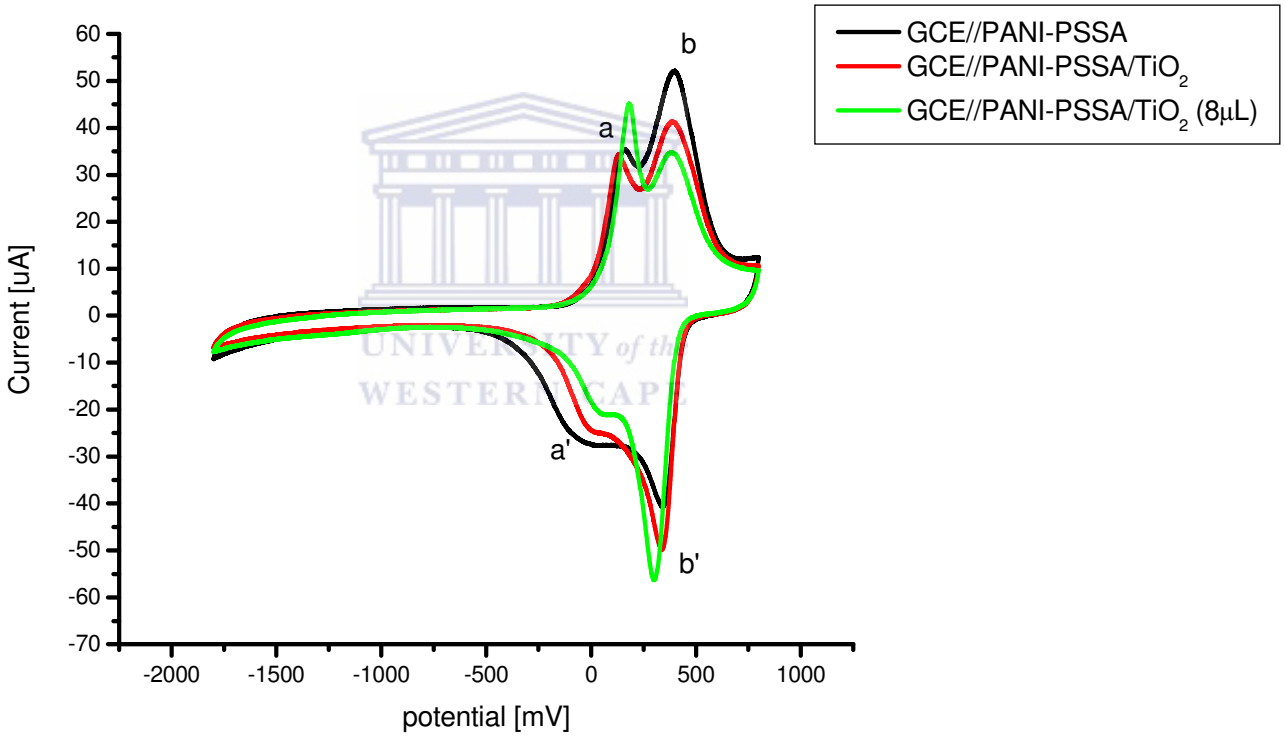


***Figure 4.13: Cyclic voltammetric analysis of the effect of the nano-$TiO_2$ metal oxide deposited on doped Polyaniline modified GC electrode against Ag/AgCl at 50 $mVs^{-1}$ scan rate in 1M KCl electrolyte solution***.

The effect of scan rate on gce//PANI-PSSA/$TiO_2$ is demonstrated in figure 4.14 showing a significant increase in current density with an increase sweep potential (scan rate). Peak potential shift is also evident for peaks (*a*), (*b*) and (*b'*), but merely not significant for peak (*a'*) as there is a fading in the intensity of that particular peak. At higher scan rates of about 1000 mV/s (which is included in the graph) a merger of anodic peaks (*a*) and (*b*) and cathodic peaks of (*a'*) and (*b'*) is witnessed. Therefore, scan rate in this particular experiment is directly proportional to current density and peak potential shift.

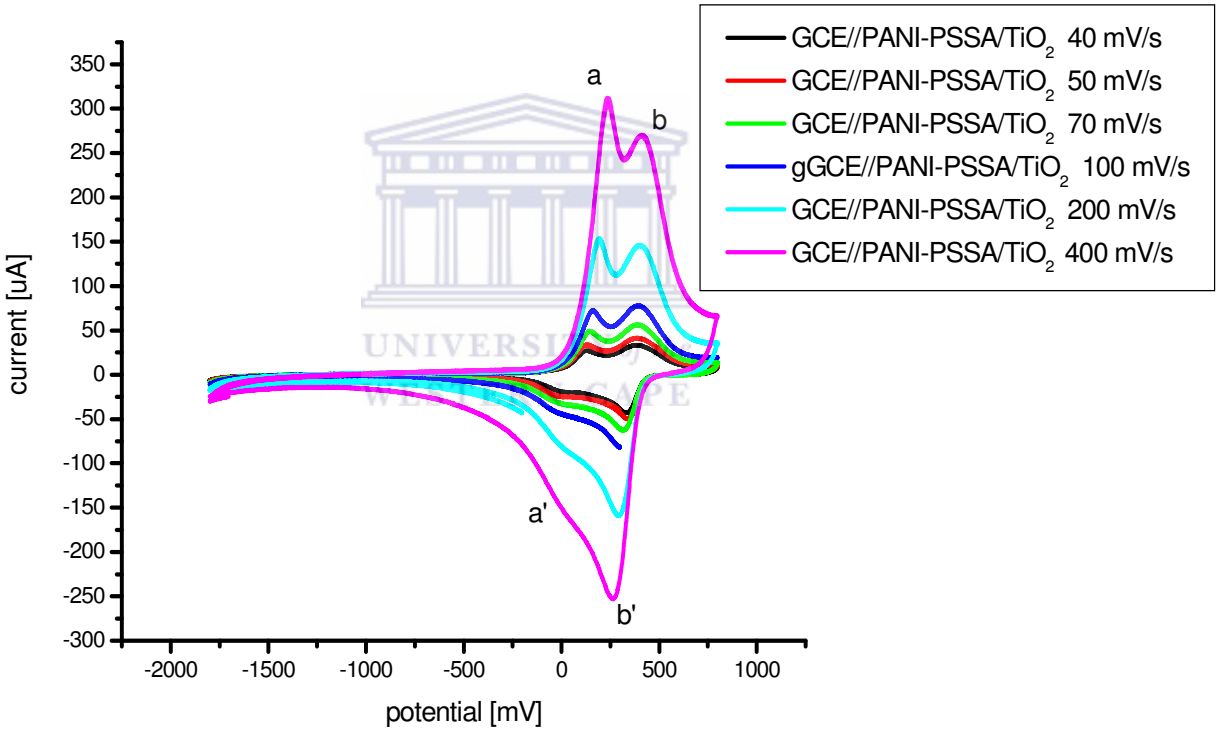


***Figure 4.14: Cyclic voltammetric effect of scan rate of the nanocomposite modified glassy carbon electrode against Ag/AgCl reference electrode.***

### 4.3 FTIR studies of electrodeposited polyaniline

The structure of PANI was also characterized with FTIR spectrum. Figure 4.15 shows the IR spectrum of the PANI synthesized electrochemically by cyclic voltammetric method. The characteristic bands at ~1575 and ~1499 $cm^{-1}$ correspond to the C=C stretching of the quinoid ring and benzenoid ring, respectively. Bands at ~1302, ~1155 and ~824 $cm^{-1}$ arose from the C-N stretching of the secondary aromatic amine, the C-H in-plane bending mode, and an aromatic C-H out of plane bending vibration individually. These characteristic bands conformed that the PANI contained the conducting emeraldine salt phase [111]. The peaks observed at 3248 $cm^{-1}$ are attributed to the N–H stretching vibrations [112].

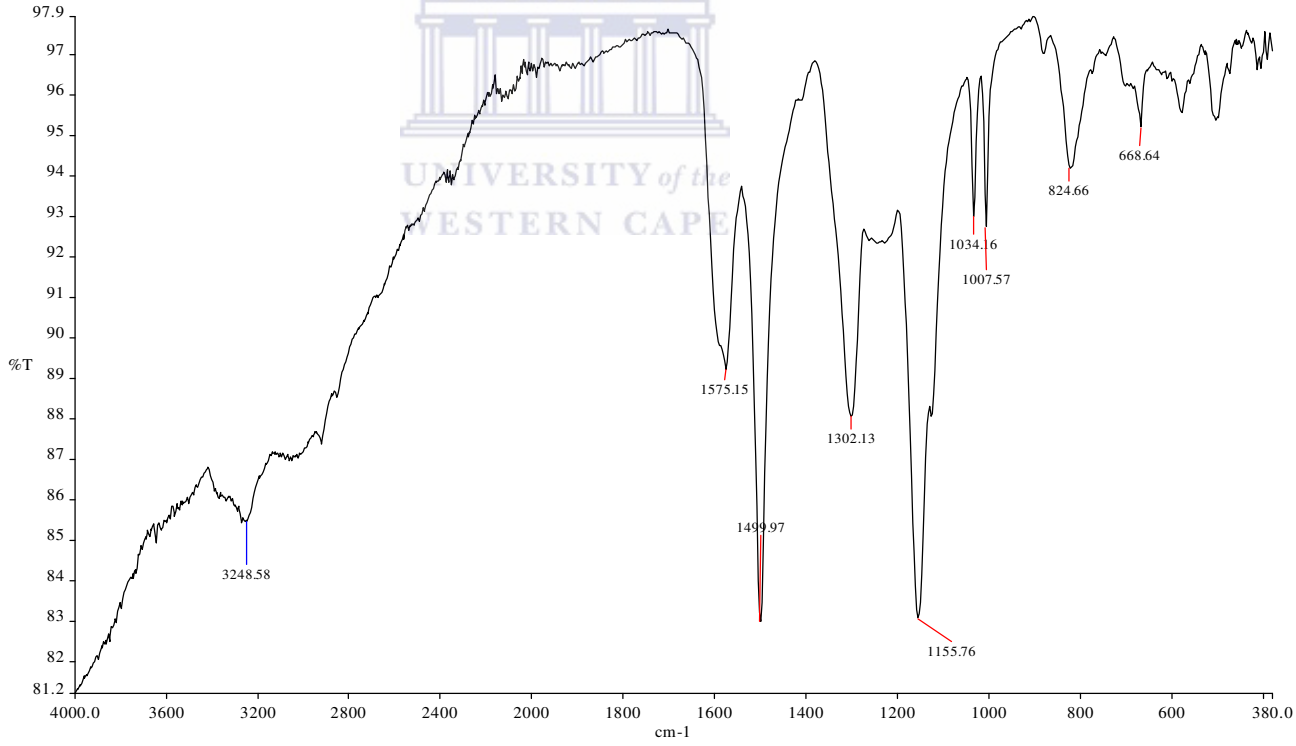


***Figure 4.15: FTIR spectrum of PSSA doped PANI***

Some of the most essential peaks observed from the FTIR spectrum are defined in Table 4.1 proving that the electropolymerized conductive polymer is indeed Polyaniline. The $SO_3^=$ dopant ions are also visible from the spectrum as shown by two intense peaks at around wavelength of approximately 1034 and 1007 $cm^{-1}$ introduced by the poly-4-styrene sulfonic acid used in the polymerization of the doped aniline.

***Table 4.1: Characteristic frequencies of potentiodynamically synthesized PANI doped in the presence of poly-4-styrene sulfonic acid***

| *Wave number (cm-1)* | *Band characteristic* |
|---|---|
| ~565 | CH out-of-plane bending vibration |
| 824 | *para*-Disubstituted aromatic rings |
| 1034 and 1007 | Due to $SO_3^=$ group of the PSSA |
| 1155 | CH in-plane bending vibration |
| 1302 | C-N stretching of the secondary aromatic amine |
| 1499 | CN stretching of benzenoid rings |
| 1575 | C=C stretching of the quinoid ring |
| 3248 | Aromatic CH stretching |
| ~3453 | NH stretching of aromatic amines |



**4.4 Galvanostatic analysis**

In order to evaluate the performance of a capacitor, galvanostatic charge-discharge analysis has to be performed. Figures 4.16 and 4.17 show charge-discharge behaviors of GCE//PANI-PSSA/$SnO_2$ and GCE//PANI-PSSA, respectively. The curves are cycles of

10 each with different current applied at 20 seconds per charging time. The curve of 1 µA and that of 10 µA show 10 cycles stretching over 400 seconds, while the 10 cycles of the 100 µA current charging stretches over a shorter period of time.

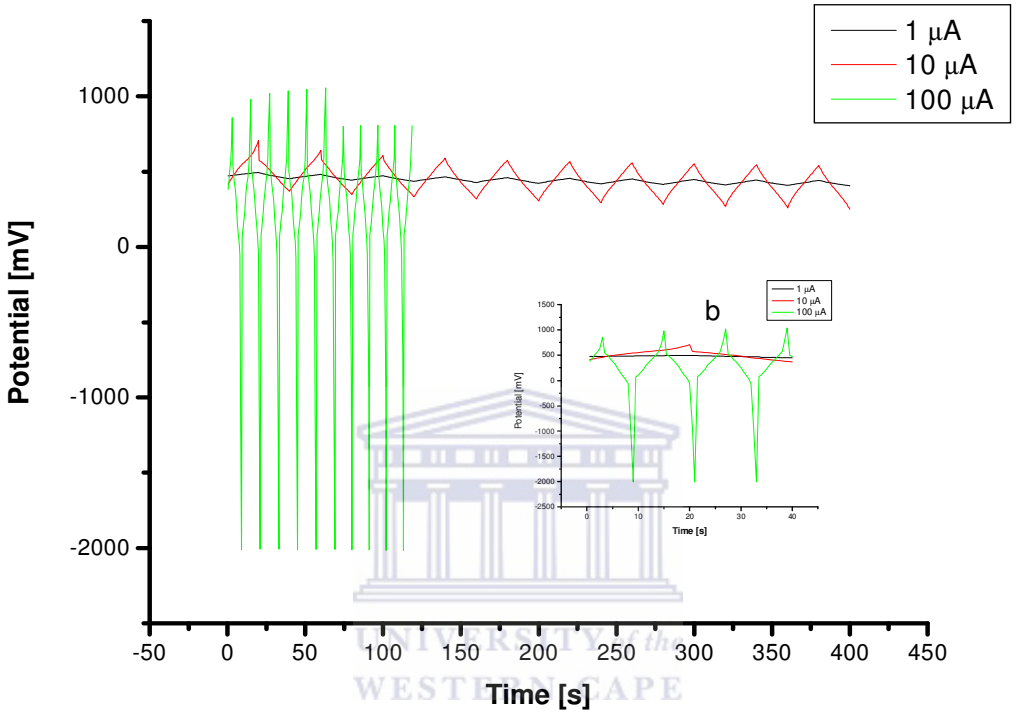


***Figure 4.16: Charge-discharge curve for the GCE//PANI-PSSA/$SnO_2$ modified electrode at different currents, 1 µA, 10 µA and 100 µA for 10 cycles.***

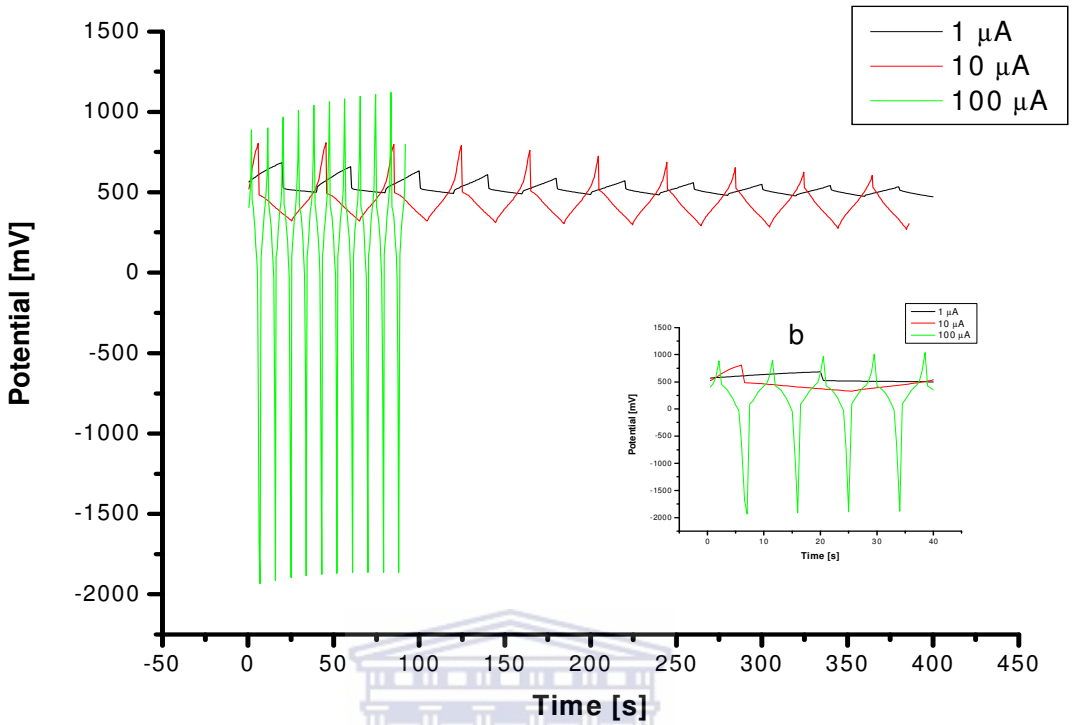


***Figure 4.17: Charge-discharge curve for the GCE//PANI-PSSA modified electrode at different currents, 1 µA, 10 µA and 100 µA for 10 cycles.***

Symmetrical charge and discharge of the curve of GCE//PANI-PSSA/$SnO_2$ is observed throughout the cycles as evidence of little or no current leakage, however, the potential of the curve of 100 µA applied current shows stepwise decrease in the potential after 5 cycles whereas the 100 µA curve of the GCE//PANI-PSSA shows gradual increase in potential over time and unsymmetrical charge and discharge curves at all applied current differences. The non-symmetry in the curves is believed to be from current leakage after charging. Figure 4.18 shows difference in charge-discharge of the GCE//PANI-PSSA and GCE//PANI-PSSA/$SnO_2$ modified electrodes over a number of 10 cycles at 10 µA

applied current. It is evident that GCE//PANI-PSSA/$SnO_2$ has longer and symmetrical charge-discharge curve though it has lower potential than bare GCE. The charge curves of GCE//PANI-PSSA/$SnO_2$ are very symmetric to their corresponding discharge counterparts in the whole potential region and the slope of every curve is potential-independence and maintains a constant value at a specified current, which the results indicate that the GCE//PANI-PSSA/$SnO_2$ has the ideal capacitive behavior for electrochemical capacitors [113-115].

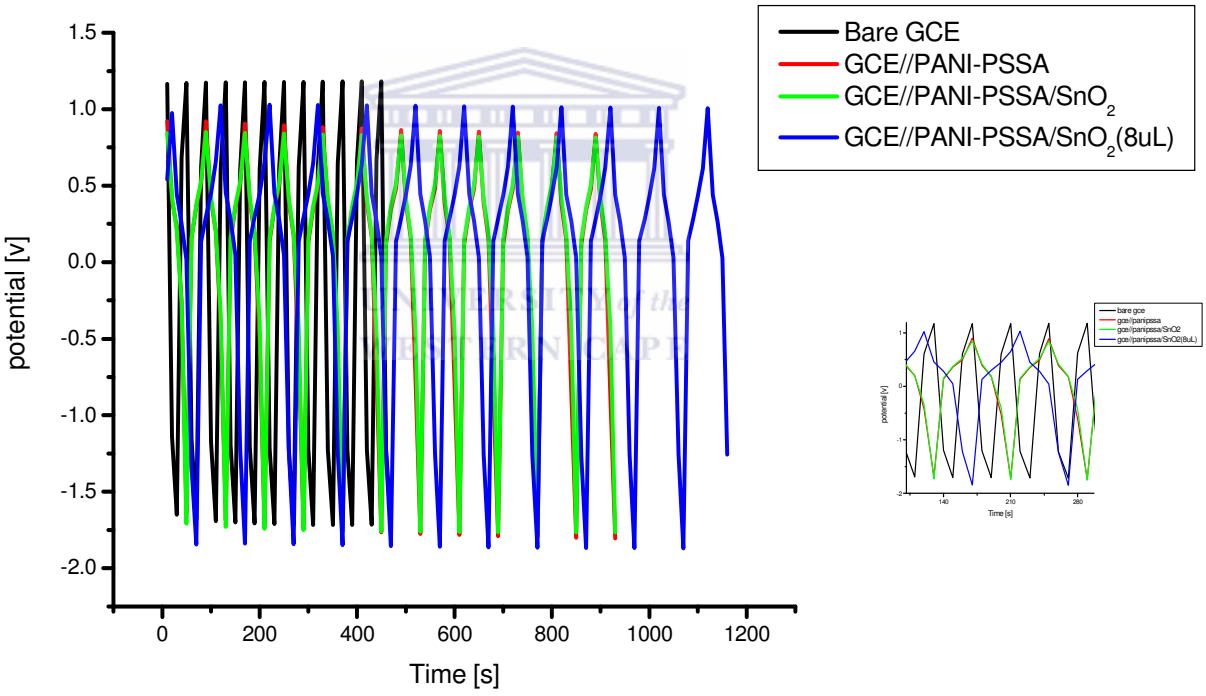


***Figure 4.18: Charge-discharge curve for both GCE//PANI-PSSA and GCE//PANI-PSSA/$SnO_2$ modified electrodes at applied current of 10 µA for 10 cycles with the insert is a magnified part of the main graph.***

Specific capacitance from charge-discharge curves is calculated according to equation (eqn. 4.5). The capacitance of GCE//PANI-PSSA/$SnO_2$ was found to be 40.043 $F.g^{-1}$.

$$C = \frac{i \times t}{m \times \Delta E} \qquad (eqn.4.5)$$

Where the parameters used are defined as, *C* being the capacitance (F), *i* being the constant current (A) applied, *m* the mass (g) of the electrode material and *ΔE* is the change in potential (V).

It is understood that a choice of the conducting polymer and the oxide material that are combined is essential to prepare a composite exhibiting good charge-discharge performances [116]. Figure 4.19 shows galvanostatic charge-discharge curves of bare GCE and the composite of gce//PANI-PSSA/nano-$TiO_2$ modified electrode recorded at constant current density of 10 uA $cm^{-1}$ at 25 $^{o}$C for a number of 10 cycles. The bare GCE electrode shows linear charge-discharge counter parts as demonstration of double layer capacitance, it can be found from the curves that the capacitor voltage varies nearly linearly with time, which indicates good capacitive behavior [117-118].

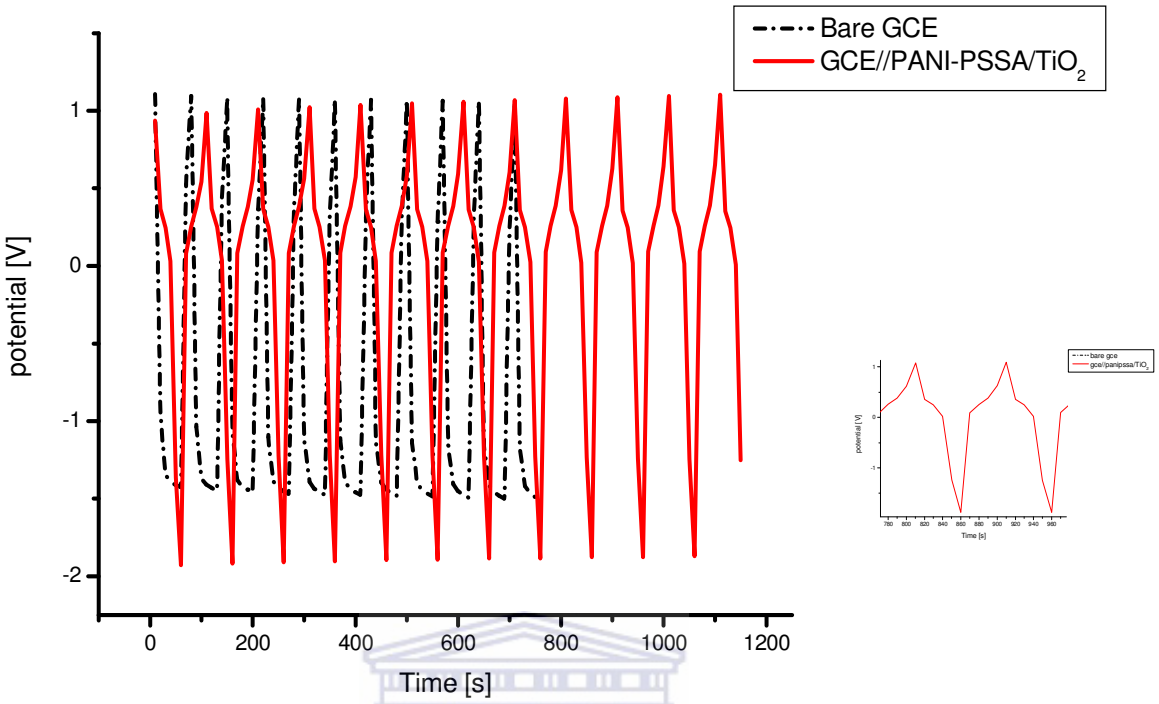


***Figure 4.19: Galvanostatic Charge-Discharge curve for composite electrode material against the bare glassy carbon working electrode with the insert is a magnified part of the main graph.***

The discharge curve consists of two sections, a sudden potential drop followed by a slow potential decay. The first potential drop results from the internal resistance and the subsequent potential decay represents the capacitive feature of the electrode. The obvious deviation of the shape of the charge-discharge curves from straight line and the shape of CV from an ideal rectangular shape revealed that the capacitance the composite is not purely double-layer, but faradaic capacitance or mainly called pseudo-capacitance, which mainly originates from the redox reaction [119-120]. It could be seen that all the curves were not ideal straight line, indicating the process of a faradic reaction. In addition, there

was an initial drop in potential caused by internal resistance [111]. Since faradaic charge-transfer is usually accompanied by the double-layer charging process, the combination of electric double-layer capacitance and faradaic capacitance is responsible for the longer charge/discharge duration [121]. Specific capacitance from charge-discharge curves is calculated using the following formula on equation (eqn. 4.5). The capacitance of gce//PANI-PSSA/$TiO_2$ is calculated to 3.363 $F.g^{-1}$.

$$C = \frac{i \times t}{m \times \Delta E} \qquad \textit{(eqn. 4.5)}$$

When the same current is used for charging and discharging, the coulombic efficiency (η) can be evaluated from the following equation (eqn.4.6).

$$\eta = \frac{t_D}{t_C} \times 100\% \qquad \textit{(eqn. 4.6)}$$



Where $t_D$ and $t_C$ are the time for galvanostatic discharging and charging respectively [113]. The Coulombic efficiency has been calculated to be 99.98%.

**4.5 Electrochemical Impedance Spectroscopic studies.**

Figure 4.20 shows Nyquist plots of the electrochemical impedance spectroscopy of bare glassy carbon electrode, GCE//PANI-PSSA and GCE//PANI-PSSA/$SnO_2$ modified electrodes scanned at 250 mV in aqueous 1M KCl electrolyte solution.

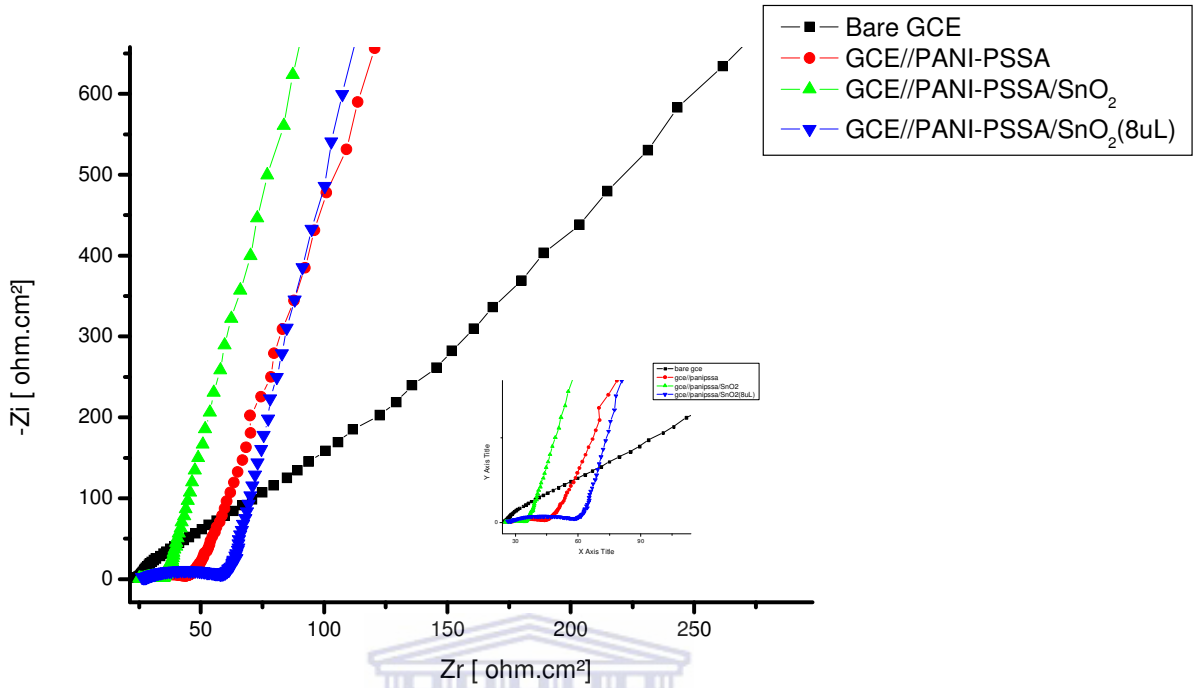


***Figure 4.20: Electrochemical impedance spectroscopy of the bare GCE, GCE//PANI-PSSA and GCE//PANi-PSSA/$SnO_2$ at 250 mV in a frequency range from 100 kHz to 10 mHz with the insert is a magnified part of the main graph.***

The complex impedance plots of different electrodes illustrated demonstrate some capacitive behavior (i.e. steep rising response of Zi asymptotically for approximately constant value of Zr, i.e. almost parallel to the Zi-axis) [97, 111]. A typical semicircle originating from electrolyte resistance and charge-transfer resistance at electrode/electrolyte interface is exhibited in the high frequency parts of the impedance spectra. The semicircle gradually becomes larger with higher potential applied on the electrode. The graph of the GCE//PANI-PSSA modified electrode demonstrates a curve with bigger semi-circle compared to that of GCE//PANI-PSSA/$SnO_2$ as evidence that the

metal oxide modified electrode has lower charge transfer resistance. At very high frequencies, a small impedance arc is observed for the bare GCE and GCE//PANI-PSSA/$SnO_2$ impedance spectrum, which is related to the double layer (dl) process [122]. Both electrodes show an increase in the impedance on the imaginary (Zi) part with decrease in frequency, which indicates the typical capacitive behaviour [22]. The slope gradually increases as frequency decreases, which is typical linear shapes of ideal electrochemical capacitor [123]. The below re-attached Figure 4.20 displays a magnified part of the lower frequency region so as to visually show the semicircles of the Nyquist plots of the differently modified electrodes hence, however, the figure caption is identical.



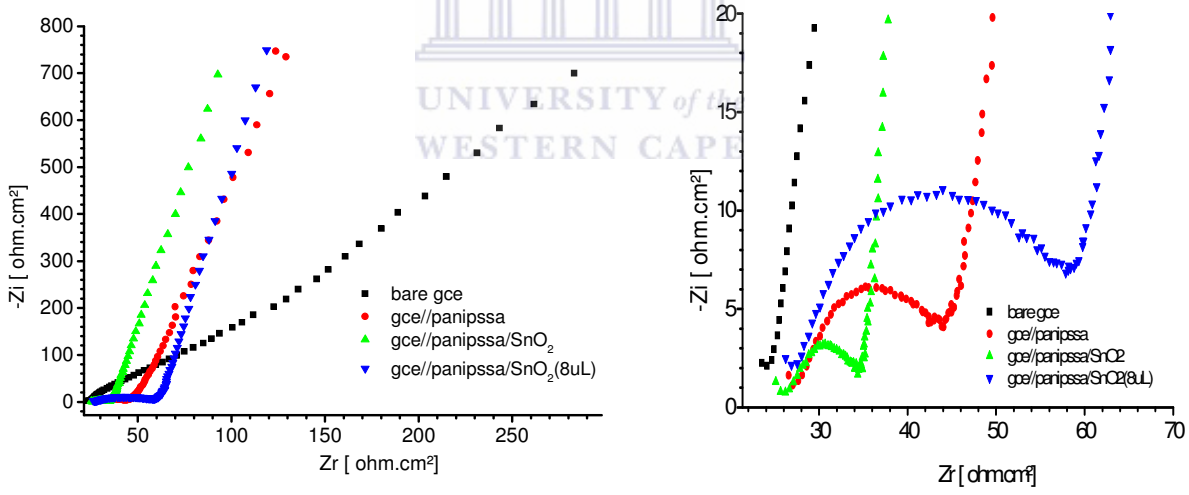


***Figure.4.20: Electrochemical impedance spectroscopy of the bare GCE, GCE//PANI-PSSA and GCE//PANi-PSSA/$SnO_2$ at 250 mV in a frequency range from 100 kHz to 10 mHz with the insert is a magnified part of the main graph.***

The data tables below show the values received after a simulation fit of the electrochemical impedance spectroscopy for a complex plot (Nyquist plot) of GCE//PANI-PSSA and GCE//PANI-PSSA/$SnO_2$ with solution resistance (Rs) denoted as R1, charge transfer resistance (Rct) as R2, Warburg as W and constant phase element as CPE. The solution resistance of both GCE//PNI-PSSA and gce//pani-pssa/$SnO_2$ is closely the same but vast difference in charge transfer resistance of which the former is 25.83 Ω and the latter being 37.03 Ω. Different circuit diagrams were fitted for both electrode leading to the metal oxide modified electrode having CPE where as the GCE//PANI-PSSA has a capacitor (C) element.

A constant phase element (CPE) is a non-intuitive circuit element, it is often used in a model in place of a capacitor due to deviation of capacitance parameters from expected values. The impedance of a CPE is represented by equation

CPE = $Z = A(j\omega)^{-\alpha}$ (*eqn. 4.7*)

= $1/(Cj\omega)^{\alpha}$ (*eqn. 4.8*)

Where, $Z$ is the impedance of the CPE, $j$ is the imaginary number ( $j = \sqrt{-1}$ ) and ω is the angular frequency ($\omega = 2\pi f$, $f$ being the frequency). The impedance of a CPE is similar to that of a capacitor except that the constant A = 1/C (the inverse of the capacitance) and the exponent α = 1 for a true capacitor. For a constant phase element, the exponent α is less than one. When α = 0.5, a 45° line is produced on the complex plane graph and could be used for an infinite length of Warburg element. During circuit fitting, the CPE is defined by two values, i.e., the capacitance, C, and the CPE exponent, α, which has a value between 0.5 and 1 for a non-ideal capacitor. If $n$ equals 1, the

equation is identical to that of a capacitor and smaller values can be related to surface roughness and in-homogeneities, which lead to frequency dispersion [124].

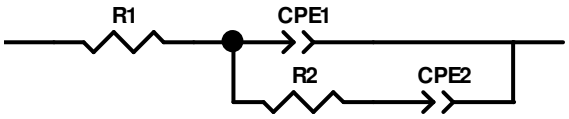


Fitting for GCE//PANI-PSSA/$SnO_2$

| Element | Freedom | Value | Error | Error % |
|---|---|---|---|---|
| R1 | Free(±) | 25.83 | 0.30308 | 1.1734 |
| CPE1-T | Free(±) | 2.0007E-05 | 2.4036E-06 | 12.014 |
| CPE1-P | Free(±) | 0.70312 | 0.012228 | 1.7391 |
| R2 | Free(±) | 37.03 | 0.56107 | 1.5152 |
| CPE2-T | Free(±) | 0.00023715 | 2.4454E-06 | 1.0312 |
| CPE2-P | Free(±) | 0.96323 | 0.002623 | 0.27231 |

***Figure 4.21: Equivalent circuit diagram for the gce//pani-pssa/$SnO_2$ modified electrode***



The equivalent circuit in accordance with the above Nyquist plot of gce//PANI-PSSA/$MO_x$ is presented in the figures 4.21 and 4.23. In these models, the double-layer capacity and the Warburg impedance for semi-infinite linear diffusion are replaced by two constant-phase elements CPE1 and CPE2 which correspond, respectively, to a capacity at an inhomogeneous electrode surface and to the diffusion of ions in the electrode. Thus, the double-layer capacity and Warburg impedance of the Randles circuit are replaced by the constant-phase elements [52, 125]. In general, the appearance of a CPE may arise from:

(i) a distribution of the relaxation times as a result of inhomogenities existing at the electrode-electrolyte interface;

(ii) porosity;

(iii) the nature of the electrode;

(iv) dynamic disorder associated with diffusion.

But, for the bare GCE electrode in the same electrolyte solution, the equivalent circuit consists of an active electrolyte resistance Rs in series with the parallel combination of the double-layer capacitance $C_d$ and an impedance of the Faradic reaction. The impedance of the Faradic reaction consists of an active charge transfer resistance Rct and a specific electrochemical element of diffusion W. The results imply that the electrode behavior follow the Randles equivalent circuit model and may be associated with inhomogeneous semi-infinite diffusion of the probe to the electrode surface indicating small deviation from the ideal semi-infinite diffusion kinetics [126].

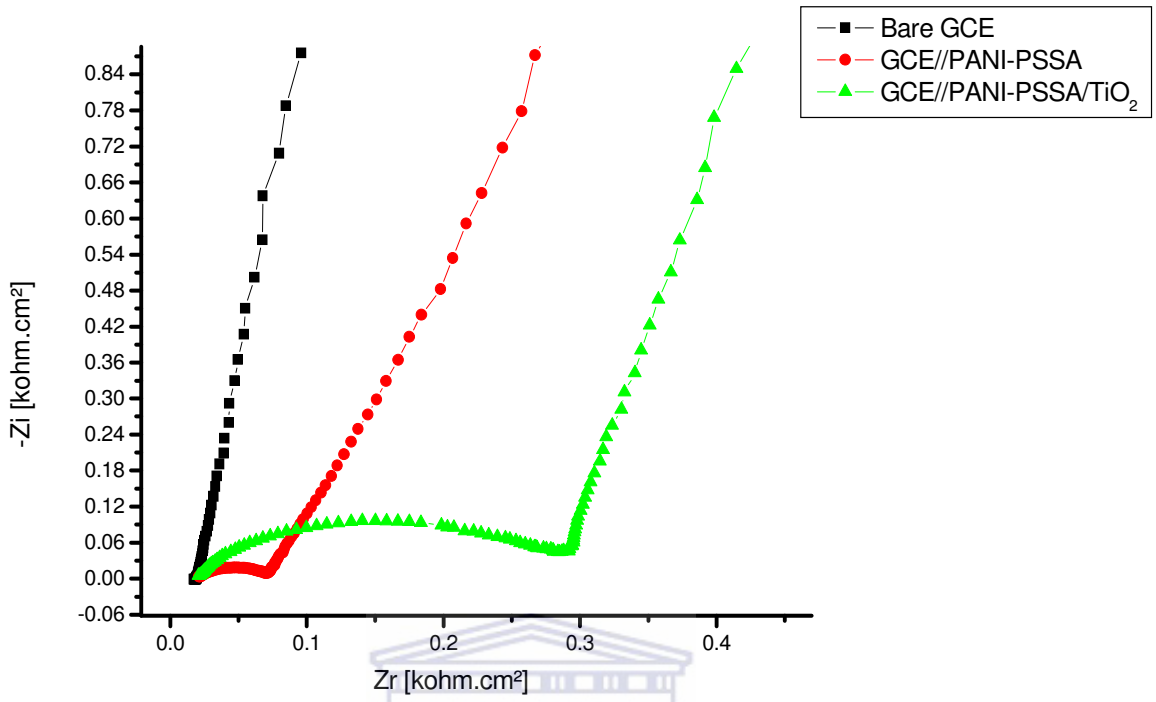


***Figure 4.22: Electrochemical impedance spectra (Nyquist plot) of electrode materials deposited on a glassy carbon working electrode***



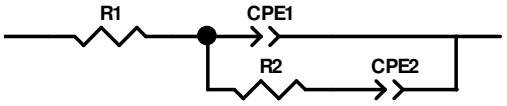


Fitting for GCE//PANI-PSSA/$TiO_2$

| Element | Freedom | Value | Error | Error % |
|---|---|---|---|---|
| R1 | Free(±) | 20.04 | 0.283 | 1.4122 |
| CPE1-T | Free(±) | 1.7133E-06 | 6.7235E-08 | 3.9243 |
| CPE1-P | Free(±) | 0.82773 | 0.0038455 | 0.46458 |
| R2 | Free(±) | 492.1 | 2.5885 | 0.52601 |
| CPE2-T | Free(±) | 0.00032429 | 1.9894E-06 | 0.61346 |
| CPE2-P | Free(±) | 0.91506 | 0.0032637 | 0.35667 |

***Figure 4.23: Equivalent circuit diagram for the GCE//PANI-PSSA/$TiO_2$ modified electrode***

In order to confirm the mechanism suggested in the voltammetric part of this work regarding the construction of the nanocomposite of $TiO_2$ interaction, EIS measurement was performed. Electrochemical impedance spectroscopy is represented in figure 4.22 by a Nyquist plot. The Nyquist plot presents the real (Z') and imaginary (Z'') parts of the complex impedance as a function of frequency [127-128]. The impedance spectra were collected at 250 mV in a frequency range from 100 Hz to 10 mHz. All of the electrode modification including the bare GCE show an increase in the impedance on the imaginary (Z'') part of the complex impedance (Nyquist) plot with a decrease in frequency, which this indicates the typical capacitive behaviour [22].

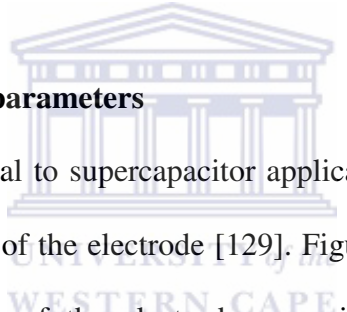


**4.6 Some other considerable parameters**

Since a long cycle-life is critical to supercapacitor applications, a cycle test was carried out to examine the service life of the electrode [129]. Figure 4.24 and figure 4.25 below show the cyclic performances of the electrodes examined by galvanostatic charge–discharge tests for 10 cycles. It is observed that the capacitances and energy of electrodes calculated from charge–discharge curves exhibit close to no decay during the tests, which implies their excellent long-term recycling capabilities [130]. Reasonably stable and constant values of capacitance have been observed for each electrode modification up to 10 cycles. A slight fluctuation in capacitance for initial cycle has been observed, which is attributed to the charge consumption due to some possible faradic reaction(s) with loosely bound surface groups at the electrode electrolyte interfaces. The variation of charge-discharge capacitance with cycle number exhibits that the capacitor has stable capacitance over number of cycles [97, 131].

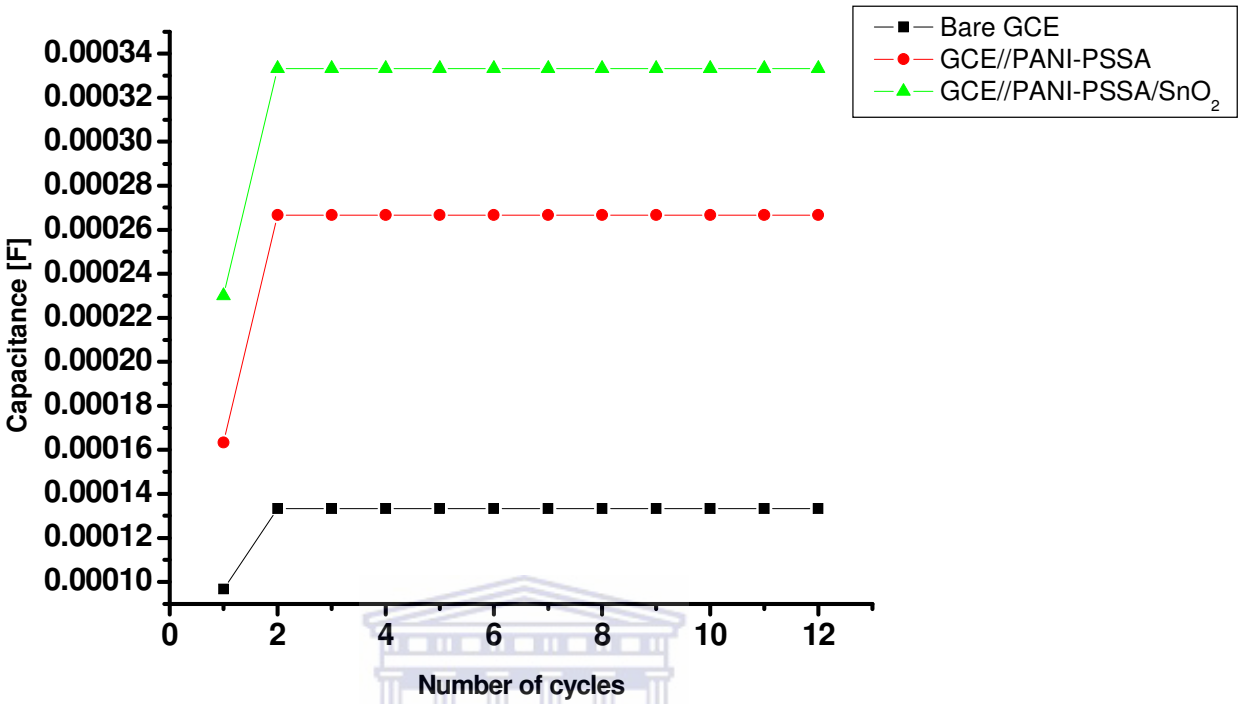


***Figure 4.24: Capacitance vs. number of cycles for bare GCE, GCE//PANI-PSSA and gce//pani-pssa/$SnO_2$.***

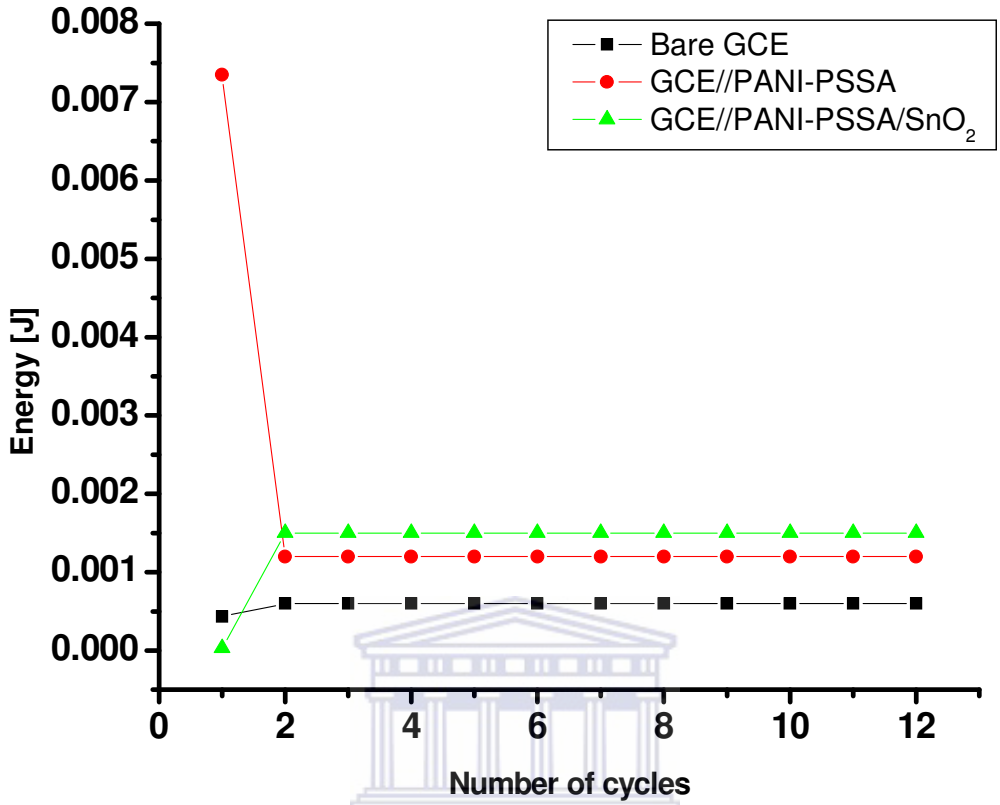




***Figure 4.25: Energy vs. number of cycles for bare GCE, GCE//PANI-PSSA and gce//pani-pssa/$SnO_2$.***

Figure 4.26 below shows power density versus number of charge-discharge cycles for both the GCE//PANI-PSSA and GCE// PANI-PSSA/$SnO_2$ modified electrodes. Same power density has been observed for both electrode modifications despite the first cycle having a decrease in density for the initial step of the gce//pani-pssa/$SnO_2$ electrode and an increase for the GCE// PANI-PSSA electrode.

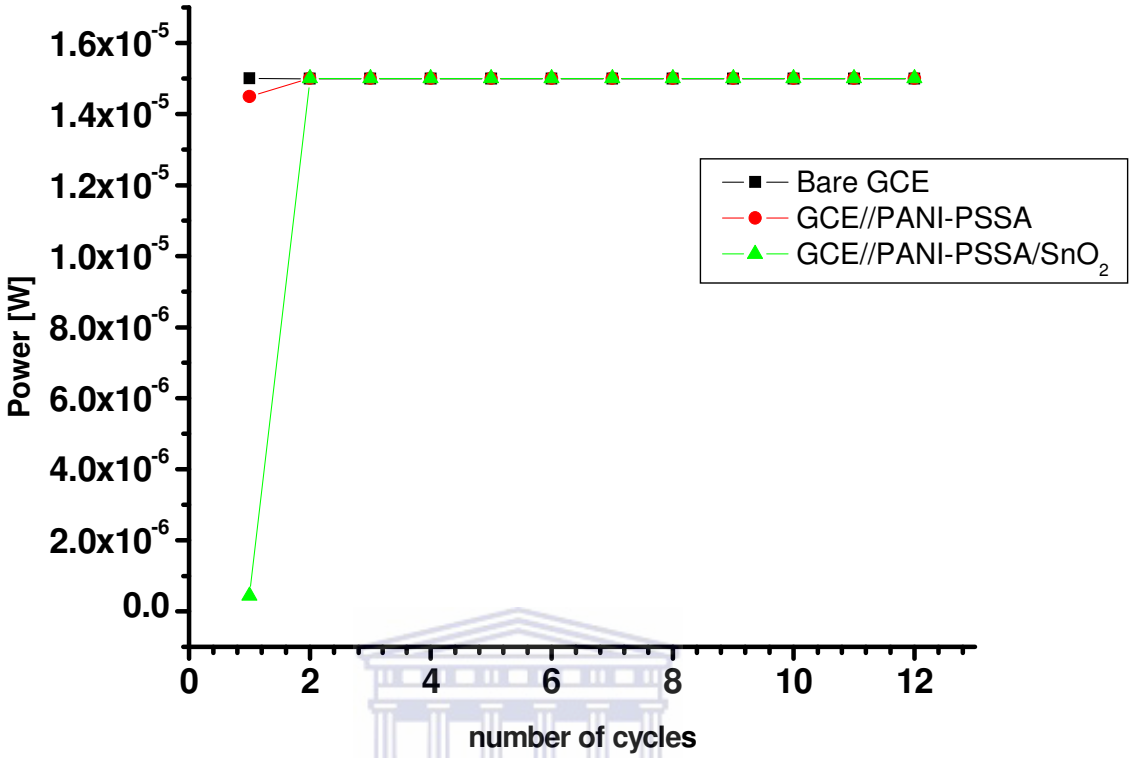


***Figure 4.26: Power vs. number of cycles for bare GCE, GCE// PANI-PSSA and GCE// PANI-PSSA/$SnO_2$.***



The relation between power density and energy density has attracted much attention in evaluation of the performance of electrochemical capacitors, especially since such devices are perceived as capable of delivering high power on discharge although intrinsically their energy density is low. An important basis for relating power density to energy density takes the form of graphical presentation by a Ragone plot displayed by figure 2.1 in Chapter 2. In evaluating the performance of electrochemical capacitors, as for batteries, characterization of their energy density and power density is one of the most important aspects of rating such electrochemical power devices [39]. The following

figures represent the improved capacitance, energy and power densities of the differently modified electrodes based on nano-$TiO_2$ electrode material.

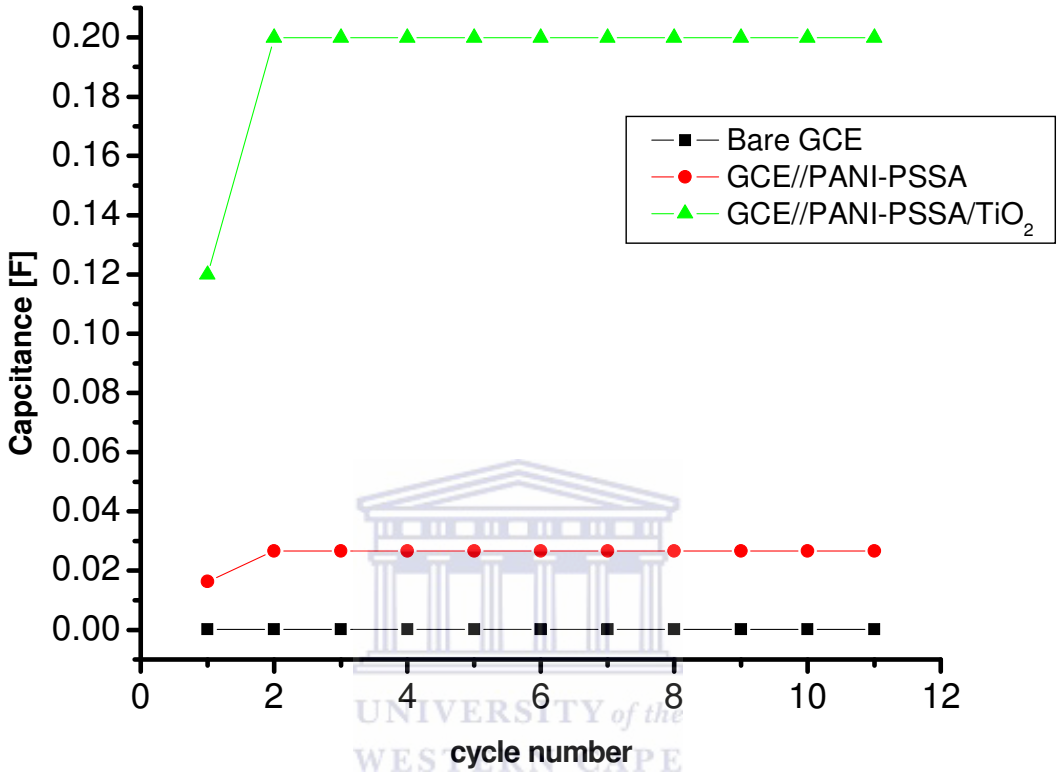




***Figure 4.27: Capacitance vs. number of cycles for bare GCE, GCE// PANI-PSSA and GCE// PANI-PSSA/$TiO_2$***

As shown in figure 4.27, the increasing trend of the specific capacitance from the lowest capacitance resulting form a non-modified bare glassy carbon electrode to the highest capacitance originating from the fully modified electrode, GCE//PANI-PSSA/$TiO_2$. An initial step of drastic increase in capacitance is observed for all the electrode modifications as a result of probably some loosely held particle and of reaction

initialization step. The initializing step is, however, not visible for a bare electrode due to there not being any redox active materials.

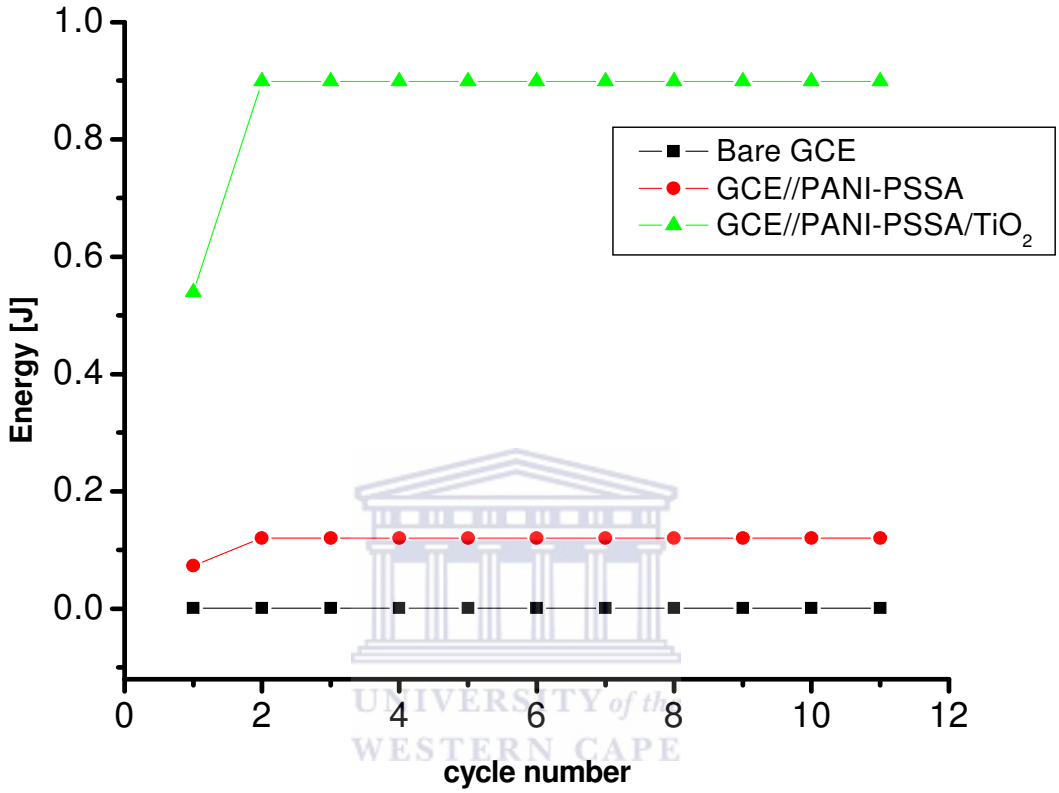




***Figure 4.28: Energy vs. number of cycles for bare GCE, GCE// PANI-PSSA and GCE// PANI-PSSA/$TiO_2$.***

Both figures 4.28 and 4.29 show energy density and power density, respectively. Similarly to the capacitance distribution, the trend here is also correspondent. Higher energy and power density is observed after modification with the metal oxide on the doped electropolymerized polyaniline.

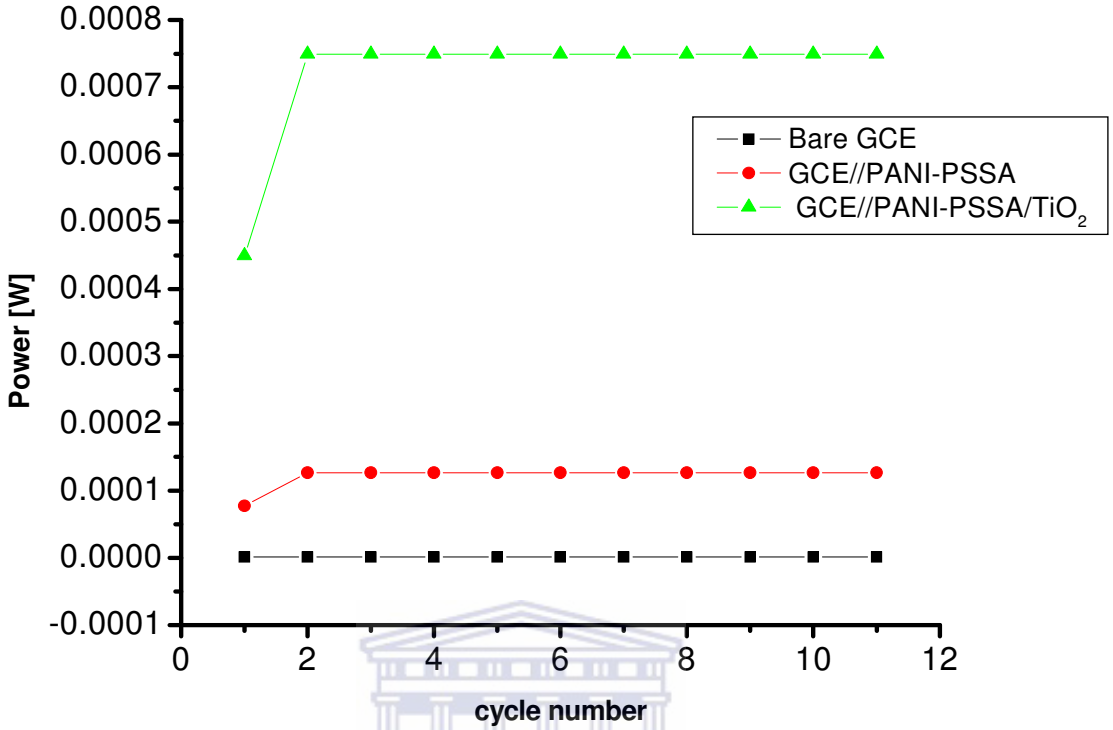


***Figure 4.29: Power vs. number of cycles for bare GCE, GCE// PANI-PSSA and GCE// PANI-PSSA/$TiO_2$***



### 4.7 Charge distribution against Scan rate

Charge is the fundamental property of a matter that exhibit electrostatic attraction or repulsion over other matter. Electric charge is a characteristic property of many subatomic particles. The charges of free-standing particles are integer multiples of the elementary charge *e* and hence we say that electric charge is *quantized*. Michael Faraday, in his electrolysis experiments, was the first to note the discrete nature of electric charge. The symbol *Q* is often used to denote a quantity of electricity or charge. The quantity of electric charge can be directly measured with an electrometer, or indirectly measured with a ballistic galvanometer and rather calculated using the following formula:

$$Q = \int_{t_i}^{t_f} Idt \qquad (eqn.\ 4.9)$$

Where, $Q$ is the charge measured in coulombs (C), $I$ denoting current density measured on amperes (A) and d$t$ denoting change in time per seconds. Table 4.2 lists the charge density of PANI-PSSA and PANI-PSSA/$SnO_2$ modified electrodes along with the respective potential scan rate. From the date obtained from the table, graphical data was constructed in order to discuss the finding of the charge against scan rate.

***Table 4.2: Charge against scan rate of modified electrodes for nano-$SnO_2$ metal oxide.***

| ***Scan rate (mV/s)*** | ***Charge (μC) GCE//PANI-PSSA/$SnO_2$*** | ***Charge (μC) GCE//PANI-PSSA*** |
|---|---|---|
| 40 | 86.23 | 45.33 |
| 50 | 50.81 | 28.25 |
| 70 | 65.81 | 49.47 |
| 100 | 50.56 | 36.62 |
| 200 | 21.66 | 11.06 |
| 400 | 11.97 | 7.568 |



Figure 4.30 shows an initial drastic decrease in charge density for lower scan rates. At scan rates of 50 to 70 mV/s, a slight increase in charge density has been observed for both modifications of electrodes, thereafter, a steady decrease in charge was witnessed. Though, however, the charge densities of the $TiO_2$ and $SnO_2$ modified electrodes have been much higher than that of the PANI-PSSA only modified electrode across all scan rates.

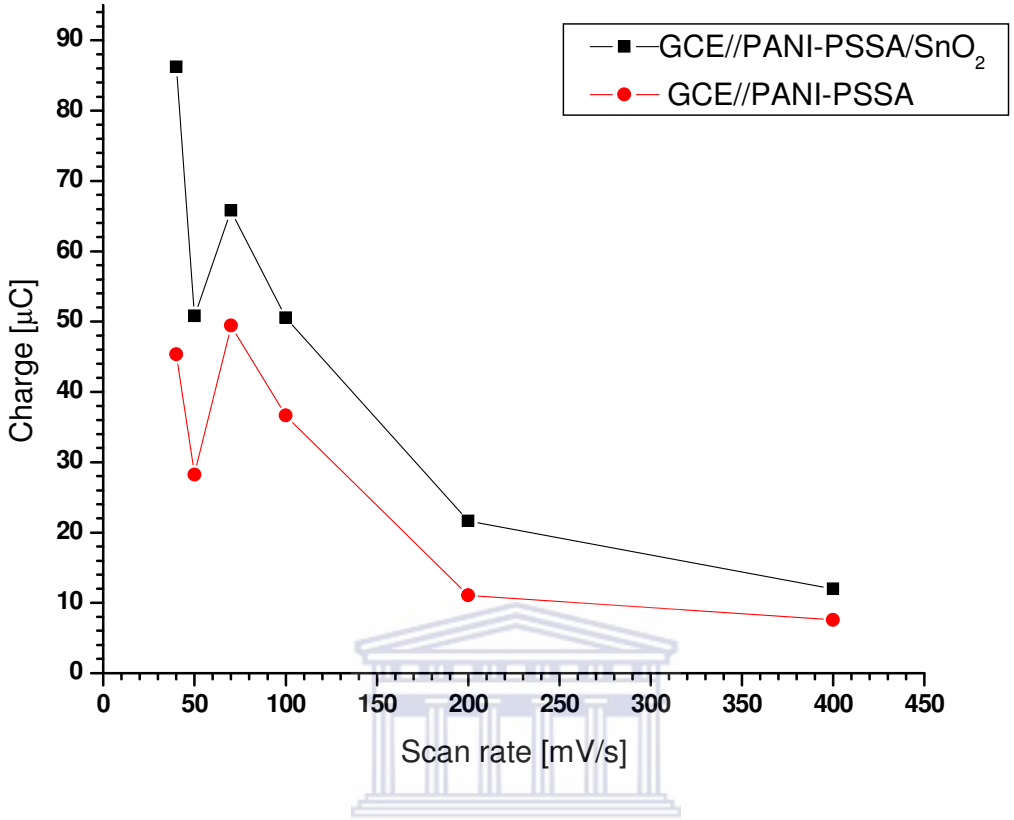


***Figure 4.30 Charge density against potential scan rate for GCE// PANI-PSSA and GCE// PANI-PSSA/$SnO_2$.***



Similarly to the above nano-$SnO_2$ electrodes, the nano-$TiO_2$ modified electrode also shows significant decrease in charge density as the potential sweep rate is increase, which then eventually leads to a decrease in capacitance against an increasing scan rate. Figure 4.31 shows the graphical decreasing trend of the capacitance as a function of scan rate. Improved capacitance is evidently witnessed at lower potential scan rate for the GCE//PANI-PSSA/$TiO_2$ modified electrode at all points compared to the PANI-PSSA modified electrodes. The increased capacitance of the $TiO_2$ modified electrode is doubled from the only polyaniline modified electrode.

*Table 4.3: Charge against scan rate of modified electrodes for nano-$TiO_2$ metal oxide*.

| *Scan rate (mV/s)* | *Charge (μC) GCE//PANI-PSSA/$TiO_2$* | *Charge (μC) GCE//PANI-PSSA* |
|---|---|---|
| 40 | 69.52 | 35.64 |
| 50 | 40.87 | 20.68 |
| 70 | 60.48 | 37.00 |
| 100 | 44.60 | 29.70 |
| 200 | 19.76 | 11.41 |
| 400 | 13.85 | 9.941 |

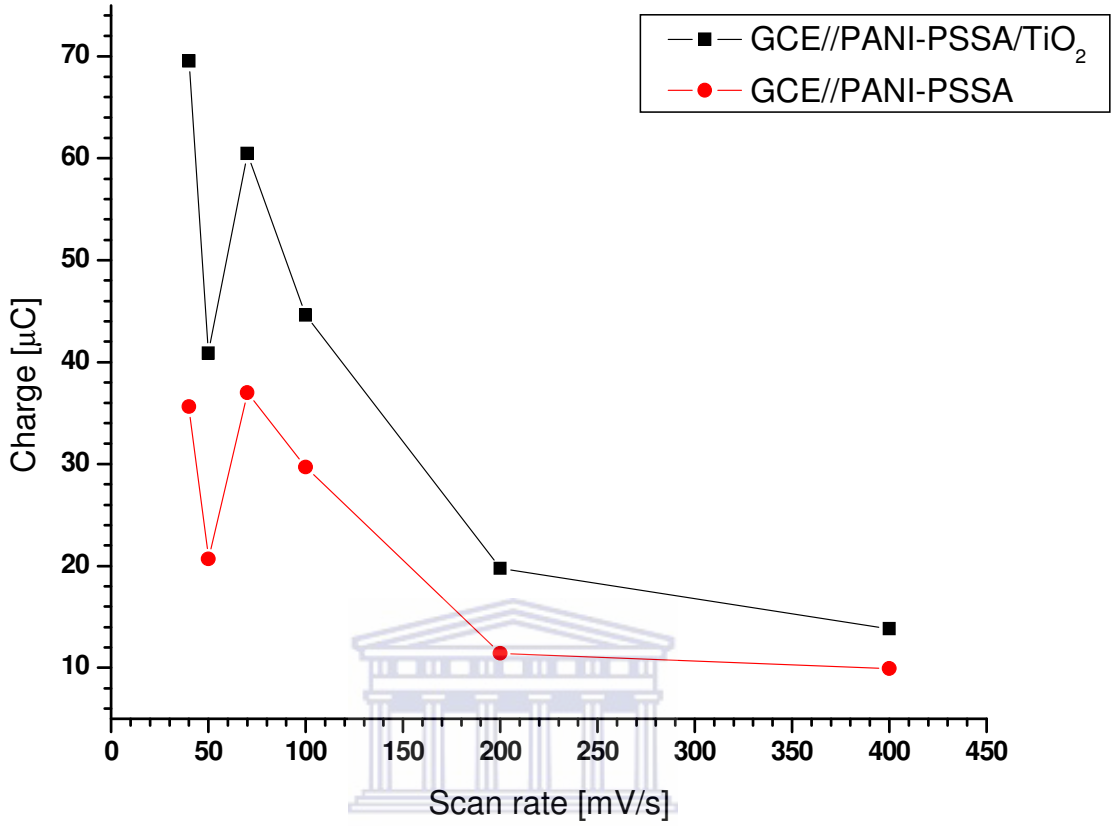




***Figure 4.31 Charge density against potential scan rate for GCE// PANI-PSSA and GCE// PANI-PSSA/$SnO_2$.***

**4.8 Performance evaluation of Capacitance against Scan rate**

The section demonstrates the importance of sweep potential (scan rate) against capacitance calculated based on cyclic voltammetry and electrochemical impedance spectroscopy. The modified electrode was characterised in 1M KCl electrolyte solution as mentioned in the experimental section at differing scan rates from 40, 50, 70, 100, 200 and up to 400 $mV.s^{-1}$. It has been mentioned that the current density was directly proportional to the scan rate witnessed on the effect of scan rate voltammograms.

Capacitance of the differently modified electrodes has been calculated using a formula stated on equation 4.10 below with all parameters mentioned above.

$$\text{Specific capacitance } C = \frac{Q}{\Delta E \times m} \qquad \textit{(eqn. 4.10)}$$

It has been also noticed that charge, however, decreases with increase of scan rate. Though not significantly so, but the trend shows inverse proportionality of charge and scan rate. Hence, capacitance is calculated to be inversely proportional to the scan rate. Thus as scan rate is increased, the capacitance decreases. The following Table 4.4 shows corresponding values of scan rate to the specific capacitance of the differently modified electrodes.



***Table 4.4: Capacitance against scan rate of modified electrodes for nano-$SnO_2$ metal oxide.***

| ***Scan rate (mV/s)*** | ***Capacitance (F/g) GCE//PANI-PSSA/$SnO_2$*** | ***Capacitance (F/g) GCE//PANI-PSSA*** |
|---|---|---|
| 40 | 3.320 | 0.0184 |
| 50 | 1.956 | 0.01148 |
| 70 | 2.534 | 0.0201 |
| 100 | 1.947 | 0.01488 |
| 200 | 0.834 | 0.00449 |
| 400 | 0.461 | 0.00308 |

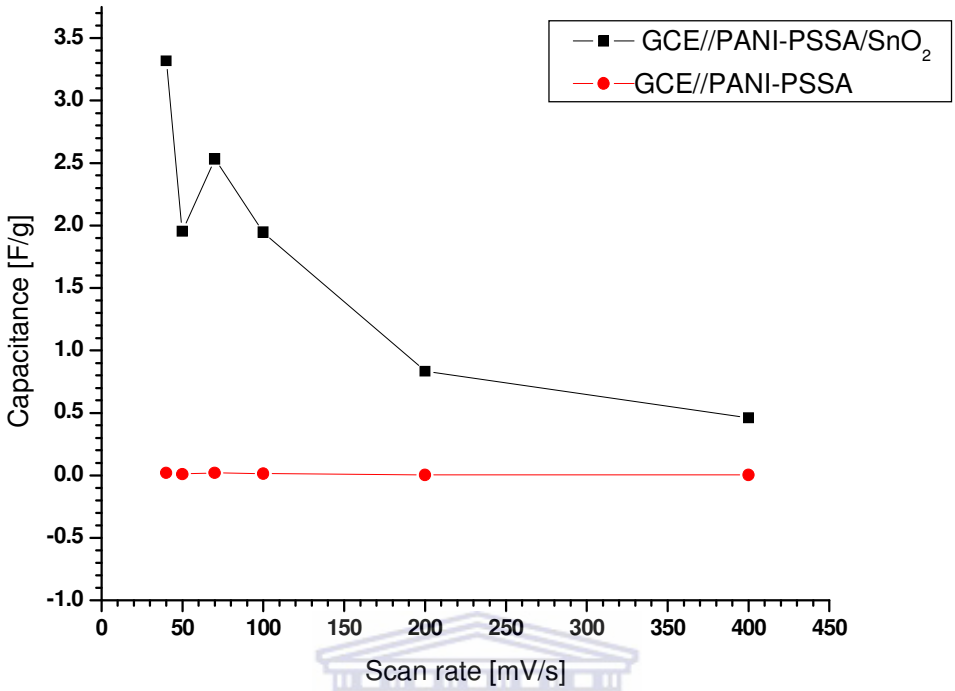


***Figure 4.32: variation of scan rate against specific capacitance of GCE// PANI-PSSA and GCE// PANI-PSSA/$SnO_2$ electrodes.***



The above figure 4.32 demonstrates the variation of potential scan rate against specific capacitance. There is much improvement of the capacitance in the $SnO_2$ modified electrode as compared to the PANI-PSSA electrode. The trend, however, is still a visible phenomenon as the potential scan rate is increased, the specific capacitance in decreasing. It is usually noted in cyclic voltammetry that when current density is increased the capacitance is decreased so as for the increase in scan rate leads to increased current density [132-133]

***Table 4.5: Capacitance against scan rate of modified electrodes for nano-$TiO_2$ metal oxide.***

| *Scan rate (mV/s)* | *Capacitance (F/g) GCE//PANI-PSSA/$TiO_2$* | *Capacitance (F/g) GCE//PANI-PSSA* |
|---|---|---|
| 40 | 16.0312 | 11.531667 |
| 50 | 9.4246 | 6.69121 |
| 70 | 13.9466 | 11.9717 |
| 100 | 10.284697 | 9.6097 |
| 200 | 4.5563 | 3.69182 |
| 400 | 3.19379 | 3.21651 |

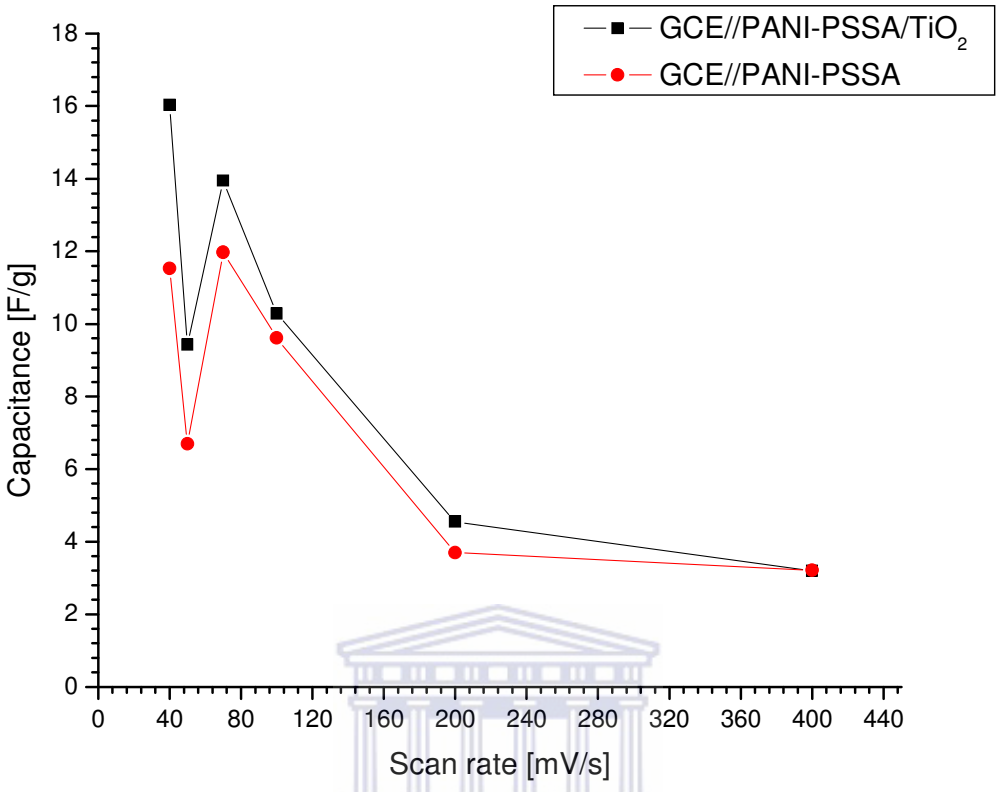


***Figure 4.33: variation of scan rate against specific capacitance of GCE// PANI-PSSA and GCE// PANI-PSSA /$TiO_2$ electrodes.***



The figure 4.33 above shows the effect of cyclic voltammetric sweeping rate on the specific capacitance. Theoretically, specific capacitance of ideal electrochemical capacitor material is not affected by potential scan rate, but if the rate is too fast, active material in electrode cannot fully react owing to material resistance, which can lead to effective specific capacitance decreasing. When cyclic voltammetric sweeping rate increases from 10 to 100mV$s^{-1}$, specific capacitance reduces to close to approximately 40% for both modifications of electrodes and thereafter as potential scan rate increases, more decrease in specific capacitance is profound [134]. Hence, lower potential scan rate

in the figures above show higher capacitance than those scanned at higher rates, evidently shown that the specific capacitance decreases with increase in scan rate.

# CHAPTER 5

# CONCLUSIONS AND RECOMMENDATIONS

## 5.1 Conclusion

Considering a lot of factors in this study, I entirely believe that every result found is worthwhile. From successfully preparing dispersion of the metal oxides used to successfully doping aniline with $SO_3^=$ ions and electro-synthesizing the doped conducting polymer. All electrochemical techniques used to characterize the materials prepared were outstandingly relevant to the study conducted.

Nanocomposite of poly-4-styrene sulfonic acid doped polyaniline with Tin dioxide ($SnO_2$) and titanium dioxide ($TiO_2$) were successfully studied on the surface of the glassy carbon microelectrode with surface area of 0.0702 $cm^{-2}$ and show potential application as supercapacitor electrode materials. The composites show symmetrical charge-discharge curves and demonstrate good stability over time. The Nyquist plots also show capacitive behavior of the constructed nanocomposite of GCE//PANI-PSSA/$SnO_2$ in the sense that the impedance increases on the imaginary part (Zi) as the frequency decreases reaching a close to parallel configuration to the imaginary impedance part. Hence, therefore, GCE//PANI-PSSA/$SnO_2$ shows ideal capacitive behavior for application in supercapacitor compared to GCE//PANI-PSSA due to the increased capacitance from 0.01148 $F.g^{-1}$ of GCE//PANI-PSSA to 1.956 $F.g^{-1}$ of the GCE//PANI-PSSA/$SnO_2$ electrode.

The study of nano-$TiO_2$/polystyrene sulfonic acid doped polyaniline has also been conducted on a GCE surface for potential application as electrode material for

supercapacitors. Improved capacitance of the electrode material has been successfully studied. It has been evaluated that nano-$TiO_2$/PANI-PSSA is a suitable material for application as electrode material for electrochemical capacitors as the capacitance increased from 6.69121 F. $g^{-1}$ of the GCE//PANI-PSSA electrode to 9.4246 F.$g^{-1}$ when $TiO_2$ was deposited to form GCE//PANI-PSSA/$TiO_2$ electrode. The $SnO_2$ based layer-by-layer composite, however, shows better specific capacitance than the $TiO_2$ based composite in most occasions concluded from the fact that the specific capacitance is almost doubled from the GCE//PANI-PSSA to the GCE//PANI-PSSA/$SnO_2$ modified electrode, whereas the specific capacitance of the $TiO_2$ based electrode is only increased about 3 orders of magnitude from GCE//PANI-PSSA to GCE//PANI-PSSA/$TiO_2$ electrode.



**5.2 Recommendation and future work**

This work gives good introductory background on double layer and pseudocapacitors and hence the overall term, supercapacitors. It is recommendable for aspiring electrochemical supercapacitor researchers as it illustrates clearly all basic capacitance behavioral techniques. We have distinctly identified the different types of capacitors as many people would just assume that there is one fundamental type of a capacitor. Due to some shortcomings such as time constraint, instrumentation, etc, we would recommend an additional future work on this study based on the following classifications;

- determining the thickness of the electrode material
- optimizing electrode surface area
- synthesis of bimetallic oxide nanoparticles, and

- synthesis of a mesh composite of conducting polymers and metal oxides.

### 5.3 References


1. Parler, S., *Electrolytic Capacitors*, in *Electrochemistry Encyclopedia*. 2005, Cornell Dubilier Electronics, Inc: Liberty, SC 29657, USA.
2. Ruiz, V., C. Blanco, M. Granda, and R. Santamaría, *Enhanced life-cycle supercapacitors by thermal treatment of mesophase-derived activated carbons.* Electrochimica Acta, 2008. **54**(2): p. 305-310.
3. Online, *Capacitor*, in *Wikipedia, The Free Encyclopedia*. 2009, http://en.wikipedia.org/wiki/Capacitor. [Accessed: Oct 3, 2009].
4. Tuite, D., *Get the Lowdown on Ultracapacitors.* http://electronicdesign.com/Articles/Index.cfm?AD=1&AD=1&AD=1&ArticleID=17465. [Accessed: Oct 3, 2009], November, 2007.
5. Ltd, W.C., *Battery and Energy Technologies*, in *Electropedia*. 2010, Woodbank Communications Ltd 2005: South Crescent Road, Chester, CH4 7AU, (United Kingdom).
6. Barrade, P., *Energy storage and applications with supercapacitors*, Laboratoire d'Electronique Industrielle, LEI, STI-ISE, Ecole Polytechnique Fédérale de Lausanne, EPF: CH 1015 Lausanne (Switzerland).
7. Tang, N., X. Tian, C. Yang, and Z. Pi, *Facile synthesis of [alpha]-MnO2 nanostructures for supercapacitors.* Materials Research Bulletin, 2009. **44**(11): p. 2062-2067.

8. Yan, J., Z. Fan, T. Wei, J. Cheng, B. Shao, K. Wang, L. Song, and M. Zhang, *Carbon nanotube/MnO2 composites synthesized by microwave-assisted method for supercapacitors with high power and energy densities.* Journal of Power Sources, 2009. **194**(2): p. 1202-1207.

9. Liu, E.-H., W. Li, J. Li, X.-Y. Meng, R. Ding, and S.-T. Tan, *Preparation and characterization of nanostructured NiO/MnO2 composite electrode for electrochemical supercapacitors.* Materials Research Bulletin, 2009. **44**(5): p. 1122-1126.

10. Lee, B.J., S.R. Sivakkumar, J.M. Ko, J.H. Kim, S.M. Jo, and D.Y. Kim, *Carbon nanofibre/hydrous RuO2 nanocomposite electrodes for supercapacitors.* Journal of Power Sources, 2007. **168**(2): p. 546-552.

11. Roberts, A.J. and R.C.T. Slade, *Effect of specific surface area on capacitance in asymmetric carbon/[alpha]-MnO2 supercapacitors.* Electrochimica Acta. **In Press, Corrected Proof**.

12. Rajendra Prasad, K. and N. Miura, *Electrochemically synthesized MnO2-based mixed oxides for high performance redox supercapacitors.* Electrochemistry Communications, 2004. **6**(10): p. 1004-1008.

13. Xia, H., J. Feng, H. Wang, M.O. Lai, and L. Lu, *MnO2 nanotube and nanowire arrays by electrochemical deposition for supercapacitors.* Journal of Power Sources. **In Press, Corrected Proof**.

14. En-Hui Liu, W.L., Jian Li, Xiang-Yun Meng, Rui Ding, Song-Ting Tan. , *Preparation and characterization of nanostructured NiO/MnO2 composite*

*electrode for electrochemical supercapacitors.* Materials Research Bulletin 2009. **44**(5): p. 1122-1126.

15. Hu, C.-C. and T.-W. Tsou, *The optimization of specific capacitance of amorphous manganese oxide for electrochemical supercapacitors using experimental strategies.* Journal of Power Sources, 2003. **115**(1): p. 179-186.

16. Huang, Q., X. Wang, and J. Li, *Characterization and performance of hydrous manganese oxide prepared by electrochemical method and its application for supercapacitors.* Electrochimica Acta, 2006. **52**(4): p. 1758-1762.

17. Magdalena Skunik, M.C., Iwona A. Rutkowska, Pawel J. Kulesza., *Improved capacitance characteristics during electrochemical charging of carbon nanotubes modified with polyoxometallate monolayers.* Electrochimica Acta 2008. **53**(11): p. 3862–3869.

18. Wang, G.-X., B.-L. Zhang, Z.-L. Yu, and M.-Z. Qu, *Manganese oxide/MWNTs composite electrodes for supercapacitors.* Solid State Ionics, 2005. **176**(11-12): p. 1169-1174.

19. Guixin Wang, M.Q., Zuolong Yu , Rongzhong Yuan, *LiNi0.8Co0.2O2/MWCNT composite electrodes for supercapacitors.* Materials Chemistry and Physics 2007. **105**(2-3): p. 169–174.

20. V.V. Pani´c, R.M.S.c., V.M. Jovanovi ´c, A.B. Dekanski, *Electrochemical and capacitive properties of thin-layer carbon black electrodes.* Journal of Power Sources 2008. **181**(1): p. 186-192.

21. Chang, J., S. Lee, T. Ganesh, R.S. Mane, S. Min, W. Lee, and S.-H. Han, *Viologen-assisted manganese oxide electrode for improved electrochemical*

*supercapacitors.* Journal of Electroanalytical Chemistry, 2008. **624**(1-2): p. 167-173.

22. Kentaro Kuratani, T.K., Nobuhiro Kuriyama, *Influence of the mesoporous structure on capacitance of the RuO2 electrode.* Journal of Power Sources, 2009. **1157**(1): p. Article in press.

23. Sang-Bok Ma, K.-W.N., Won-Sub Yoon, Xiao-Qing Yang, Kyun-Young Ahn, Ki-Hwan Oh, Kwang-Bum Kim, *Electrochemical properties of manganese oxide coated onto carbon nanotubes for energy-storage applications.* Journal of Power Sources 2008. **178**(1): p(483–489).

24. Mao-SungWu, C.-Y.H., Kun-Hao Lin., *Electrophoretic deposition of nickel oxide electrode for high-rate electrochemical capacitors.* Journal of Power Sources 2009. **186**(2): p. 557-564.

25. Guang-Yu Zhao, H.-L.L., *Preparation of polyaniline nanowire arrayed electrodes for electrochemical supercapacitors.* Microporous and Mesoporous Materials 2008. **110**(2-3): p. 590–594.

26. Philip Lessner, T.-Y., Randolf S. Hahn, Veeriya Rajasekaran, *Preparation of conductive polymers from stabilized precursor solution*. 1999, Kemet Electronics Corparation: United States Patent.

27. Hideo Yamamoto, M.O., Minoru Fukuda, Isao Isa, Katsumi Yoshino., *Characteristics of aluminium solid electrolytic capacitors using conducting polymer.* Journal of Power Sources 1996. **60**(2): p. 173-177.

28. P. Zhao, R., B.K. Lok , F.K. Lai, C.C. Tin, J.H. Zhao, R.M. Yar, *Investigation of Ta2O5/SiO2/4H-SiC MIS capacitors.* Microelectronic Engineering 2006. **83**(1): p. 58-60.

29. E. Atanassova, D.S., A. Paskaleva, M. Georgieva, J. Koprinarova. , *Electrical characteristics of Ti-doped Ta2O5 stacked capacitors.* Thin Solid Films 2008. **516**(23): p. 8684–8692.

30. Jae-Chan Kwak, Y.-H.L., Byung-Ho Choi., *Preparation of tantalum oxide thin films by photo-assisted atomic layer deposition.* Applied Surface Science, 2004. **230**(1-4): p. 249–253.

31. C. Chaneliere, J.L.A., R.A.B. Devine, B. Balland, *Tantalum pentoxide (Ta2Os) thin films for advanced dielectric applications. A review.* Materials Science and Engineering, 1998. **R22**(6): p. 269-322.

32. G. Aygun a, R.T., *Electrical and dielectrical properties of tantalum oxide films grown by Nd:YAG laser assisted oxidation.* Thin Solid Films 2008. **517**(2): p. 994-999.

33. J.W. Schultze, H.K., *Application potential of conducting polymers.* Electrochimica Acta 2005. **50**(7-8): p. 1739–1745.

34. C. Constantinescu, N.S., A. Moldovan, M. Dinescu, C. Vasiliu, *Thin films of polyaniline deposited by MAPLE technique.* Applied Surface Science 2007. **253**(19): p. 7711–7714.

35. Daniel A. Scherson, A.P., *Batteries and Electrochemical Capacitors.* The Electrochemical Society Interface, 2006(Spring 2006).

36. Christen, T. and M.W. Carlen, *Theory of Ragone plots.* Journal of Power Sources, 2000. **91**(2): p. 210-216.

37. Su, Y.-f., F. Wu, L.-y. Bao, and Z.-h. Yang, *RuO2/activated carbon composites as a positive electrode in an alkaline electrochemical capacitor.* New Carbon Materials, 2007. **22**(1): p. 53-57.

38. Reddy, R.N. and R.G. Reddy, *Sol-gel MnO2 as an electrode material for electrochemical capacitors.* Journal of Power Sources, 2003. **124**(1): p. 330-337.

39. Conway, B.E., *Electrochemical Supercapacitors: Scientific Fundamentals and Technological Applications*. 1999, New York: Kluwer Academic/Plenum.

40. Shu-Juan Bao, B.-L.H., Yan-Yu Liang, Wen-Jia Zhou, Hu-Lin Li. , *Synthesis and electrochemical characterization of amorphous MnO2 for electrochemical capacitor.* Materials Science and Engineering, 2005. **A 397**(1-2): p. 305-309.

41. Conway, B.E., V. Birss, and J. Wojtowicz, *The role and utilization of pseudocapacitance for energy storage by supercapacitors.* Journal of Power Sources. **66**(1-2): p. 1-14.

42. Miura, V.G.a.N., *Electrochemically Deposited Polyaniline Nanowire's Network: A High-Performance Electrode Material for Redox Supercapacitor.* Electrochemical and Solid-State Letters, 2005. **8**(12): p. A630-A632.

43. Sharma, P. and T.S. Bhatti, *A review on electrochemical double-layer capacitors.* Energy Conversion and Management. **In Press, Corrected Proof**.

44. Zhang, Y., H. Feng, X. Wu, L. Wang, A. Zhang, T. Xia, H. Dong, X. Li, and L. Zhang, *Progress of electrochemical capacitor electrode materials: A review.* International Journal of Hydrogen Energy, 2009. **34**(11): p. 4889-4899.

45. M. Jayalakshmi, K.B., *Simple capacitors to supercapacitors- An Overview.* International Journal of Electrochemical Science, 2008. **3**: p. 1196-1217.

46. Niwa, S. and Y. Taketani, *Development of new series of aluminium solid capacitors with organic semiconductive electrolyte (OS-CON).* Journal of Power Sources, 1996. **60**(2): p. 165-171.

47. Burke, A., *Ultracapacitors: why, how, and where is the technology.* Journal of Power Sources, 2000. **91**(1): p. 37-50.

48. Jayalakshmi, M., M.M. Rao, N. Venugopal, and K.-B. Kim, *Hydrothermal synthesis of SnO2-V2O5 mixed oxide and electrochemical screening of carbon nano-tubes (CNT), V2O5, V2O5-CNT, and SnO2-V2O5-CNT electrodes for supercapacitor applications.* Journal of Power Sources, 2007. **166**(2): p. 578-583.

49. Shi, H., *Activated carbons and double layer capacitance.* Electrochimica Acta, 1996. **41**(10): p. 1633-1639.



50. Qu, D. and H. Shi, *Studies of activated carbons used in double-layer capacitors.* Journal of Power Sources, 1998. **74**(1): p. 99-107.

51. Bagotsky, V.S., *Fundamentals of Electochemistry*. Second Edition ed. 2006, Hoboken, New Jersey: John Wiley & Sons, Inc.

52. Girija, T.C. and M.V. Sangaranarayanan, *Investigation of polyaniline-coated stainless steel electrodes for electrochemical supercapacitors.* Synthetic Metals, 2006. **156**(2-4): p. 244-250.

53. Richard Akinyeye, I.M., Shaniel Botha, Priscilla Baker, Emmanuel Iwuoha, *Electrocatalytic sensor applications of nanostructured polypyrroles and*

*polythiophenes*, in *Transworld Research Network*, K.I. Ozoemena, Editor. 2007: Kerila, India.

54. Immaculate Michira, M.K., R. O. Akinyeye, V. Somerset, M. Sekota, A. Al-Ahmed, Priscilla Baker, Emmanuel Iwuoha, *Anthracene sulphonic acid-doped polyanilines: Electrodynamics and application as amperometric peroxide biosensor*, in *Transworld Research Networks*, K.I. Ozoemena, Editor. 2007: Kerala, India.

55. Ntlaseng G.R, M., Aoife Morrin, Emmanuel I. Iwuoha, *Electrochemistry and scanning electron microscopy of polyaniline/peroxidase-based biosensor.* Talanta, 2004. **64**(1): p. 115-120.

56. Emmanuel I. Iwuoha, D.S.D.V., Nuria P. Garcia, Malcolm R. Smyth, Jose M. Pingarron, *Reactivity of organic phase biosensors. The amperometric behaviour of horseradish peroxidase immobilised on a platinum electrode modified with an electrosynthetic polyaniline film.* Biosensors and Bioelectronics, 1997. **12**(8): p. 749-761.

57. Deepak Verma, V.D., *Role of novel microstructure of polyaniline-CSA thin film in ammonia sensing at room temperature.* . Sensors and Actuators 2008. **B 134**(2): p. 373–376.

58. Yin-Hou Chen, J.-Y.W., Yi-Chang Chung, *Preparation of polyaniline-modified electrodes containing sulfonated polyelectrolytes using layer-by-layer techniques.* Biosensors and Bioelectronics 2006. **22**(4): p. 489-494.

59. Ming Huanga, C.-H.C.a.T.-C.W., *Development and characterization of flexible electrochromic devices based on polyaniline and poly(3,4-*

*ethylenedioxythiophene)-poly(styrene sulfonic acid)* Electrochimica Acta, 2006. **51**(26): p. 5858-5863.

60. Xing Hu, Y.-Y.Z., Kai Tang, Guo-Lin Zou, *Hemoglobin-biocatalysts synthesis of a conducting molecular complex of polyaniline and sulfonated polystyrene.* Synthetic Metals, 2005. **150**(1): p. 1-7.

61. Sambhu Bhadraa, D.K., Nikhil K. Singha, Joong Hee Lee, *Progress in preparation, processing and applications of polyaniline.* Progress in Polymer Science, 2009. **34**(8): p. 783-810.

62. Bhadra, S., N.K. Singha, and D. Khastgir, *Polyaniline by new miniemulsion polymerization and the effect of reducing agent on conductivity.* Synthetic Metals, 2006. **156**(16-17): p. 1148-1154.

63. Fielda, J.S. and M.V. Swain, *The indentation characterisation of the mechanical properties of various carbon materials: Glassy carbon, coke and pyrolytic graphite.* Carbon, 1996. **34**(11): p. 1357-1366.

64. Henning Lund, O.H., *Organic Electrochemistry*. Fourth ed. 2001, New York: Marcel Dekker Inc.

65. Maier, K. *Wisegeek: What is Titanium Dioxide*. 2003 - 2010 [cited 2010 06 April 2010]; Available from: http://www.wisegeek.com/what-is-titanium-dioxide.htm.

66. Winkler, J., *Titanium Dioxide*. 2003, Hannover, Germany: Vincentz Network.

67. Nishino, A., *Capacitors: operating principles, current market and technical trends.* Journal of Power Sources, 1996. **60**(2): p. 137-147.

68. Raül Díaz, I.D.-P., Pau Gorostiza, Fausto Sanz and Joan R. Morante, *An Electrochemical Study of Tin Oxide Thin Film in Borate Buffer Solutions.* Chem. Soc, 2003. **14**(4): p. 523-529.

69. R. Díaz, I.D.-P., P. Gorostiza, F. Sanz, J. R. Morante, *Tin oxide thin films: electronic properties and growth mechanism under electrochemical control*. 2003, LCTEM and EME, University of Barcelona: Barcelona, Spain.

70. Delgado, R.D., *Tin Oxide Gas Sensors: An Electrochemical Approach*. 2002, University of Barcelona: Barcelona, Spain.

71. M. C. Roco, S.W., P. Alivisatos, *Nanotechnology Research Directions: IWGN Workshop Report - Vision for Nanotechnology R&D in the Next Decade"*. 1999, WTEC, Loyola College in Maryland.

72. F.G Thomas, G.H., *Introduction to voltammetric analysis: Theory and practice*, ed. B. Hamilton. 2001, Collingwood, Australia: CSIRO publishing. p12-14.

73. Wang, J., *Analytical electrochemistry. Study of electrode reactions and interfacial properties*. Third Edition ed. 2006, Hoboken, New Jersey: John Wiley & Sons Inc. p29-33.

74. Nicholson, R.S. and I. Shain, *Theory of Stationary Electrode Polarography. Single Scan and Cyclic Methods Applied to Reversible, Irreversible, and Kinetic Systems.* Analytical Chemistry, 1964. **36**(4): p. 706-723.

75. Monk, P.M.S., *Fundamentals of Electroanalytical Chemistry*. 2001: John Wiley & Sons LTD.

76. Rieger, P.H., *Electrochemistry*. Second Edition ed. 1993: Chapman & Hall.

77. Plambeck, J.A., *Electroanalytical Chemistry: Basic principal and applications*. 1982: John Wiley & Sons Inc.

78. Karden, E., S. Buller, and R.W. De Doncker, *A method for measurement and interpretation of impedance spectra for industrial batteries.* Journal of Power Sources, 2000. **85**(1): p. 72-78.

79. Evgenij Barsoukov, J.R.M., *Impedance spectroscopy: theory, experiment, and applications*. 2nd Edition ed. 2005: John Wiley and Sons.

80. R. Winston Revie, H.H.U., *Corrosion and Corrosion Control*. 4th Eddition ed. 2008: Wiley-Interscience.

81. John R. Scully, D.C.S., Martin W. Kendig, *Electrochemical impedance: Analysis and interpretation*. 1993: ASTM international.

82. Mário G. S. Ferreira, C.M., *Electrochemical and optical techniques for the study and monitoring of metallic corrosion*. Illustrated ed. 1991: Springer.

83. Macdonald, J.R., *Impedance Spectroscopy Theory, Experiment, and Applications*. Second Edition ed, ed. J.R.M. Evgenij Barsoukov. 2005, Hoboken, New Jersey: John Wiley & Sons, Inc.

84. Watt, I.M., *The principles and practice of Electron Microscopy*. Second Edition ed. 1997, New York: Cambridge University Press.

85. David B. Williams, C.B.C., *Transmission Electron Microscopy*. Second Edition ed. Vol. Part 1: Basics. 2009, New York: Springer.

86. Reimer, L., *Transmission Electron Microscopy: Physics of image formation and microanaysis*. 1984, Berlin, Heidelberg, New York, Tokyo: Springer-Verlag.

87. Headridge, J.B., *Electrochemical Techniques for Inorganic Chemists*. 1969, London and New York: Academic Press Inc. (London) Ltd.

88. Bioanalytical Systems, I. *Instruction manual for BASi epsilon for electrochemistry*. 2000-2009 [cited 2010 March, 01.2010]; Available from: http://www.basinc.com/mans/EC_epsilon/Techniques/Cpot/cp.html.

89. Meyer, J.E.P.a.R.T. *FTIR Spectroscopy*. 1994-2009 [cited 2010 April, 13]; Available from: http://www.irgas.com/ftir_spectroscopy.html.

90. SiliconFarEast.com. *FTIR Spectroscopy*. 2001-2005 13 April 2010; Available from: http://www.siliconfareast.com/FTIR.htm.

91. Zheng J.P., H.J., Jow T.R. , *The limitations of energy density for electrochemical capacitors* Journal of the Electrochemical Society, 1997. **144**(6): p. 2026-2031. .

92. Conway, B.E., *Transition from 'supercapacitor' to 'battery' behavior in electrochemical energy storage* Journal of the Electrochemical Society, 1991. **138**(6): p. 1539-1548. .

93. S. Sarangapani, B.V.T., C.-P. Chen, *Materials for electrochemical capacitors theoretical and experimental constraints.* Journal of the Electrochemical Society, 1996. **143**(11): p. 3791-3799. .

94. Sarangapani, S., P. Lessner, J. Forchione, A. Griffith, and A.B. Laconti, *Advanced double layer capacitors.* Journal of Power Sources, 1990. **29**(3-4): p. 355-364.

95. Wen, J. and Z. Zhou, *Pseudocapacitance characterization of hydrous ruthenium oxide prepared via cyclic voltammetric deposition.* Materials Chemistry and Physics, 2006. **98**(2-3): p. 442-446.

96. Conway, B.E., V. Birss, and J. Wojtowicz, *The role and utilization of pseudocapacitance for energy storage by supercapacitors.* Journal of Power Sources, 1997. **66**(1-2): p. 1-14.

97. Hashmi, S.A., A. Kumar, and S.K. Tripathi, *Investigations on electrochemical supercapacitors using polypyrrole redox electrodes and PMMA based gel electrolytes.* European Polymer Journal, 2005. **41**(6): p. 1373-1379.

98. Lee, J.-G., J.-Y. Kim, and S.-H. Kim, *Effects of microporosity on the specific capacitance of polyacrylonitrile-based activated carbon fiber.* Journal of Power Sources, 2006. **160**(2): p. 1495-1500.

99. Prasad, K.R. and N. Miura, *Potentiodynamically deposited nanostructured manganese dioxide as electrode material for electrochemical redox supercapacitors.* Journal of Power Sources, 2004. **135**(1-2): p. 354-360.

100. E. L. Run, J.L.R., *Apparatus for Distilling Aniline*, Standard Oil development Co., Standard inspection Laboratory: Bayonne, NJ.

101. Ndangili, P.M., T.T. Waryo, M. Muchindu, P.G.L. Baker, C.J. Ngila, and E.I. Iwuoha, *Ferrocenium hexafluorophosphate-induced nanofibrillarity of polyaniline-polyvinyl sulfonate electropolymer and application in an amperometric enzyme biosensor.* Electrochimica Acta. **In Press, Corrected Proof**.

102. Mathebe, N.G.R., A. Morrin, and E.I. Iwuoha, *Electrochemistry and scanning electron microscopy of polyaniline/peroxidase-based biosensor.* Talanta, 2004. **64**(1): p. 115-120.

103. Engel, A. and C. Colliex, *Application of scanning transmission electron microscopy to the study of biological structure.* Current Opinion in Biotechnology, 1993. **4**(4): p. 403-411.

104. Skandan, G., Y.J. Chen, N. Glumac, and B.H. Kear, *Synthesis of oxide nanoparticles in low pressure flames.* Nanostructured Materials, 1999. **11**(2): p. 149-158.

105. Yang Liu, J.Y., Wensheng Yang, Tengfeng Xie, Yubai Bai and Tiejin Li, *Influence of hydrothermal temperature on structures and photovoltaic properties of SnO2 nanoparticles.* Journal of Nanoparticle Research, 2000. **2**(3): p.(309–313).

106. Muchindu, M., T. Waryo, O. Arotiba, E. Kazimierska, A. Morrin, A.J. Killard, M.R. Smyth, N. Jahed, B. Kgarebe, P.G.L. Baker, and E.I. Iwuoha, *Electrochemical nitrite nanosensor developed with amine- and sulphate-functionalised polystyrene latex beads self-assembled on polyaniline.* Electrochimica Acta. **In Press, Corrected Proof**.

107. Michalak, F. and P. Aldebert, *A flexible electrochromic device based on colloidal tungsten oxide and polyaniline.* Solid State Ionics, 1996. **85**(1-4): p. 265-272.

108. Li, H., J. Wang, Q. Chu, Z. Wang, F. Zhang, and S. Wang, *Theoretical and experimental specific capacitance of polyaniline in sulfuric acid.* Journal of Power Sources, 2009. **190**(2): p. 578-586.

109. Songa, E.A., O.A. Arotiba, J.H.O. Owino, N. Jahed, P.G.L. Baker, and E.I. Iwuoha, *Electrochemical detection of glyphosate herbicide using horseradish*

*peroxidase immobilized on sulfonated polymer matrix.* Bioelectrochemistry, 2009. **75**(2): p. 117-123.

110. Gurunathan, K. and D.C. Trivedi, *Studies on polyaniline and colloidal TiO2 composites.* Materials Letters, 2000. **45**(5): p. 262-268.

111. Mi, H., X. Zhang, S. Yang, X. Ye, and J. Luo, *Polyaniline nanofibers as the electrode material for supercapacitors.* Materials Chemistry and Physics, 2008. **112**(1): p. 127-131.

112. Girija, T.C. and M.V. Sangaranarayanan, *Polyaniline-based nickel electrodes for electrochemical supercapacitors--Influence of Triton X-100.* Journal of Power Sources, 2006. **159**(2): p. 1519-1526.

113. Bao, S.-J., B.-L. He, Y.-Y. Liang, W.-J. Zhou, and H.-L. Li, *Synthesis and electrochemical characterization of amorphous MnO2 for electrochemical capacitor.* Materials Science and Engineering A, 2005. **397**(1-2): p. 305-309.

114. Liu, H. and G. Zhu, *The electrochemical capacitance of nanoporous carbons in aqueous and ionic liquids.* Journal of Power Sources, 2007. **171**(2): p. 1054-1061.

115. Ye, J.-S., X. Liu, H.F. Cui, W.-D. Zhang, F.-S. Sheu, and T.M. Lim, *Electrochemical oxidation of multi-walled carbon nanotubes and its application to electrochemical double layer capacitors.* Electrochemistry Communications, 2005. **7**(3): p. 249-255.

116. Kuwabata, S., S. Masui, H. Tomiyori, and H. Yoneyama, *Charge-discharge properties of chemically prepared composites of V2O5 and polypyrrole as positive electrode materials in rechargeable Li batteries.* Electrochimica Acta, 2000. **46**(1): p. 91-97.

117. Xu, Y., J. Wang, W. Sun, and S. Wang, *Capacitance properties of poly(3,4-ethylenedioxythiophene)/polypyrrole composites.* Journal of Power Sources, 2006. **159**(1): p. 370-373.

118. Huang, Q., X. Wang, J. Li, C. Dai, S. Gamboa, and P.J. Sebastian, *Nickel hydroxide/activated carbon composite electrodes for electrochemical capacitors.* Journal of Power Sources, 2007. **164**(1): p. 425-429.

119. Gao, Y., S. Chen, D. Cao, G. Wang, and J. Yin, *Electrochemical capacitance of Co3O4 nanowire arrays supported on nickel foam.* Journal of Power Sources. **195**(6): p. 1757-1760.

120. Mitra, S., A.K. Shukla, and S. Sampath, *Electrochemical capacitors with plasticized gel-polymer electrolytes.* Journal of Power Sources, 2001. **101**(2): p. 213-218.

121. Li, X.-l., Y. Xing, H. Wang, H.-l. Wang, W.-d. Wang, and X.-y. Chen, *Synthesis and characterization of uniform nanoparticles of [gamma]-Mo2N for supercapacitors.* Transactions of Nonferrous Metals Society of China, 2009. **19**(3): p. 620-625.

122. Wei, W., X. Cui, W. Chen, and D.G. Ivey, *Improved electrochemical impedance response induced by morphological and structural evolution in nanocrystalline MnO2 electrodes.* Electrochimica Acta, 2009. **54**(8): p. 2271-2275.

123. Zheng, Y.-Z., H.-Y. Ding, and M.-L. Zhang, *Hydrous-ruthenium-oxide thin film electrodes prepared by cathodic electrodeposition for supercapacitors.* Thin Solid Films, 2008. **516**(21): p. 7381-7385.

124. Akinyeye, R.O., *Nanostructured Polypyrrole impedimetric sensors for Athropogenic organic pollutants*, in *Department of Chemistry*. 2007, University of the Western Cape: Cape Town. p. 271.

125. Girija, T.C. and M.V. Sangaranarayanan, *Analysis of polyaniline-based nickel electrodes for electrochemical supercapacitors.* Journal of Power Sources, 2006. **156**(2): p. 705-711.

126. Miao, F., B. Tao, P. Ci, J. Shi, L. Wang, and P.K. Chu, *3D ordered NiO/silicon MCP array electrode materials for electrochemical supercapacitors.* Materials Research Bulletin, 2009. **44**(9): p. 1920-1925.

127. C.R. Martins, C.P.L.R., L.C. Costa, R.M. Rubinger, *Dielectric properties of ternary melt processed blends.* . Journal of Non-Crystalline Solids 2008. **354**(47-51): p. 5323–5325.

128. Zejli, H., J.L.H.-H.d. Cisneros, I. Naranjo-Rodriguez, and K.R. Temsamani, *Stripping voltammetry of silver ions at polythiophene-modified platinum electrodes.* Talanta, 2007. **71**(4): p. 1594-1598.

129. Kim, Y.J., Y. Abe, T. Yanagiura, K.C. Park, M. Shimizu, T. Iwazaki, S. Nakagawa, M. Endo, and M.S. Dresselhaus, *Easy preparation of nitrogen-enriched carbon materials from peptides of silk fibroins and their use to produce a high volumetric energy density in supercapacitors.* Carbon, 2007. **45**(10): p. 2116-2125.

130. Lu, T., Y. Zhang, H. Li, L. Pan, Y. Li, and Z. Sun, *Electrochemical behaviors of graphene-ZnO and graphene-SnO2 composite films for supercapacitors.* Electrochimica Acta. **55**(13): p. 4170-4173.

131. Hsieh, C.-T., W.-Y. Chen, and Y.-S. Cheng, *Influence of oxidation level on capacitance of electrochemical capacitors fabricated with carbon nanotube/carbon paper composites.* Electrochimica Acta, 2010. **55**(19): p. 5294-5300.

132. Li, J., X. Wang, Q. Huang, S. Gamboa, and P.J. Sebastian, *A new type of MnO2·xH2O/CRF composite electrode for supercapacitors.* Journal of Power Sources, 2006. **160**(2): p. 1501-1505.

133. Horng, Y.-Y., Y.-C. Lu, Y.-K. Hsu, C.-C. Chen, L.-C. Chen, and K.-H. Chen, *Flexible supercapacitor based on polyaniline nanowires/carbon cloth with both high gravimetric and area-normalized capacitance.* Journal of Power Sources. **195**(13): p. 4418-4422.

134. Chen, C., D. Zhao, and X. Wang, *Influence of addition of tantalum oxide on electrochemical capacitor performance of molybdenum nitride.* Materials Chemistry and Physics, 2006. **97**(1): p. 156-161.